수의학박사학위논문

The roles of voltage-gated K^+ channels, Kv3.3 and Kv3.4 as oxidation sensor

산화 감지자로서 전압의존성 K^+ 채널 Kv3.3과 Kv3.4의 역할

2018년 8월

서울대학교 대학원

수의학과 수의약리학 전공

송 민 석

Doctoral Thesis

The roles of voltage-gated K^+ channels, Kv3.3 and Kv3.4 as oxidation sensor

Min Seok Song

Academic advisor: So Yeong Lee, D.V.M, Ph.D

Graduate School

Seoul National University

August 2018

The roles of voltage-gated K^+ channels, Kv3.3 and Kv3.4 as oxidation sensor

산화 감지자로서 전압의존성 K^+ 채널

Kv3.3과 Kv3.4의 역할

지도교수 이 소 영

이 논문을 수의학 박사학위 논문으로 제출함
2018년 6월

서울대학교 대학원
수의학과 수의생명과학 전공
(수의약리학)
송 민 석

송민석의 수의학 박사학위 논문을 인준함
2018년 7월

위 원 장 _____ (인)

부위원장 _____ (인)

위 원 _____ (인)

위 원 _____ (인)

위 원 _____ (인)

ABSTRACT

The functions and roles of voltage-gated potassium (Kv) channels in cell physiology, including cell proliferation, apoptosis, and wound healing, have been well investigated. However, the function of Kv channels as oxidation-sensitive channels have not yet been much investigated.

The impact of oxidation-sensitive Kv channels on cell behavior was evaluated in the context of an increase in oxidative stress in this study. The function of the Kv3.1, Kv3.3, and Kv3.4 channels was the focus of the research because they have not been adequately investigated, despite being well-recognized as oxidation-sensitive channels.

Kv3.3 was demonstrated to be involved in the hemin-induced erythroid differentiation of human leukemia cells, namely K562, via interaction with several signaling pathways, including mitogen-activated protein kinase (MAPK), cAMP response element-binding protein (CREB), and c-fos. Knockdown of Kv3.3 using siRNA-Kv3.3 increased hemin-induced erythroid differentiation, whereas overexpression of Kv3.3 did not have any effect on the cell differentiation. However, in the presence of fibronectin, the effect of siRNA-Kv3.3 contributed on the cell adhesion properties through the regulation of integrin β3 without having any effect on K562 erythroid differentiation.

Kv3.4 was also found to play a pivotal role in the death of human SH-SY5Y neuroblastoma cells induced by oxidative stress and HIF-1α was suggested as a key regulator of Kv3.4. Accumulated HIF-1α by $CoCl_2$ inhibited

Kv3.4 to protect SH-SY5Y cells against $CoCl_2$-induced oxidative damage. Although there was no accumulated HIF-1α by MPP^+ treatment, inhibition of Kv3.4 using BDS-II, a Kv3.4 selective blocker, blocked apoptosis by inhibiting cytochrome c release from mitochondrial intermembrane space to cytosol and mitochondrial membrane potential depolarization during MPP^+-induced SH-SY5Y cell death.

Not normal cells but only cancer cells, such as A549 and MDA-MB-231 increased the expression levels of Kv3.1 and Kv3.4 in cell density dependent manner because they were exposed to the pericellular hypoxia and ROS accumulation according to the cell density increment. Increased Kv3.1 and Kv3.4 were involved in cancer cell migration and invasion to help the cells avoiding oxidative damage and excessive ROS accumulation and BDS-II blocked the cell migration and invasion by inhibiting pH regulation and ERK activation of the cancer cells.

The present study demonstrates the role of the Kv channels as oxidation-sensitive channels and it would not only provide a new paradigm for studying Kv channels but also suggest oxidation-sensitive Kv channels as new biomarkers and therapeutic targets in oxidative stress-related disease.

Keyword: cell differentiation, cell invasion, cell migration, Kv channel, Kv3, oxidative stress

Student Number: 2012-21540

CONTENTS

LIST OF FIGURES AND TABLES

CHAPTER I

CHAPTER II

CHAPTER III

ABBREVIATIONS

Kv	voltage-gated potassium channels
MAPK	mitogen-activated protein kinase
CREB	cAMP response element-binding protein
ROS	reactive oxygen species
RNS	reactive nitrogen species
MIRP2	MinK-Related Peptide 2
NF-κB	nuclear factor kappa light chain enhancer of activated B cells
ERK1/2	extracellular signal–regulated kinases1/2
CBP	CREB binding protein
FBS	fetal bovine serum
HIF-1α	hypoxia inducible factor-1α
BDS-II	blood depressing substance-II
MPP^+	1-methyl-4-phenylpyridinium
NDFIP1	NEDD4 family-interacting protein 1
MMP	mitochondrial membrane potential
Nedd4	neural precursor cell expressed developmentally down-regulated protein 4
tERK	total ERK
pERK	phosphorylated ERK

Literature review

1. Oxidation-sensitive voltage-gated potassium channels

The functions of Kv channels have been investigated in previous studies in relation to proliferation, apoptosis, and oxygen sensing. (Wang et al., 2002; Pardo, 2004; Wang, 2004; Kunzelmann, 2005; Lang et al., 2005; O'Grady and Lee, 2005). However, there may be an overlooked part in the case of their function of oxygen sensing. Because most of Kv channels, known as oxygen sensing channels, are oxidation-sensitive channels which have the ability to sense numerous oxidation-inducing factors. (Kaab et al., 2005; Li and Schultz, 2006).

Various protocols and phenomenology have been applied in previous studies with regard to oxidative modification, site-directed mutagenesis, and structural and kinetic modeling, in order to gain mechanistic insight into the roles and functions of oxidation-sensitive Kv channels. The modification of cysteine, methionine, tyrosine, histidine, and tryptophan (often observed in protein during oxidative stress and the oxidation of specific protein residue in Kv channels) may alter the structure or function of Kv channels (Sahoo et al., 2014). The oxidation of cysteine and methionine residue, in particular, is known to affect Kv channel currents (Ruppersberg et al., 1991; Sahoo et al., 2014). For example, oxidation of the protein residue in Kv channels induced by reactive oxygen species (ROS) modulates N-type inactivation or P/C-type inactivation of those channels (Schlief et al., 1996; Chen et al., 2000; Xu et al.,

2001). Potentially reversible oxidative regulation of the Kv channels by ROS is considered to be a contributory mechanism to cellular plasticity, including cell differentiation and fusion, and may also have an important role in diverse oxidative stress-related disease (Sahoo et al., 2014; Sesti, 2016).

2. Oxidative stress and disease

Free radicals are unstable molecules that damage or oxidize cells in the body during a process that is referred to as oxidative stress. Oxidative stress reflects an imbalance between the systemic manifestation of ROS or reactive nitrogen species (RNS) and the ability of the biological system to readily detoxify the reactive intermediates or repair the resulting damage.

Oxidative stress induces DNA, lipid, and protein damage to the cell structure. Oxidative stress-induced DNA damage by ROS manifests as apurinic/apyrimidinic (abasic) DNA sites, oxidized purines and pyrimidines, single- and double-stranded DNA breaks; of which the most two common endogenous DNA base modifications are 8-oxo-7,8-dihydroguanine and 2,6-diamino-4-hydroxy-5-formamidopyrimidine (Barzilai and Yamamoto, 2004; Kryston et al., 2011). Increased ROS affects membrane lipid peroxidation, leading to the loss of membrane fluidity and elasticity, impaired cellular functioning, and even cell rupture. The direct products of lipid peroxidation, such as malondialdehyde, isoprostanes, and 4-hydroxynonenal, are considered to be the most important biomarkers of oxidative stress in tissues (Milei et al., 2007; Barrera, 2012). In the case of protein damage, this results in the

inactivation and denaturation of essential proteins, such as enzymes and membrane ion transporters. The most at-risk proteins are those with sulfur-containing amino acids, such as methionine and cysteine (Friguet, 2006; Martinez et al., 2017).

Oxidative stress-induced damage causes disease states. For example, oxidative stress is associated with a variety of neurodegenerative diseases, such as Alzheimer's and Parkinson's, with increasing evidence that it plays a key role in these diseases (Markesbery, 1997; Gandhi and Abramov, 2012; Hwang, 2013). The most common neurodegenerative disease, Alzheimer's, is characterized by progressive neuronal loss and the accumulation of proteins, including extracellular amyloid plaques and intracellular tau-containing neurofibrillary tangles. It has been suggested that the accumulation of oxidative stress-induced neuronal damage is one of the main causes of this disease and is critical to its initiation and progression (Mattson, 2004; Wang et al., 2014). However, the origin of increased ROS production and the exact mechanisms that underlie the disruption in the redox balance remain elusive. Parkinson's disease is characterized by the death of *substantia nigra pars compacta* dopaminergic neurons and decreased dopaminergic levels in the nigrostriatal dopaminergic pathway in the brain (Blesa et al., 2015). Although the exact mechanism for the initiation and progression of Parkinson's disease remains unclear, oxidative stress is considered to be a major responsible pathophysiological mechanism (Blesa et al., 2015).

Carcinogenesis is another example of a disease state that is caused by oxidative stress as a consequence of the overproduction of ROS and RNS due to

endogenous or exogenous insult. Oxidative stress-induced DNA, lipid, and protein damage contributes to abnormal cell function, i.e., cell cycle impairment, dysregulation of the DNA repair system, and an imbalance in the redox state (Klaunig and Kamendulis, 2004; Klaunig et al., 2010). In addition to inducing DNA, lipid, and protein oxidative damage; oxidative damage to protein-coding or noncoding RNA may potentially cause errors in protein synthesis or the dysregulation of gene expression, and contribute to the initiation and progression of cancer (Nunomura et al., 2007). DNA damage, mutation, and altered gene expression have recently been demonstrated to be requirements for carcinogenesis progression (Klaunig and Kamendulis, 2004; Klaunig et al., 2010). Such damage induces the malfunctioning and/or dysregulation of key DNA repair, cell growth, and apoptosis-related proteins, and may be influential in the promotion of chromosomal instability and malignancy (Holt et al., 2009; Kryston et al., 2011). In addition, there is a need for new molecular approaches, such as epigenetics and proteomics, as this would facilitate the ability to gain further insight into the mechanisms at work. Although these events may derive from different mechanisms, a common denominator is that cellular oxidants are involved in tumorigenic development.

Aside from neurodegenerative disease and carcinogenesis, many diseases have been identified as having a close relationship with oxidative stress; including diabetes mellitus; heart, pulmonary, and autoimmune disease; nephropathy, and ocular disease (Halliwell, 1994; Florence, 1995; Pham-Huy et al., 2008).

3. Kv3.3 and Kv3.4 as oxidation sensitive channels

The role of Kv3 channels is poorly understood when compared against scientific knowledge of other Kv channels. Although it is well-recognized that Kv3.3 and Kv3.4 are oxidation-sensitive channels (Duprat et al., 1995; Patel and Honore, 2001), the specific mechanisms behind their role of Kv3.3 and Kv3.4 as oxidation-sensitive channels have been poorly elucidated. In particular, although Kv3.3 has its own fast inactivating potassium currents when transfected into the Human embryonic kidney (HEK) cell or Chinese hamster ovary (CHO) cell system (Rae and Shepard, 2000; Fernandez et al., 2003), few studies have reported the electrophysiological recordings of endogenously expressed Kv3.3 in other cells. This is likely to influence why it has been more poorly researched than the other three Kv3 subfamilies (i.e., Kv3.1, Kv3.2, and Kv3.4). Considering that Kv3.3 is an oxygen-sensitive channel that opens in the presence of oxygen and inversely closes in response to hypoxia, and Kv3.3 is one of the channels that loses its fast inactivation upon the external application of H_2O_2 (Ruppersberg et al., 1991; Vega-Saenz de Miera and Rudy, 1992; Patel and Honore, 2001), its role in cell physiology needs to be explored while bearing these considerations in mind.

By contrast, Kv3.4 is relatively more studied than Kv3.3. Several reports have focused on the function of Kv3.4 in cell physiology and on its role as an oxygen-sensitive channel (Baranauskas et al., 2003; Kaab et al., 2005; Pannaccione et al., 2007; Menendez et al., 2010; Palme et al., 2013). Kv3.4 is also well documented as a potential therapeutic target for Alzheimer's disease.

It is overexpressed in both the early and advanced stages of this neurodegenerative disease, and its upregulation leads to altered electrical and synaptic activity that may trigger the neurodegeneration (Angulo et al., 2004). Kv3.4 and its accessory protein, MIRP2 are involved in neuronal cell death induced by the neurotoxic amyloid β peptide, which is generated from the amyloid precursor protein and whose amyloid fibrillar form is the primary component of amyloid plaques found in the brains of patients with Alzheimer's disease (Pannaccione et al., 2007). In addition, during exposure of the amyloid β-peptide, nuclear factor kappa light chain enhancer of activated B cells (NF-κB), a signal molecule that is closely involved in the cellular response to the oxidative stress, mediates the transcriptional regulation of KV3.4 (van den Berg et al., 2001; Pannaccione et al., 2007).

Referring to other oxidation-sensitive Kv channels, which are relatively well investigated than Kv3.3 and Kv3.4, it is certain that much more research about those two channels needs to be done in the future. In particular, in the case of Kv2.1, the channel is considered to be one of the most significant potassium channels in terms of its involvement in the apoptotic pathway. Its mechanisms and function have been investigated extensively when compared to the other oxidation-sensitive channels (Pal et al., 2003; Yao et al., 2009; McCord and Aizenman, 2013). In detail, Kv2.1 is abundantly expressed in the cortex and hippocampus, and is oxidized in the brains of aging mice. The oxidized Kv2.1 channels form oligomers that are held together by disulfide bonds obtained through the mutation of an N-terminal cysteine (involving Cys-73, accumulate in the plasma membrane as a consequence of defective

endocytosis (Misonou et al., 2005; Wu et al., 2013). The accumulation of Kv2.1 oligomers in the membrane disrupts the integrity of the planar lipid raft, thereby causing apoptosis via activation of the c-Src/JNK signaling pathway (Wu et al., 2013).

Kv channels, such as Kv1.1, Kv2.1, Kv1.3, and Kv4.2, known to have oxygen sensing, are involved in neuronal apoptosis (Plant et al., 2006; Koeberle et al., 2010). In addition, like Kv2.1 and Kv4.2, Kv3.4 is thought to be connected to Alzheimer's disease and therefore has potential as a novel therapeutic target in Parkinson's disease. Based on the available evidence, at the very least, Kv3.4 is involved in neuronal apoptosis, with potentially more functions in cell physiology based on its sensitivity to oxidation.

4. Hypothesis and Purposes

It was hypothesized in the current study that Kv3.3 and Kv3.4 play a significant role as oxidation-sensitive Kv channels in cell physiology. Although their prominence as oxidation-sensitive Kv channels is well established, there is a scarcity of available evidence in the literature on their oxidation-sensing properties. It is possible that Kv3.3 and Kv3.4 play a pivotal role in oxidative stress-related disease or cell physiology, and an attempt was made to determine this in the current research. Erythroid differentiation, neurodegenerative disease, and cancer cell migration and invasion, were the focus of the current study in this regard. An endeavor was also made to establish whether or not signal molecules interact with oxidation-sensitive Kv channels. The primary objective

of the current study was not only to provide a new paradigm within which Kv channels could be studied, but also to identify which oxidation-sensitive Kv channels could be new biomarkers and therapeutic targets in oxidative stress-related disease.

CHAPTER I

Voltage-gated K^+ channel, Kv3.3 is involved in hemin-induced K562 differentiation

(Data in this chapter have been published in

Song et al., PLoS One, 2016, 11(2):e0148633)

ABSTRACT

Kv channels are well known to be involved in cell proliferation. However, even though cell proliferation is closely related to cell differentiation, the relationship between Kv channels and cell differentiation remains poorly investigated. This study demonstrates that Kv3.3 is involved in K562 cell erythroid differentiation. Down-regulation of Kv3.3 using siRNA-Kv3.3 increased hemin-induced K562 erythroid differentiation through decreased activation of signal molecules such as p38, cAMP response element-binding protein, and c-fos. Down-regulation of Kv3.3 also enhanced cell adhesion by increasing integrin β3 and this effect was amplified when the cells were cultured with fibronectin. The Kv channels, or at least Kv3.3, appear to be associated with cell differentiation; therefore, understanding the mechanisms of Kv channel regulation of cell differentiation would provide important information regarding vital cellular processes.

INTRODUCTION

Kv channels are well-established ion channels in excitable cells, where they serve as regulators of membrane potential and neuronal activities; however, these channels are also found in non-excitable cells, including cancer cells (Hille, 2001; Pardo and Suhmer, 2008; Bardou et al., 2009). Previous studies have revealed cellular functions of Kv channels that include cell proliferation, apoptosis, and oxygen sensing (Wang et al., 2002; Pardo, 2004; Wang, 2004; Kunzelmann, 2005; Lang et al., 2005; O'Grady and Lee, 2005). Specifically, the modulation of certain Kv channel subunits, such as Kv1.1, Kv1.3, Kv4.1, Kv10.1, and Kv11.1, significantly affects cancer cell proliferation (Wang et al., 2002; Hemmerlein et al., 2006; Jang et al., 2009; Jang et al., 2011; Jang et al., 2011). Nevertheless, even though a relationship is known to exist between cell proliferation and cell differentiation (Golding et al., 1988; Langdon et al., 1988; Volpi et al., 1994), a function for Kv channels in cell differentiation has not been well established. However, Kv channels may be involved in a series of cell differentiation mechanisms, and specific Kv channel subunits may have direct effects on cell differentiation.

K562 cells are human immortalized myelogenous leukemia cells obtained from the pleural fluid of patients with chronic myeloid leukemia in blast crisis (Lozzio and Lozzio, 1975). These cells have been useful for studying hematopoietic cell proliferation and differentiation (Koeffler and Golde, 1980) and can differentiate into an erythroid lineage when treated with differentiation-

inducing reagents such as hemin, sodium butyrate, and nicotinic acid (Rutherford et al., 1979; Ida et al., 2009). The induced cells produce hemoglobin, and differentiation can be validated by benzidine staining or hemoglobin quantification (Koeffler and Golde, 1980; Yi et al., 2004; Zhang et al., 2007; Yang et al., 2009). K562 cells also can differentiate into megakaryotic lineages when treated with megakaryotic differentiation-inducing reagents, such as phorbol 12-myristate 13-acetate (Pettiford and Herbst, 2003; Limb et al., 2009).

K562 cell differentiation involves the MAPK and CREB signaling pathways; extracellular signal-regulated kinase 1/2 (ERK1/2), CREB, and p38 have been specifically identified as important factors in K562 erythroid differentiation and hemoglobin synthesis (Huang et al., 2004; Sangerman et al., 2006; Akel et al., 2007; Di Pietro et al., 2007). In addition, certain Kv channels have close links to signaling molecules including CREB and CREB binding protein (CBP); they modulate Kv channel expression (Tong et al., 2010; Kim et al., 2012).

Taken together, the available evidence suggests that Kv channels may be involved in the cell differentiation process through a range of signal pathways. An understating of the relationship between Kv channels and cell differentiation mechanisms might therefore suggest a new paradigm for cell differentiation research. This study investigated the roles of Kv channels and underlying signal mechanisms in the differentiation of K562 cells.

MATERIALS AND METHODS

Cell culture and hemin-induced cell differentiation

K562 cells obtained from Korean Cell Line Bank were cultured in RPMI1640 medium (Welgene, Daegu, Korea) supplemented with 10% fetal bovine serum (FBS) and 1% antibiotic-antimycotic solution (Sigma, St. Louis, MO) at 37°C incubation with 5% CO_2. T25 flasks (SPL Life Sciences, Gyeonggi-do, Korea) were used for culturing the cells. When sufficient growth was achieved, 1 x 10^5 cells were plated into a new T25 flask (SPL Life Sciences, Gyeonggi-do, Korea) and incubated with 50 μM hemin (Sigma, St. Louis, MO) to induce erythroid differentiation.

Reverse transcription-polymerase chain reaction (RT-PCR)

Total RNA was isolated using RNeasy Micro Kit (Quiagen, Valencia, CA) according to the manufacturer's instructions. The cDNA was synthesized by reverse transcribing 1 μg of extracted RNA using random hexamers and an M-MLV reverse transcription kit (Promega, Madison, WI). The PCR reaction was performed with 2 μl of cDNA, 1× GoTaq® green master mix (Promega), and target Kv channel specific primers using the following reaction conditions: initial denaturation at 94°C for 5 min, 35 cycles of cycling process (94°C for 40 s, the indicated annealing temperature (Table 1) for 40 s, 72°C for 1 min, and an extension at 72°C for 1 min), and a final extension at 72°C for 7 min (Table 1).

All PCR products were subjected to electrophoresis on 1.6% agarose gel and analyzed using an ABI Prism 3730 XL DNA Analyzer (Applied Biosystems, Foster City, CA) to confirm their amplified sequences.

Western blotting

K562 cells were lysed with 1X passive lysis buffer (Promega, Madison, WI) and total protein was quantified with a BCA protein assay kit (Pierce, Rockford, IL). The extracted proteins were separated on a 10% SDS-PAGE and then transferred to Nitrocellulose membranes (Whatman, Maidstone, Kent). After blocking in 1x TBS-Tween 20 containing 5% nonfat milk (5% TTBS) (Difco Franklin Lakes, NJ), membranes were probed with specific antibodies (in 5% TTBS) for Kv2.1, Kv3.3, p38, phospho-p38 (Abcam, Cambridge, MA), Kv1.2, Kv1.3, CREB, phospho-CREB (Millipore, Billerica, MA), ERK, phospho-ERK (Cell Signaling Technology, Inc, Danver, MA), Kv9.3, c-fos or β-actin (Santa Cruz Biotechnology, CA, USA). After overnight incubation, membranes were treated with horseradish peroxidase-conjugated goat, anti-rabbit secondary antibody (Santa Cruz Biotechnology, CA, USA) and visualized using an enhanced chemiluminescent detection kit (iNtron Biotechnology, Gyeonggi-do, Korea)

Real-time RT-PCR

A standard curve and primer efficiency were analyzed from the standard curve prepared from diluted cDNAs (2 or 10 fold) using a primer of GAPDH, a house

keeping gene, as a reference. The real-time RT-PCR reaction was performed with 2 μl of cDNA, 1x SYBR Green Master Mix (Applied Biosystems, Foster City, CA), and 0.2 μM forward and reverse primers in the following reaction: initial step 95°C 30 s, then 40 cycles of the at 95°C for 5 s, and either 60°C (Kv3.3) or 55°C (integrin) for 45 s. A dissociation protocol was used to confirm that paired primers produced only a single product. All of the procedures were performed using an Applied Biosystems StepOnePlus™ Real-Time PCR System (Applied Biosystems, Foster City, CA). The relative mRNA expressions of the Kv channel gene were normalized to the GAPDH gene and expressed as a fold change relative to the control group.

Benzidine staining

Cultured cells were collected and centrifuged at 400 g for 5 min to obtain cell pellets. The cell pellets were washed using PBS and recentrifuged for 5 min. A benzidine working solution was prepared by mixing 20 μl of hydrogen peroxide solution (Sigma, St. Louis, MO) in 1 ml benzidine stock solution [0.2% 3,3′-dimethoxybenzidine (Sigma, St. Louis, MO) dissolved in 3% glacial acetic acid solution (Sigma, St. Louis, MO)]. The cell pellets were incubated at room temperature with the solution for 2 min and passed through the washing step again. Benzidine positive cells were analyzed by light microscopy. The K562 cells that were cultured in fibronectin coated wells underwent the washing and staining steps without centrifugation.

Hemoglobin quantification

Cell pellets were collected for protein extraction. Extracted protein was quantified using a BCA protein assay kit (Pierce, Rockford, IL). Quantitative analysis of hemoglobin was performed using a QuantiChromTM Heme Assay Kit (BioAssay Systems, Hayward, CA) following manufacturer's instructions. The unit-hemoglobin contents (ng Hb/μg Protein) were calculated by dividing the amount of hemoglobin by the total amount of protein.

Patch clamp recordings

Poly-L-lysine coated 12 mm coverslips (SPL) was put into the recording chamber to allow the cells to be attached on the bottom of the chamber. K562 cells were centrifuged and then resuspended with bath solution to be transferred to the chamber. The cells were visualized by the differential interference contrast video microscopy (Olympus, Tokyo, Japan). Patch pipettes were pulled from the borosilicate glass capillaries (1.7 mm diameter; 0.5 mm wall thickness) (World Precision Instruments, Sarasota, FL); the range of the seal resistance was from 8 to 10 MΩ. The internal pipette solution (in mM concentration) was consist of 135 K-gluconate, 5 KCl, 20 HEPES, 0.5 $CaCl_2$, 5 EGTA, and 5 ATP-Mg and the bath solution is consist of 126 NaCl, 26 $NaHCO_3$, 5 KCl, 1.2 NaH_2PO_4, 2.4 $CaCl_2$, 1.2 $MgCl_2$, and 10 glucose. The currents were recorded in the whole cell configuration by using Axoclamp 2B amplifier (Axon Instruments, Foster City, CA). Electric signal was filtered at 1 kHz and digitized at 10 kHz using analog-digital converter (Digidata 1320A,

Axon Instruments) and pClamp software (Version 9.0, Axon Instruments). For the voltage-clamp mode, following protocol was used: cells were hyperpolarized by -90 mV pulse for 320 ms and the membrane currents were activated by depolarizing pulse for 400 ms from a holding potential -80 mV to the test potential which are ranged from -70 to 40 mV in 10 mV increments.

Inducing cell differentiation after transfection with small interference RNA (siRNA)

Cells were transfected with siRNA-Kv3.3 using ON-TARGET plus SMART pool Human KCNC3 (Thermo Scientific Dharmacon, Lafayette, CO) and Lipofectamine™ 2000 reagent (Invitrogen, Carlsbad, CA, USA) following the manufacturer's instructions for suspension cells. The ON-TARGET plus® Control pool (Thermo Scientific Dharmacon, Lafayette, CO) was used as a control siRNA. The K562 cells (1 x 10^5) were plated in 6 well plates immediately prior to the transfection step in RPMI 1640 (Welgene, Daegu, Korea) containing 10% FBS without any antibiotics. After 24 h, the siRNA-Kv3.3 transfected cells were incubated with 50 μM hemin in 6 well plates. The incubation time was 24 or 48 h for benzidine staining or hemoglobin quantification, respectively. To induce cell adhesion, 6 well plates containing 10 μg/ml of fibronectin (Sigma, St. Louis, MO) dissolved in DPBS were incubated at 4°C for one day, and the coated plates were used for the experiment in place of uncoated plates.

Kv3.3 overexpressed K562 cell line establishment

HEK293T cells (GE lifesciences) were maintained in 10% fetal bovine serum and 1% penicillin/streptomycin in Dulbecco's modified Eagle medium (DMEM) at 37°C and 5% CO_2. 24 hours before transfection, 6×10^6 HEK293T cells were seeded into 100 mm dish. The following day, 50 μL (47.5 μg) of a Trans-lentiviral packaging mix encoding viral proteins Gag-Pol, Rev, and VSV-G and 42 μg of lentiviral transgene plasmids were transfected into each well for lentivirus production using Calcium phosphate. 14 hours after transfection, the DNA-reagent mixture was removed and replaced with 5% FBS in 14 ml fresh DMEM. At 48 hours post-transfection, lentiviral supernatants were harvested and filtrated with 0.45-μm filters. 1 volume of cold (4°C) PEG-it Virus Precipitation Solution (Systembio) was added to every 4 volumes of lentiviral particle-containing supernatant. The supernatant/PEG-it mixture was centrifuged at 1,500 x g for 30 minutes at 4°C. The viral pellet was resuspended and combined the lentiviral particles in 10 μL using cold (4°C), DMEM media. To determine transduction efficiency, HEK293T cells were transduced with lentivirus harvested from HEK293T cell transfection. At 72 hours post-transduction, GFP-positive cells were observed by fluorescence microscope (NiKon). Lentivirus was added to K562 cell culture in RPMI media. Lentivirus was then added to give a multiplicity of infection (MOI) of 1. After overnight incubation, lentivirus was removed and fresh media added. K562 cells were then transduced with KCNC3 (Openbiosystem, OHS5898-202623948) construct and selected by 2 μg/ml Blastcidin to create K562-KCNC3.

Statistical analysis

All data are shown as means ± standard error (SE) and the Student's *t*-test or One-way ANOVA was used to analyze the data (GraphPad Prism version 5.0).

Table 1. RT-PCR primers for Kv channel screening in K562 cells

Subtype	Accession No.	Size (bp)	Primer sequence (Forward/Reverse)	Annealing (°C)
Kv1.1	L02750	498	5’-ACATTGTGGCCATCATTCCT-3’ 5’-GCTCTTCCCCCTCAGTTTCT-3’	55
Kv1.2	NM_004974.3	200	5'-ATGAGAGAATTGGGCCTCCT-3' 5'-CCCACTATCTTTCCCCCAAT-3'	58
Kv1.3	NM_002232.3	177	5'-TGTCATGGCATCTCTTGC-3' 5'-TGCATTTGGGATTCATTT-3'	60
Kv1.4	NM_002233.3	170	5'-ACGAGGGCTTTGTGAGAGAA-3' 5'-GGTTTCCAGGCAAAAGATGA-3'	58
Kv1.5	M55513	917	5’-TGCGTCATCTGGTTCACCTTCG-3’ 5’-TGTTCAGCAAGCCTCCCATTCC-3’	60
Kv2.1	L02840	451	5’-GGAAGCCTGCTGTCTTCTTG-3’ 5’-CTTCATCTGAGAGCCCAAGG-3’	65
Kv3.3	AF055989	284	5’-CCTCATCTCCATCACCACCT-3’ 5’-CGAGATAGAAGGGCAGGATG-3’	60
Kv3.4	M64676	631	5’-TTCAAGCTCACACGCCACTTCG-3’ 5’-TGCCAAATCCCAAGGTCTGAGG-3’	65
Kv4.3	AF048712	349	5’-TGAGCTGATTGTCCTCAACG-3’ 5’-GTTCTCCGAGTCGTTGTCGT-3’	60
Kv9.3	NM_002252.3	200	5'-CAGTGAGGATGCACCAGAGA-3' 5'-TTGCTGTGCAATTCTCCAAG-3'	60

Table 2. Real-time RT-PCR primers for Kv channels and integrins in K562 cells

Subtype	Accession No.	Size (bp)	Primer sequence (Forward/Reverse)	Annealing (°C)
Kv2.1	NM_004975.2	173	5'-GTTGGCCATTCTGCCATACT-3' 5'- GCAAAGTGAAGCCCAGAGAC-3'	60
Kv3.3	NM_004977.2	147	5'- CCTTCCTGACCTACGTGGAG-3' 5'- CGAGATAGAAGGGCAGGATG-3'	60
Kv3.4	NM_004978.4	178	5'- AATATCCCAGGGTGGTGACA-3' 5'- GGTCTTCAAAGCTCCAGTGC-3'	60
Kv9.3	NM_002252.3	200	5'- CAGTGAGGATGCACCAGAGA-3' 5'- TTGCTGTGCAATTCTCCAAG-3'	60
integrin β1	NM_002211.3	209	5'- CATCTGCGAGTGTGGTGTCT-3' 5'- GGGGTAATTTGTCCCGACTT-3'	55
integrin β3	NM_000212.2	176	5'- GCAATGGGACCTTTGAGTGT-3' 5'- GTGGCAGACACATTGACCAC-3'	55

RESULTS

Expression of Kv channels in K562 cells and the induction of K562 cell erythroid differentiation using hemin

RT-PCR analysis revealed that seven different Kv channels (Kv1.2, Kv1.4, Kv2.1, Kv3.3, Kv3.4, Kv4.3, and Kv9.3) were detected in K562 cells (Figure 1A). Kv1.1, Kv1.3, and Kv1.5 were also detected; however, the expression was too low. Western blot analysis demonstrated that Kv1.3, Kv2.1, Kv3.3, and Kv9.3 exist in K562 cells (Figure 1A). Hemin was used to induce K562 cell differentiation into erythroids (Figure 1B). Negative control data showed few stained cells. At an early stage of differentiation, the percentage of benzidine-positive cells, which were dyed black, rapidly increased and later reached a plateau (Figure 1C). The concentration of hemoglobin, on the other hand, showed no significant changes in the early stage of differentiation and started to increase between 24 and 48 h (Figure 1D). Only Kv3.3 was selected for the further analysis since Western blot data showed the Kv3.3 band more clearly than Kv2.1 in K562 cells.

A

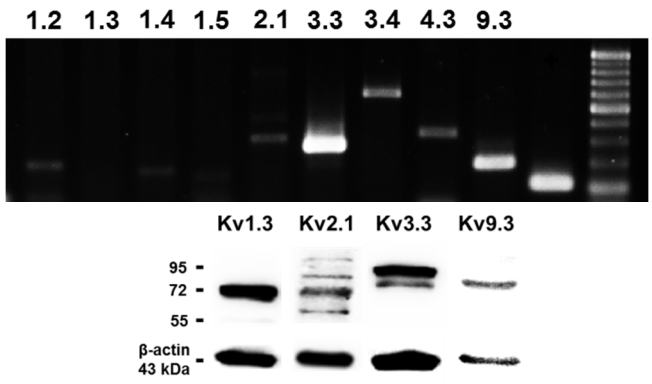
1.2 1.3 1.4 1.5 2.1 3.3 3.4 4.3 9.3
Kv1.3 Kv2.1 Kv3.3 Kv9.3
95
72
55
β-actin
43 kDa

B

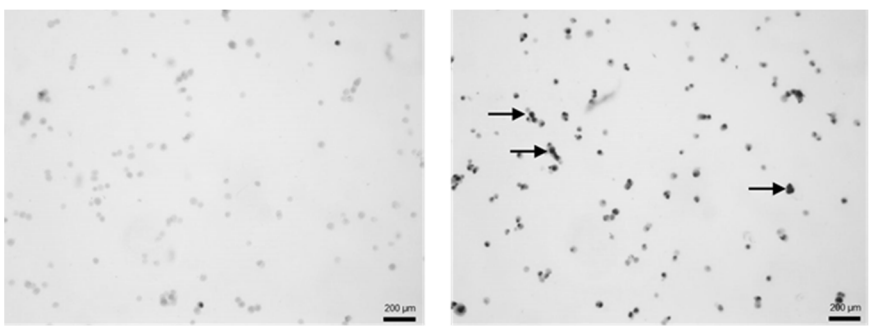
200 μm
200 μm
Control (72 h)
hemin (72 h)

C

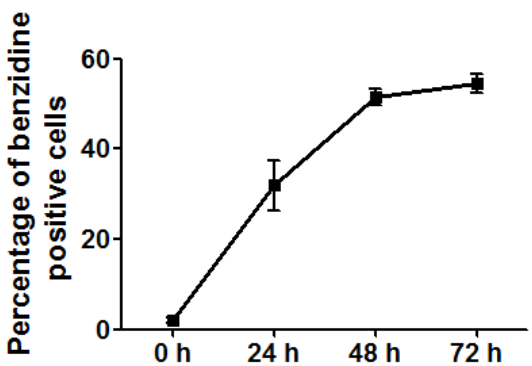
Percentage of benzidine positive cells
60
40
20
0
0 h
24 h
48 h
72 h

D

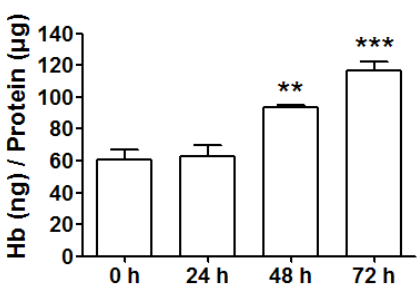
Hb (ng) / Protein (μg)
140
120
100
80
60
40
20
0
**
***
0 h
24 h
48 h
72 h

Figure 1. Identification of Kv channels in K562 cells and the erythroid differentiation of K562 cells using hemin (A) RT-PCR data analysis demonstrated 7 different subtypes of Kv channels (Kv1.2, Kv1.4, Kv1.5, Kv2.1, Kv3.3, Kv3.4, Kv4.3, and Kv9.3). Western blot demonstrated the protein expression of Kv1.3, Kv2.1, Kv3.3, and Kv9.3. (B) K562 cells differentiated into erythroid cells were stained with benzidine after 72 h of differentiation using hemin (magnification ×40). Benzidine-positive cells appeared black, indicated by colored arrows. (C) The percentage of benzidine-positive cells was counted at 4 different time points (0, 24, 48, and 72 h). (D) The hemoglobin content of the differentiated K562 cells was measured at each indicated time point using a modified QuantiChrom Heme Assay. The concentration of hemoglobin at each time point was expressed as nanograms of heme per microgram of total protein.

The expression of Kv channels and whole cell patch clamp recording during the late stage of differentiation

The real-time quantitative RT-PCR data demonstrated that the mRNA expression level of Kv3.3 was decreased by half after 24 hours of erythroid differentiation and the reduction rate gradually slowed down, whereas Kv2.1 increased during the K562 erythroid differentiation (Figure 2A). Kv3.4 and Kv9.3 showed no change and Kv1 subunits were not detected (Figure 2A). The protein expression level of Kv3.3 was also significantly lower during erythroid differentiation as a result of hemin treatment at the indicated time points (24, 48, and 72 h) (Figure 2B). Figure 2C demonstrated representative current traces recorded from K562 cells. Despite the fact that the mRNA and protein expression levels of Kv channels were detected, there was no TEA-sensitive current before and after hemin-induced erythroid differentiation (Figure 2C).

Kv3.3 knockdown using siRNA-Kv3.3 increased hemin-induced K562 cell differentiation, whereas Kv3.3 overexpression did not decrease the hemin-induced K562 erythroid differentiation effectively

To verify whether Kv3.3 directly affects K562 cell differentiation, siRNA-Kv3.3 was transfected into the K562 cells. After 24 h of transfection, the K562 cells were cultured with hemin for 48 h (Figure 3A). The degree of siRNA

transfection was confirmed by RT-PCR and Western blot analysis (Figure 3B and 3C). The benzidine staining and hemoglobin quantification data demonstrated that decreased Kv3.3 expression increased hemin-induced K562 cell differentiation (Figure 3D and 3E). The numbers of benzidine-positive cells, stained black, were increased in siRNA-Kv3.3-transfected cells compared to the control cells. Hemoglobin quantification confirmed an approximately 50% increase in hemoglobin content following transfection with siRNA-Kv3.3. The knockdown of Kv3.3 using siRNA-Kv3.3 increased the expression level of Kv2.1, but it did not have any effect on the expression levels of Kv3.4 and Kv9.3 (Figure 3F). Interestingly, siRNA-Kv3.3 transfection without hemin did not induce K562 erythroid differentiation (Figure 3G).

Next, Kv3.3-overexpressed K562 cells were established (Figure 4A and 4B) to verify whether Kv3.3 overexpression inhibits hemin-induced K562 erythroid differentiation. Benzidine staining data demonstrated that the overexpression of Kv3.3 slightly inhibited the hemin-induced K562 erythroid differentiation (Figure 4C). However, in the case of hemoglobin kit assay, the data demonstrated that Kv3.3 overexpression did not significantly decrease the hemin-induced K562 erythroid differentiation effectively (Figure 4D), whereas the down-regulation of Kv3.3 using siRNA- Kv3.3 enhanced the differentiation more clearly (Figure 3E).

A

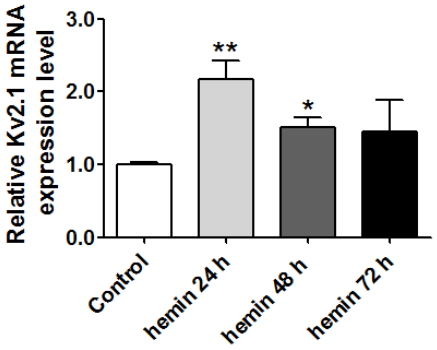
Relative Kv2.1 mRNA expression level
3.0
2.0
1.0
0.0
**
*
Control
hemin 24 h
hemin 48 h
hemin 72 h

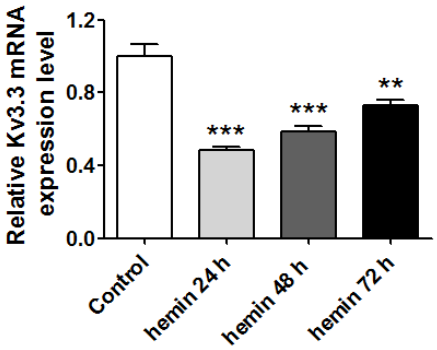
Relative Kv3.3 mRNA expression level
1.2
0.8
0.4
0.0
***
***
**
Control
hemin 24 h
hemin 48 h
hemin 72 h

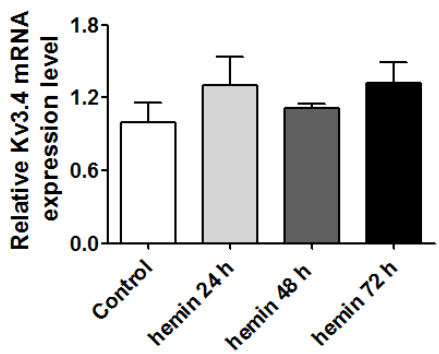
Relative Kv3.4 mRNA expression level
1.8
1.2
0.6
0.0
Control
hemin 24 h
hemin 48 h
hemin 72 h

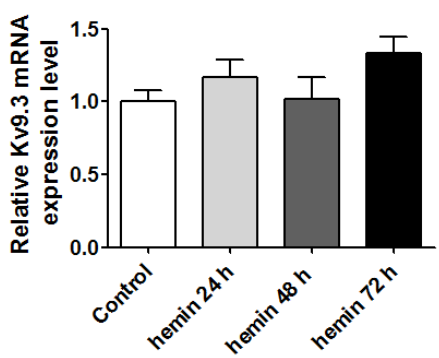
Relative Kv9.3 mRNA expression level
1.5
1.0
0.5
0.0
Control
hemin 24 h
hemin 48 h
hemin 72 h

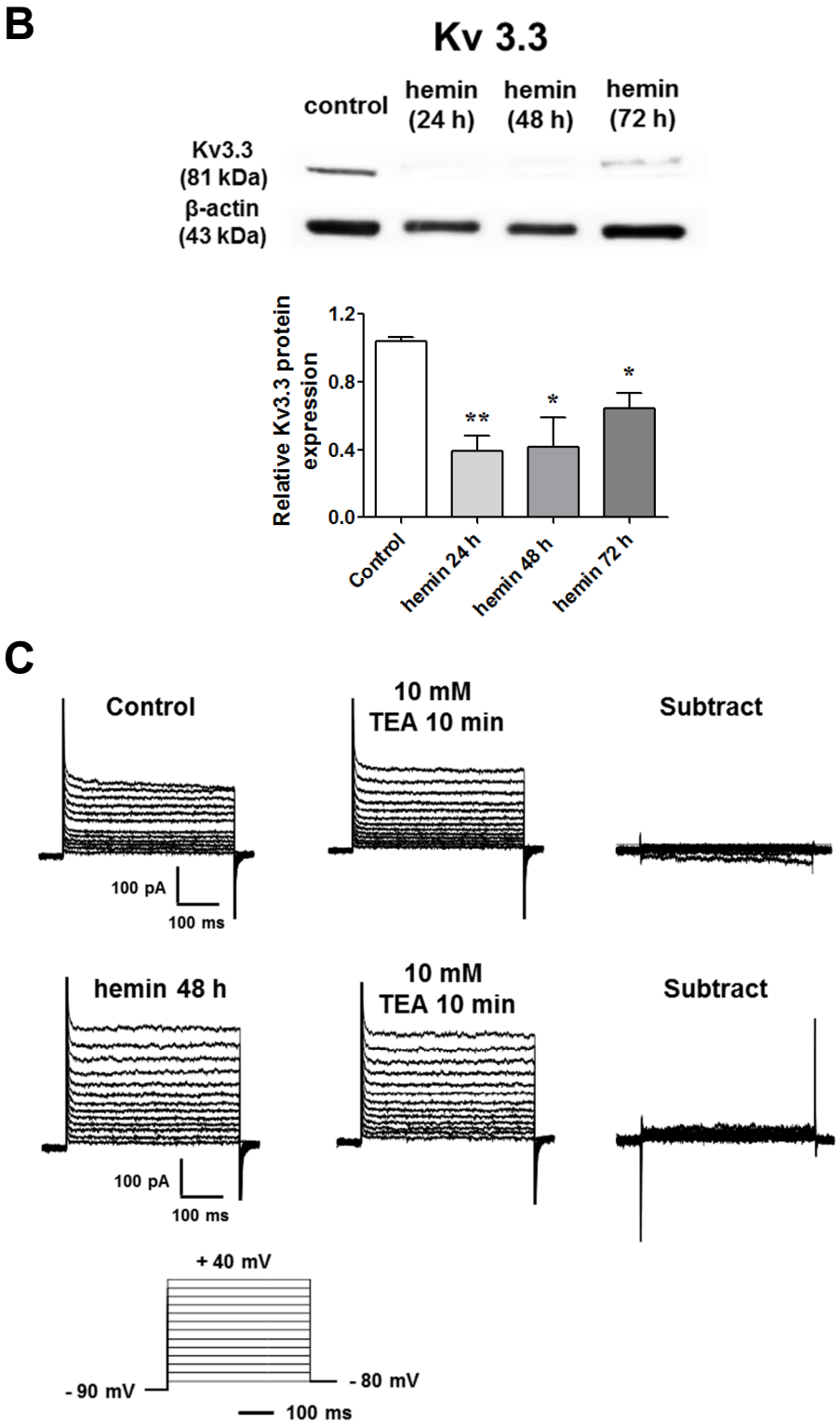
B
Kv 3.3
control
hemin (24 h)
hemin (48 h)
hemin (72 h)
Kv3.3 (81 kDa)
β-actin (43 kDa)
Relative Kv3.3 protein expression
1.2
0.8
0.4
0.0
**
*
*
Control
hemin 24 h
hemin 48 h
hemin 72 h
C
Control
10 mM TEA 10 min
Subtract
100 pA
100 ms
hemin 48 h
10 mM TEA 10 min
Subtract
100 pA
100 ms
+ 40 mV
- 90 mV
- 80 mV
100 ms

Figure 2. The expression of Kv channels and whole cell patch clamp recording during the late stage of differentiation (A) After hemin-induced K562 cell differentiation, the mRNA expression levels of Kv channels, including Kv2.1, Kv3.3, Kv3.4, and Kv9.3, were compared with those of undifferentiated cells. The mRNA expression level of Kv2.1 was increased, whereas the mRNA expression level of Kv3.3 was decreased during erythroid differentiation. The mRNA expression of Kv3.4 and Kv9.3 were not altered during erythroid differentiation. (B) The protein level of Kv3.3 decreased significantly after 24 hours of hemin-induced erythroid differentiation in K562 cells. The relative protein expression of the Kv3.3 was expressed as a fold change relative to the control group. (C) Representative current traces recorded from K562 cells. There was no TEA-sensitive current before and after hemin-induced erythroid differentiation. Experiments were performed in triplicate, and data are expressed as mean ± standard error. **$p<0.01$ compared with control value.

A

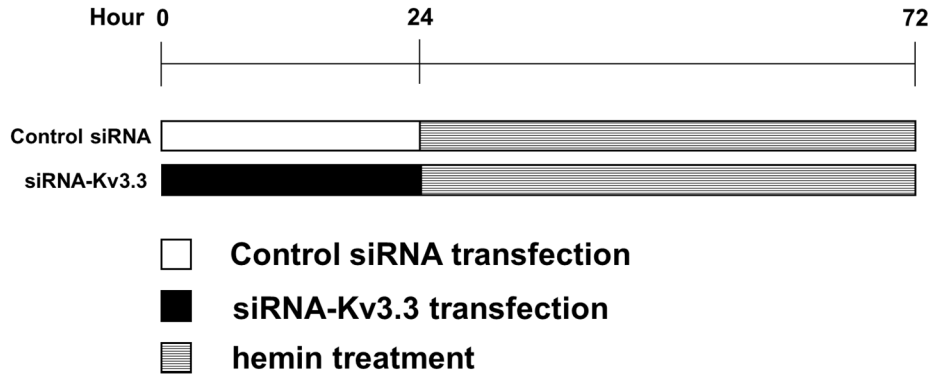
Hour 0
24
72
Control siRNA
siRNA-Kv3.3
Control siRNA transfection
siRNA-Kv3.3 transfection
hemin treatment

B

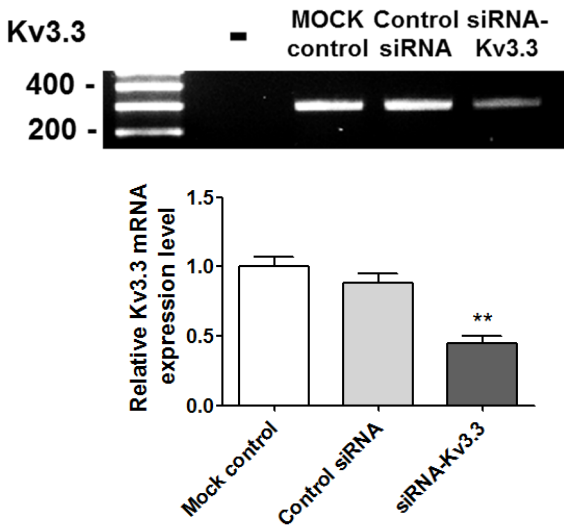
Kv3.3
-
MOCK control
Control siRNA
siRNA-Kv3.3
400 -
200 -
Relative Kv3.3 mRNA expression level
1.5
1.0
0.5
0.0
**
Mock control
Control siRNA
siRNA-Kv3.3

C

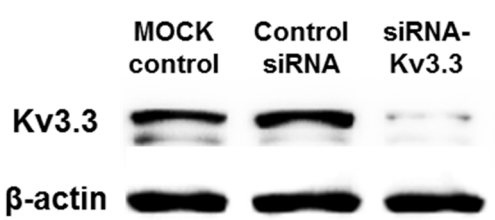
MOCK control
Control siRNA
siRNA-Kv3.3
Kv3.3
β-actin

D

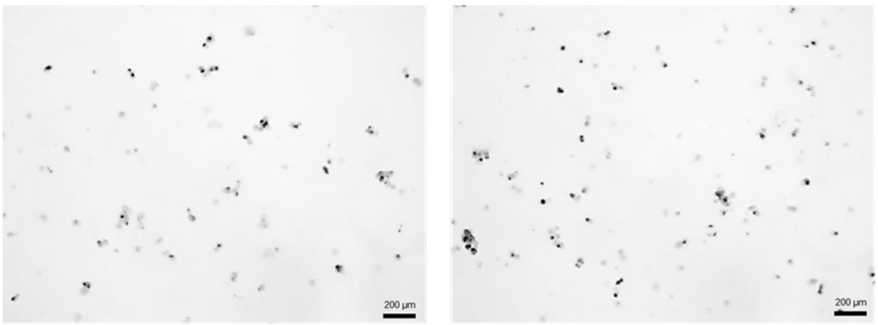

Control siRNA siRNA-Kv3.3

E

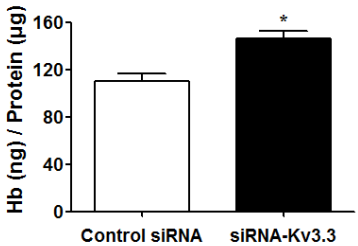

F

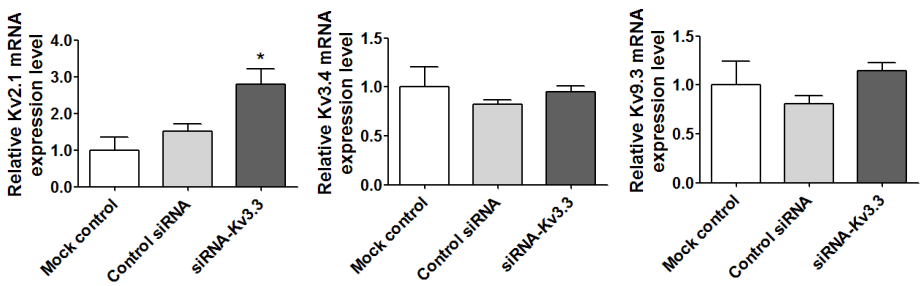

G

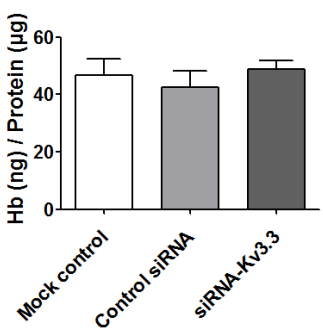

Figure 3. Silenced Kv3.3 increased hemin-induced K562 cell differentiation

Hemin-induced K562 cell differentiation was significantly increased by decreasing the Kv3.3 expression using siRNA-Kv3.3. (A) Protocol for control siRNA and siRNA-Kv3.3 transfection and hemin treatment. After 24 h of transfection, the K562 cells were cultured with hemin for 48 h. (B), (C) mRNA and protein expressions were suppressed when the cells were transfected with siRNA-Kv3.3. RT-PCR was performed after 48 h of transfection. The relative mRNA expression of the Kv3.3 was normalized to the GAPDH gene and expressed as a fold change relative to the Mock control group. (D) Benzidine staining demonstrated greater hemoglobin formation in siRNA-Kv3.3-transfected cells (right) compared to control siRNA-transfected cells (left) during hemin-induced K562 cell erythroid differentiation (magnification ×40). Staining was performed after 24 h of transfection and 24 h of differentiation. (E) The amounts of hemoglobin content were increased by siRNA-Kv3.3 transfection compared to control. The hemoglobin content was increased by about 50% by siRNA-Kv3.3 transfection. (F) The knockdown of Kv3.3 using siRNA-Kv3.3 increased the expression level of Kv2.1, but it did not have any effect on the expression levels of Kv3.4 and Kv9.3. The relative mRNA expressions of the Kv channels were normalized to the GAPDH gene and expressed as a fold change relative to the Mock control group. (G) siRNA-Kv3.3 transfection without hemin did not induce K562 erythroid differentiation. Experiments were performed in triplicate, and data are expressed as mean ± standard error. *$p<0.05$ compared with control value.

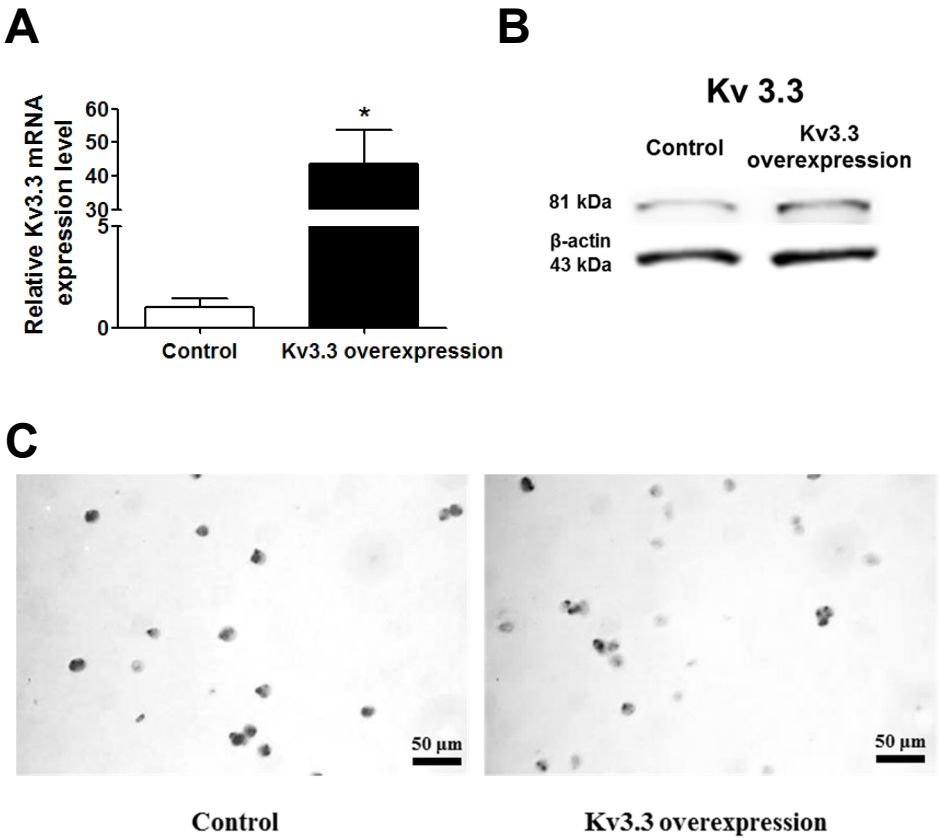
A
B
Relative Kv3.3 mRNA expression level
60
50
40
30
5
0
*
Control
Kv3.3 overexpression
Kv 3.3
Control
Kv3.3 overexpression
81 kDa
β-actin
43 kDa
C
50 μm
50 μm
Control
Kv3.3 overexpression
D
Hb (ng) / Protein (μg)
140
105
70
35
0
Control
Kv3.3 overexpression

Figure 4. Overexpression of Kv3.3 did not have a clear effect on hemin-induced erythroid differentiation (A),(B) mRNA and protein expression levels of Kv3.3 were increased in the K562 overexpressed cell line compared to the normal K562 cell line. The relative mRNA expression of the Kv3.3 was normalized to the GAPDH gene and expressed as a fold change relative to the Mock control group. (C) The degree of hemin-induced erythroid differentiation was measured using benzidine staining in Kv3.3-overexpressed K562 cells or normal K562 cells. There was no significant difference between the two, however. (D) Hemoglobin quantification demonstrated that overexpressed Kv3.3 did not have any effect on hemin-induced K562 erythroid differentiation.

Signaling mechanisms involved in the regulation of K562 erythroid differentiation by siRNA-Kv3.3 transfection

Signal cascades involving in K562 erythroid differentiation have been well established (Huang et al., 2004; Sangerman et al., 2006; Akel et al., 2007; Di Pietro et al., 2007). p38, ERK1/2, CREB, and c-fos were examined during hemin-induced K562 erythroid differentiation in siRNA-Kv3.3-transfected K562 cells. As shown in Figure 5, the levels of phosphorylated forms of p38 and CREB and the levels of c-fos were reduced significantly by transfection with siRNA-Kv3.3 compared to the controls. Although the protein expression levels of the activated (phosphorylated) forms of p38 and CREB were reduced, the total amounts of p38 and total CREB were not significantly reduced. The protein expression levels of total and phosphorylated ERK1/2 (Figure 5) and the phosphorylated form of ERK2 (p-42 MAPK) also decreased; however, the difference was not statistically significant. Phosphorylated ERK1 (p-44 MAPK) was not detected in K562 cells. These changes indicated that decreased Kv3.3 expression in K562 cells increased hemin-induced K562 cell differentiation through the reduced activation of p38, p-CREB, and c-fos.

Kv channels are not involved in the early stage of hemin-induced K562 erythroid differentiation

The mRNA expression levels of Kv2.1, Kv3.3, Kv3.4, and Kv9.3 were measured at the presented time points (10 min, 30 min, and 1 h) after inducing

differentiation, and the expression levels of Kv channels including Kv3.3 were not changed in the early stage of hemin-induced K562 erythroid differentiation (Figure 6A). The protein expression level of Kv3.3 was also not changed after 10 min and 30 min of the erythroid differentiation (Figure 6B). Kv3.3 knockdown using siRNA-Kv3.3 was also performed during the early stage of hemin-induced K562 erythroid differentiation, and the transfection had no effect on the signaling mechanisms, such as p38 and ERK, which are known to be involved in the early stage of erythroid differentiation (Figure 7).

Kv3.3 knockdown using siRNA-Kv3.3 increased cell adhesion in K562 cells

The K562 cells transfected with siRNA-Kv3.3 showed interesting morphological changes. Even though K562 cells are suspension and sphenoid cells, the adhesion of a few K562 cells to the bottom of the 6 well plates was observed when the cells were incubated with hemin for one or two days. The adherent cells had spindle-like shapes and more adherent cells were detected when the cells were transfected by siRNA-Kv3.3 compared to the control cells (Figure 8A). Real time RT-PCR data demonstrated that the mRNA expression

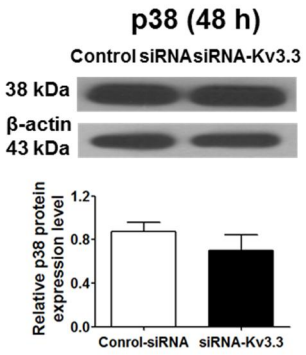
p38 (48 h)
Control siRNA siRNA-Kv3.3
38 kDa
β-actin
43 kDa
Relative p38 protein expression level
1.2
0.8
0.4
0.0
Conrol-siRNA
siRNA-Kv3.3

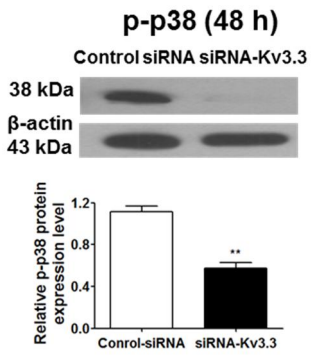
p-p38 (48 h)
Control siRNA siRNA-Kv3.3
38 kDa
β-actin
43 kDa
Relative p-p38 protein expression level
1.2
0.8
0.4
0.0
**
Conrol-siRNA
siRNA-Kv3.3

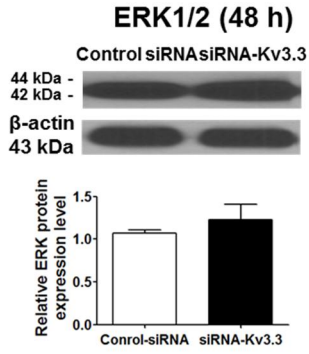
ERK1/2 (48 h)
Control siRNA siRNA-Kv3.3
44 kDa -
42 kDa -
β-actin
43 kDa
Relative ERK protein expression level
1.5
1.0
0.5
0.0
Conrol-siRNA
siRNA-Kv3.3

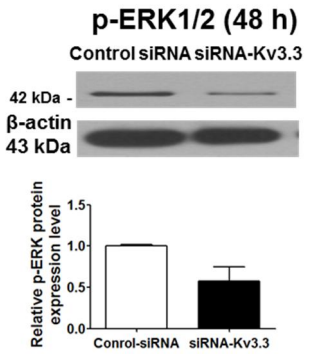
p-ERK1/2 (48 h)
Control siRNA siRNA-Kv3.3
42 kDa -
β-actin
43 kDa
Relative p-ERK protein expression level
1.5
1.0
0.5
0.0
Conrol-siRNA
siRNA-Kv3.3

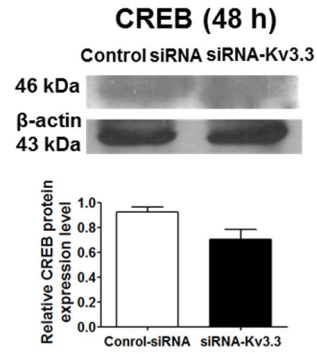
CREB (48 h)
Control siRNA siRNA-Kv3.3
46 kDa
β-actin
43 kDa
Relative CREB protein expression level
1.0
0.8
0.6
0.4
0.2
0.0
Conrol-siRNA
siRNA-Kv3.3

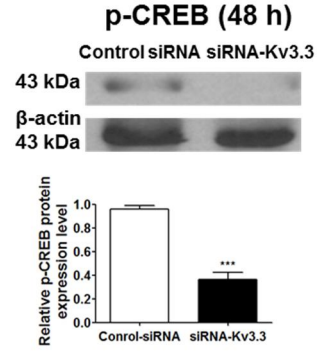
p-CREB (48 h)
Control siRNA siRNA-Kv3.3
43 kDa
β-actin
43 kDa
Relative p-CREB protein expression level
1.0
0.8
0.6
0.4
0.2
0.0
***
Conrol-siRNA
siRNA-Kv3.3

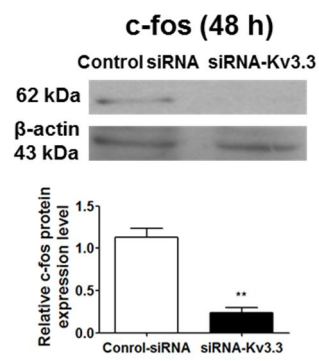
c-fos (48 h)
Control siRNA siRNA-Kv3.3
62 kDa
β-actin
43 kDa
Relative c-fos protein expression level
1.5
1.0
0.5
0.0
**
Conrol-siRNA
siRNA-Kv3.3

Figure 5. Signaling mechanisms of K562 erythroid differentiation regulation by siRNA- Kv3.3 transfection The expressions of p38, ERK1/2, CREB, and c-fos during cell differentiation changed with siRNA-Kv3.3 transfection. The levels of the phosphorylated, activated forms of p38 and CREB were lower in siRNA-Kv3.3 transfected cells than in control cells. The levels of c-fos during cell differentiation were also reduced after siRNA- Kv3.3 transfection. The levels of phosphorylated ERK2 (p-42 MAPK) also seemed lower; however, the differences were not statistically significant. Phosphorylated ERK1 (p-44 MAPK) was not detected. No changes were noted for the total p38, total ERK1/2, and total CREB. The graphs show the quantitative analysis of each protein. Western blot assay was performed when transfected cells were differentiated for 48 h with hemin; each assay was performed in triplicate, and data are expressed as mean ± standard error. **$p<0.01$ compared with control value. The relative protein expressions of the signal molecules were expressed as a fold change relative to the control group.

A

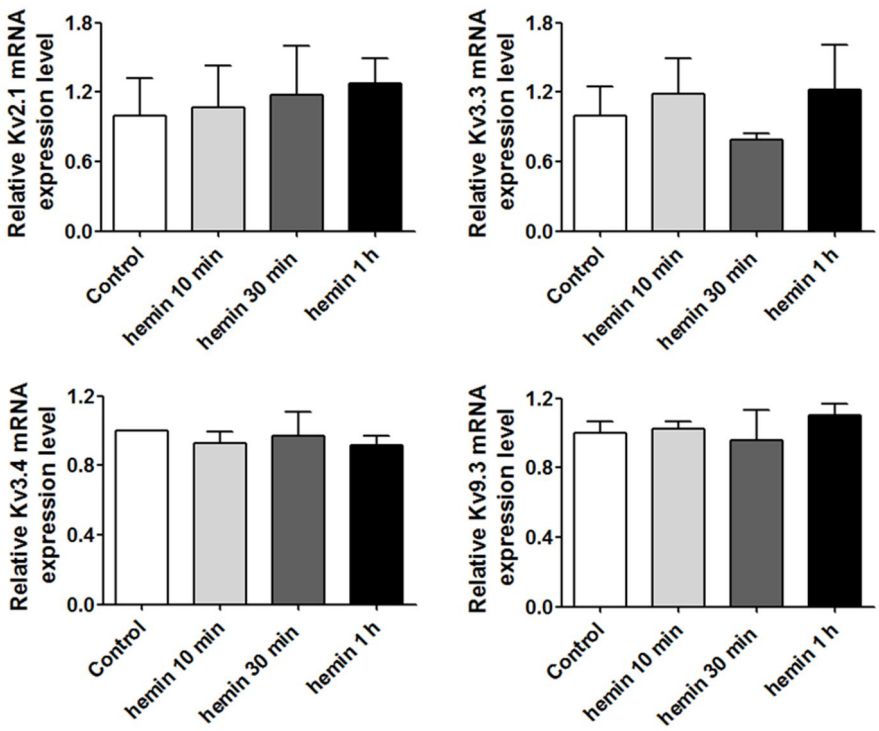
Relative Kv2.1 mRNA expression level
1.8
1.2
0.6
0.0
Control
hemin 10 min
hemin 30 min
hemin 1 h
Relative Kv3.3 mRNA expression level
1.8
1.2
0.6
0.0
Control
hemin 10 min
hemin 30 min
hemin 1 h
Relative Kv3.4 mRNA expression level
1.2
0.8
0.4
0.0
Control
hemin 10 min
hemin 30 min
hemin 1 h
Relative Kv9.3 mRNA expression level
1.2
0.8
0.4
0.0
Control
hemin 10 min
hemin 30 min
hemin 1 h

B

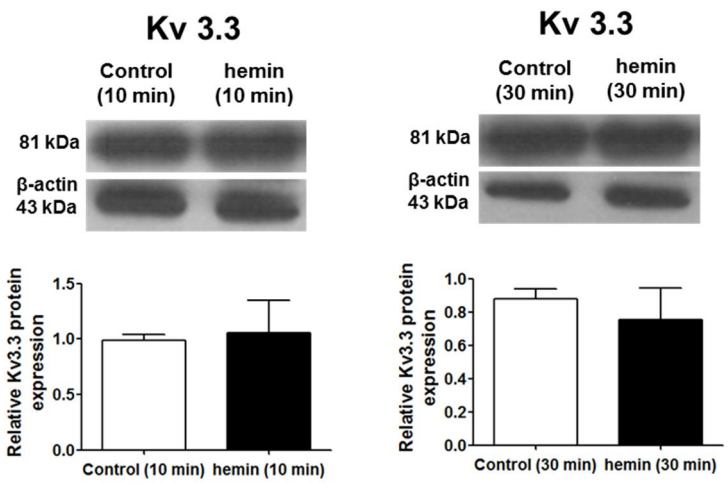
Kv 3.3
Control (10 min)
hemin (10 min)
81 kDa
β-actin 43 kDa
Relative Kv3.3 protein expression
1.5
1.0
0.5
0.0
Control (10 min)
hemin (10 min)
Kv 3.3
Control (30 min)
hemin (30 min)
81 kDa
β-actin 43 kDa
Relative Kv3.3 protein expression
1.0
0.8
0.6
0.4
0.2
0.0
Control (30 min)
hemin (30 min)

Figure 6. The relationship between Kv3.3 and the early stage of K562 erythroid differentiation (A) The mRNA expression levels of the Kv channels, including Kv2.1, Kv3.3, Kv3.4, and Kv9.3, did not correlate with the hemin-induced K562 erythroid differentiation at the indicated time points (10 min, 30 min, and 1 h). (B) The protein expression level of Kv3.3 was estimated after inducing 10 min and 30 min of erythroid differentiation, and there was no change compared to the control cells. The relative mRNA expressions of the Kv channels were normalized to the GAPDH gene and expressed as a fold change relative to the Mock control group.

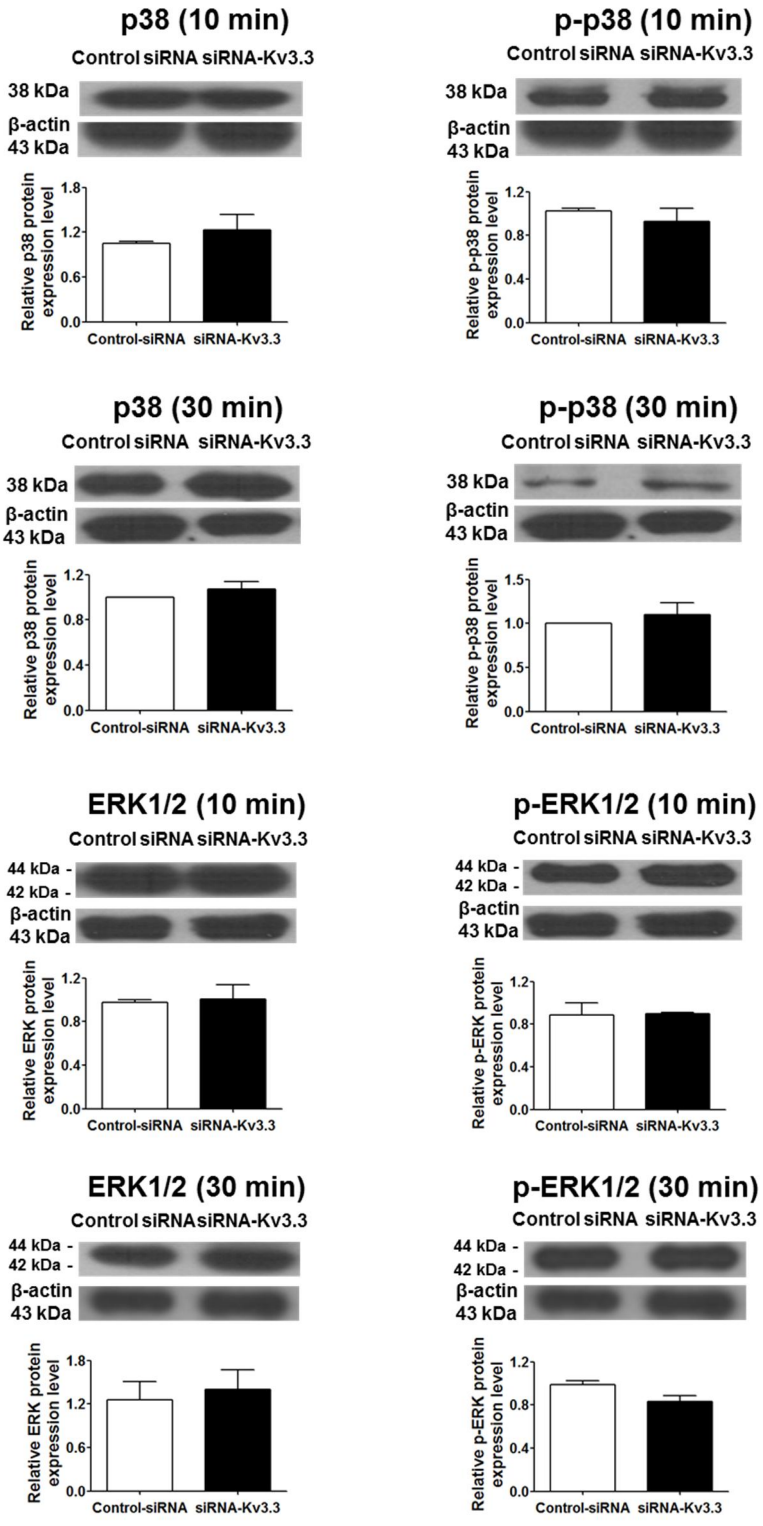
p38 (10 min)
Control siRNA siRNA-Kv3.3
38 kDa
β-actin
43 kDa
Relative p38 protein expression level
1.8
1.2
0.6
0.0
Control-siRNA siRNA-Kv3.3
p-p38 (10 min)
Control siRNA siRNA-Kv3.3
38 kDa
β-actin
43 kDa
Relative p-p38 protein expression level
1.2
0.8
0.4
0.0
Control-siRNA siRNA-Kv3.3
p38 (30 min)
Control siRNA siRNA-Kv3.3
38 kDa
β-actin
43 kDa
Relative p38 protein expression level
1.2
0.8
0.4
0.0
Control-siRNA siRNA-Kv3.3
p-p38 (30 min)
Control siRNA siRNA-Kv3.3
38 kDa
β-actin
43 kDa
Relative p-p38 protein expression level
1.5
1.0
0.5
0.0
Control-siRNA siRNA-Kv3.3
ERK1/2 (10 min)
Control siRNA siRNA-Kv3.3
44 kDa -
42 kDa -
β-actin
43 kDa
Relative ERK protein expression level
1.2
0.8
0.4
0.0
Control-siRNA siRNA-Kv3.3
p-ERK1/2 (10 min)
Control siRNA siRNA-Kv3.3
44 kDa -
42 kDa -
β-actin
43 kDa
Relative p-ERK protein expression level
1.2
0.8
0.4
0.0
Control-siRNA siRNA-Kv3.3
ERK1/2 (30 min)
Control siRNA siRNA-Kv3.3
44 kDa -
42 kDa -
β-actin
43 kDa
Relative ERK protein expression level
1.8
1.2
0.6
0.0
Control-siRNA siRNA-Kv3.3
p-ERK1/2 (30 min)
Control siRNA siRNA-Kv3.3
44 kDa -
42 kDa -
β-actin
43 kDa
Relative p-ERK protein expression level
1.2
0.8
0.4
0.0
Control-siRNA siRNA-Kv3.3

Figure 7. In the early stage of K562 erythroid differentiation, Kv3.3 knockdown using siRNA-Kv3.3 did not have any effect on the expression levels of signaling molecules involved in K562 erythroid differentiation The protein expression levels of p38 and ERK were measured after 24 h of siRNA-Kv3.3 transfection and 10 min or 30 min of erythroid differentiation. During the early stage of erythroid differentiation, down-regulated Kv3.3 had no effect on the protein levels of p38 and ERK.

levels for integrins β3 (Figure 8B left) and β1 (Figure 8B right), which are well-known adhesion molecules, were not statistically changed by siRNA-Kv3.3 transfection.

Next, the K562 cells were incubated in fibronectin-coated plates to enhance cell adhesion because fibronectin binds to integrins (Pankov and Yamada, 2002). After 24 h of transfection, the K562 cells were cultured with hemin in fibronectin-coated well for 48 h (Figure 8C). As shown in Figure 8D, when siRNA-Kv3.3 was transfected, many more cells adhered to the bottom of the plates compared to the controls (Figure 8D). In addition, the mRNA expression level of integrin β3 significantly increased in siRNA-Kv3.3-transfected cells (Figure 8E left), whereas integrin β1 showed no difference (Figure 8E right). On the other hand, when the cells were cultured in fibronectin-coated plates with hemin, erythroid differentiation was not enhanced by siRNA– Kv3.3 transfection. Benzidine staining and hemoglobin quantification indicated no significant differences between control and siRNA-transfected cells (Figure 8F). These results suggest that the erythroid differentiation effect induced by reduced Kv3.3 expression in K562 cells was transformed into a cell adhesion-enhancing effect when K562 cells were provided with fibronectin.

Signaling mechanisms involved in the regulation of K562 differentiation by the siRNA-Kv3.3 transfection of cells cultured in fibronectin plates

Cultures in fibronectin-coated wells eliminated the Kv3.3-mediated erythroid differentiation-inducing effect. Therefore, the signaling mechanisms in the presence and absence of fibronectin were compared with each other. As demonstrated in Figure 9, none of the total and activated forms of ERK1/2, p38, and CREB showed any differences in the control and siRNA-transfected cells. These results are consistent with the lack of erythroid differentiation in siRNA-Kv3.3 cells cultured in fibronectin-coated wells.

A

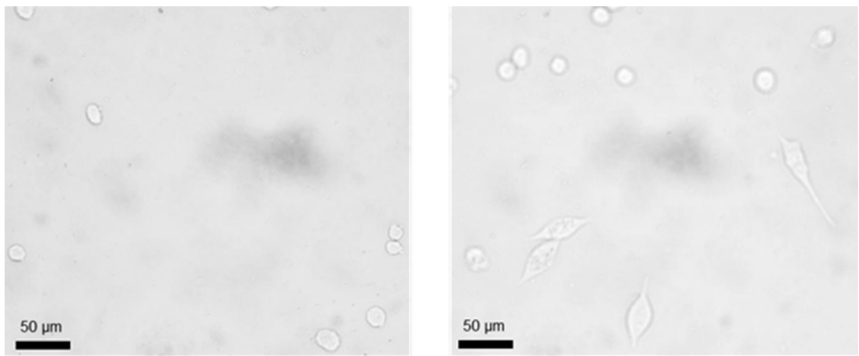
50 μm
50 μm
Control siRNA
siRNA-Kv3.3

B

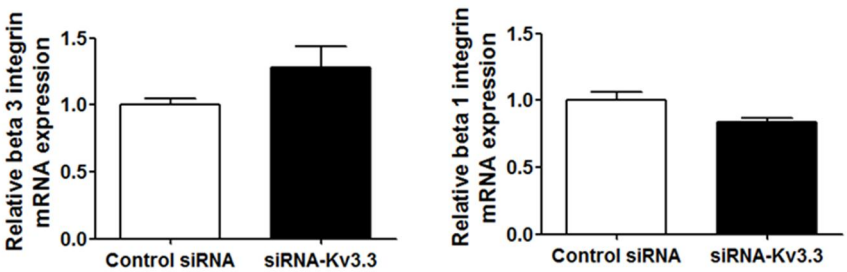
Relative beta 3 integrin mRNA expression
1.5
1.0
0.5
0.0
Control siRNA
siRNA-Kv3.3
Relative beta 1 integrin mRNA expression
1.5
1.0
0.5
0.0
Control siRNA
siRNA-Kv3.3

C

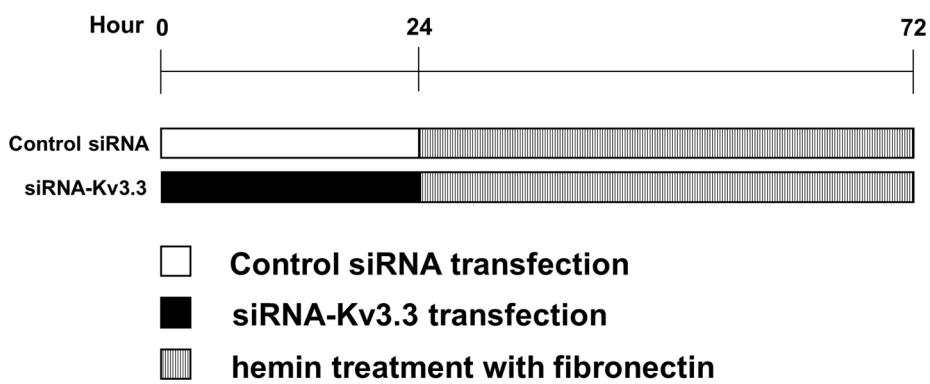
Hour
0
24
72
Control siRNA
siRNA-Kv3.3
Control siRNA transfection
siRNA-Kv3.3 transfection
hemin treatment with fibronectin

D

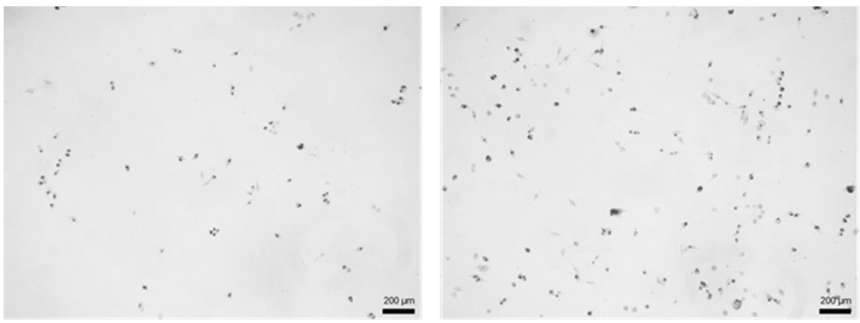

Control siRNA siRNA-Kv3.3

E

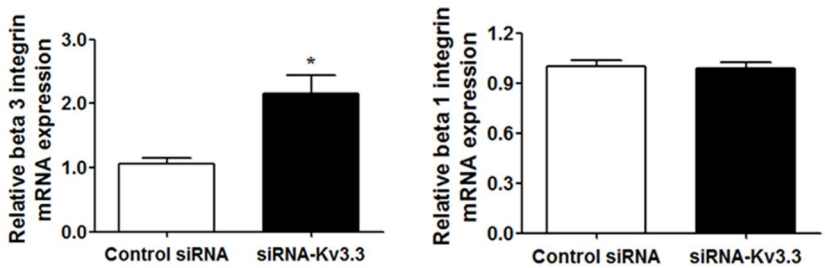

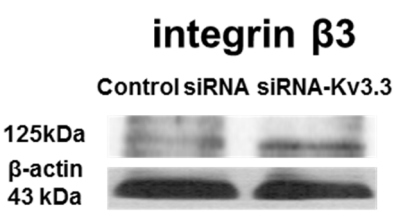

F

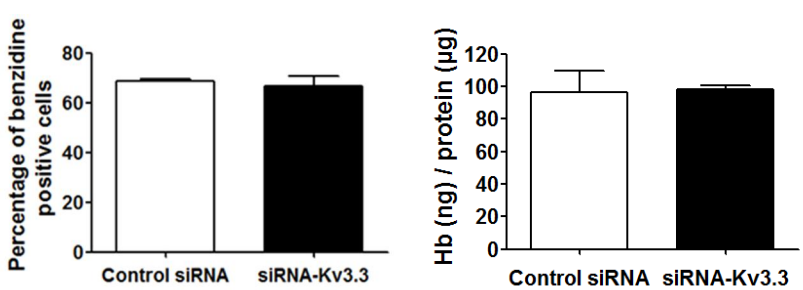

Figure 8. Effects of siRNA-Kv3.3 transfection on cell adhesion (A) Attached K562 cells were detected in siRNA-Kv3.3-transfected cell cultures (right), whereas fewer attached cells were found in control cultures (left) (magnification ×200). (B) The mRNA expression levels of integrin β3 (left) and integrin β1 (right) during hemin-induced K562 cell erythroid differentiation by transfection of siRNA-Kv3.3. (C) The protocol for control siRNA and siRNA-Kv3.3 transfection and hemin treatment with fibronectin. After 24 h of transfection, the K562 cells were cultured with hemin in fibronectin-coated wells for 48 h. (D) Culturing the cells in fibronectin-coated wells (10 μg/ml) significantly improved cell adhesion during the hemin-induced erythroid differentiation of siRNA-Kv3.3-transfected cells (magnification ×40). (E) Cells cultured in fibronectin-coated wells showed amplified effects of decreased Kv3.3 on integrin β3 levels. The mRNA and protein expression levels of integrin β3 in siRNA-Kv3.3-transfected cells increased much more during hemin-induced K562 cell erythroid differentiation than in the control group (*$p<0.05$). On the other hand, no differences were noted in integrin β1 expression between the control and siRNA-Kv3.3 transfected-cells when the cells were cultured in fibronectin-coated wells. (F) Benzidine staining (left) and hemoglobin quantification (right) indicated that increased erythroid differentiation by siRNA-Kv3.3 was not detected when the cells were cultured in fibronectin-coated wells. The relative mRNA expressions of the inegrins were normalized to the GAPDH gene and expressed as a fold change relative to the control siRNA group.

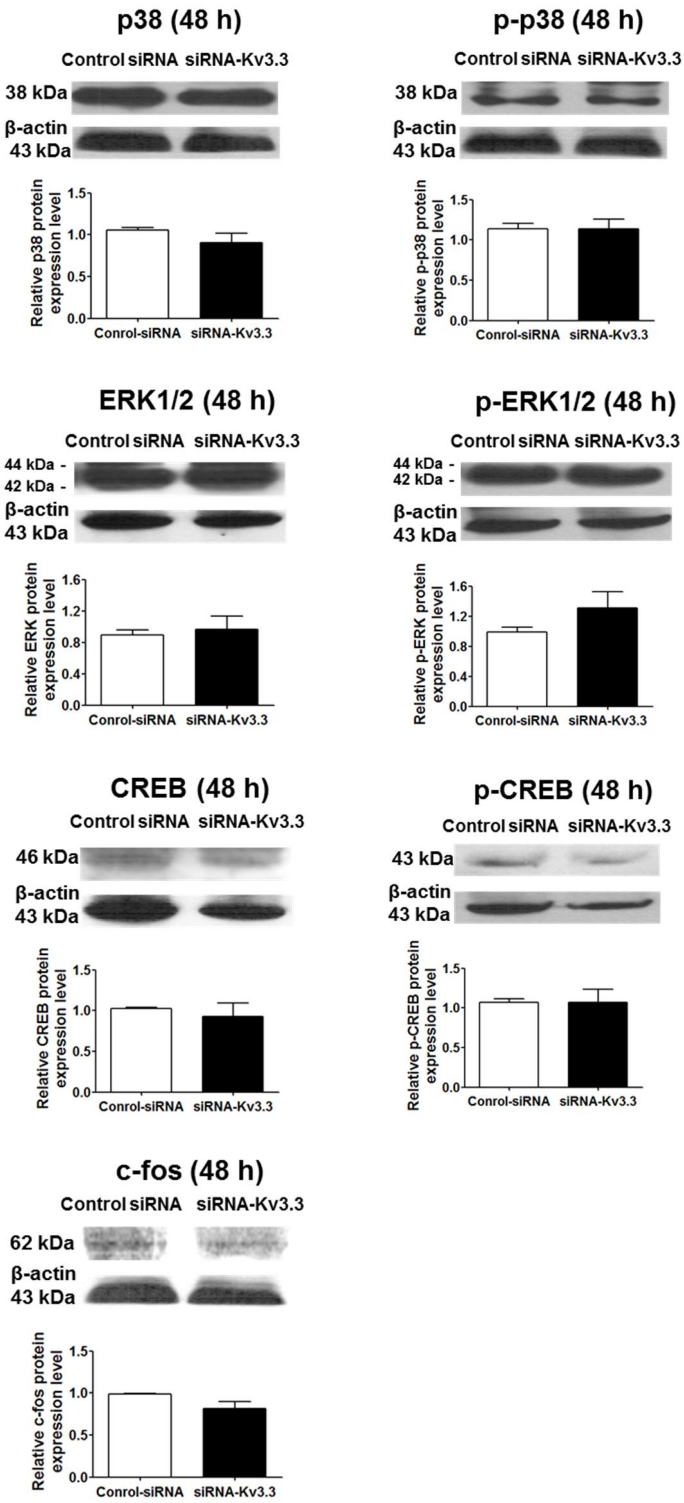
p38 (48 h)
Control siRNA siRNA-Kv3.3
38 kDa
β-actin
43 kDa
Relative p38 protein expression level
1.5
1.0
0.5
0.0
Conrol-siRNA siRNA-Kv3.3
p-p38 (48 h)
Control siRNA siRNA-Kv3.3
38 kDa
β-actin
43 kDa
Relative p-p38 protein expression level
1.5
1.0
0.5
0.0
Conrol-siRNA siRNA-Kv3.3
ERK1/2 (48 h)
Control siRNA siRNA-Kv3.3
44 kDa -
42 kDa -
β-actin
43 kDa
Relative ERK protein expression level
1.6
1.2
0.8
0.4
0.0
Conrol-siRNA siRNA-Kv3.3
p-ERK1/2 (48 h)
Control siRNA siRNA-Kv3.3
44 kDa -
42 kDa -
β-actin
43 kDa
Relative p-ERK protein expression level
1.6
1.2
0.8
0.4
0.0
Conrol-siRNA siRNA-Kv3.3
CREB (48 h)
Control siRNA siRNA-Kv3.3
46 kDa
β-actin
43 kDa
Relative CREB protein expression level
1.5
1.0
0.5
0.0
Conrol-siRNA siRNA-Kv3.3
p-CREB (48 h)
Control siRNA siRNA-Kv3.3
43 kDa
β-actin
43 kDa
Relative p-CREB protein expression level
1.5
1.0
0.5
0.0
Conrol-siRNA siRNA-Kv3.3
c-fos (48 h)
Control siRNA siRNA-Kv3.3
62 kDa
β-actin
43 kDa
Relative c-fos protein expression level
1.5
1.0
0.5
0.0
Conrol-siRNA siRNA-Kv3.3

Figure 9. Signaling mechanisms of K562 differentiation regulation by siRNA-Kv3.3 transfection and cultures in fibronectin plates No changes in the expression levels of p38, ERK1/2, CREB, and c-fos were noted in response to decreased Kv3.3 levels compared to control cells during cell differentiation in fibronectin-coated wells. No differences were noted in the total amounts or amounts of phosphorylated forms of ERK1/2, p38, and CREB expression in the control and siRNA-transfected cells. No differences were observed in the c-fos levels following siRNA-Kv3.3 transfection when the cells were cultured with fibronectin. The graphs indicate the quantitative analysis of each protein. Western blot assays were performed when the transfected cells were differentiated for 48 h with hemin and fibronectin. Each assay was performed in triplicate, and data are expressed as mean ± standard error.

DISCUSSION

In the present study, first of all, Kv channel subunits exist in K562 cells and the roles of Kv channels in K562 cell differentiation were identified. RT-PCR and Western blot analyses demonstrated that Kv3.3 was highly expressed in K562 cells, and that its expression level was down-regulated during the late stage of erythroid differentiation, whereas Kv2.1 was increased and other Kv channels did not show any change. In Kv3.3-silenced cells, erythroid differentiation was significantly increased during the late stage (48 h) via p-p38, p-CREB, and c-fos, whereas in the early stage of differentiation, there was no change compared to the control cells (10 min and 30 min). Interestingly, the adhesion of K562 cells was increased in Kv3.3-silenced cells and that adhesion was enhanced in the presence of fibronectin.

Kv channels have a known involvement in a range of essential cellular functions, including cell proliferation, wound healing, apoptosis, and oxygen sensing (Wang et al., 2002; Pardo, 2004; Wang, 2004; Kunzelmann, 2005; Lang et al., 2005; O'Grady and Lee, 2005). Cell differentiation is another important fundamental event that is regarded as having a close relationship with cell proliferation (Golding et al., 1988; Langdon et al., 1988; Volpi et al., 1994). Several reports have demonstrated the relevance of qualitative and quantitative changes in Kv currents to the differentiation state of peripheral murine $CD4^+$ lymphocytes (Liu et al., 2002). More recently, Kv channels have been suggested to play roles in cell differentiation (Leung, 2012). Wild-type *Xenopus* Kv1.1

overexpression in *Xenopus* retinal ganglion cells results in morphological differentiation in the form of increased dendritic branching (Hocking et al., 2012). In particular, You et al. demonstrated that Kv2.1 and Kv3.3 may play important roles in the differentiation of human mesenchymal stem cells into adipocytes (You et al., 2013).

To date, many voltage-dependent channels have been identified in hematopoietic stem cells, and these channels function distinctly in proliferation and differentiation (Pillozzi and Becchetti, 2012). The expressions of Kv1.3 and Kv7.1 have been identified in $CD34^{+}/CD45^{+}/CD133^{high}$ cells from peripheral blood by RT-PCR. In particular, Kv11.1, which is upregulated in leukemic hematopoietic cells, appears to be involved in the physiology of leukemic and stem cells in processes such as cell adhesion and proliferation (Pillozzi and Becchetti, 2012).

The importance of p38, ERK1/2, CREB, and c-fos in regulating erythroid differentiation has been demonstrated. K562 erythroid differentiation is well known to involve p38, while ERK1/2 shows an opposite or no effect (Witt et al., 2000; Huang et al., 2004; Di Pietro et al., 2007; Liu et al., 2010), and CREB protein activation is involved in K562 erythroleukemia cell differentiation (Di Pietro et al., 2007). In the present study, the signal molecules p38, CREB, and c-fos showed a tendency to decrease during the late stage of hemin-induced erythroid differentiation due to reduced Kv3.3. The regulation of CREB by Kv3.3 was previously demonstrated. Tong et al. (2010) showed that the blocking of CREB reduced the expression of Kv3.3 and c-fos in medial nucleus of the trapezoid body neurons (Tong et al., 2010).

Compared to what is known for other Kv channels, the roles of Kv3.3 are poorly understood. Although Kv3.3 has its own fast inactivating potassium currents when it is transfected into the HEK cell or CHO cell system (Rae and Shepard, 2000; Fernandez et al., 2003), there are few reports dealing with the electrophysiological recordings on Kv3.3. Kv3.3 is a known oxygen-sensitive channel; it opens in the presence of oxygen and reversely closes in response to hypoxia (Patel and Honore, 2001). Several reports demonstrated that hypoxia reduces the production of oxygen-reactive intermediates, including H_2O_2, and Kv3.3 is one of the channels that lose its fast inactivation upon external application of H_2O_2 (Ruppersberg et al., 1991; Vega-Saenz de Miera and Rudy, 1992; Patel and Honore, 2001). The relationship between the function of potassium channels and oxidative stress has been well established (Liu and Gutterman, 2002), and Kv3.3 function can be inferred to have relevance to oxidative stress. On the other hand, differentiated K562 cells produce heme contents, resulting in the increased production of reactive oxygen species (Ryter and Tyrrell, 2000) and naturally this causes oxidative stress. Kv3.3 may be involved in protection against oxidative stress during erythroid differentiation, which may increase oxidative stress as a side effect. Therefore, decreases in Kv3.3 expression in K562 cells would induce erythroid differentiation. Furthermore, expressions of signal molecules, such as MAPK and CREB, which are involve in oxidation-sensitive mechanisms (de Nigris et al., 2003), were altered during the hemin-induced erythroid differentiation of K562 cells transfected by siRNA-Kv3.3.

According to the data of this study, it would be clear that there may be

some relationship between Kv2.1 and Kv3.3. The mRNA expression level of Kv2.1 was increased during hemin-induced K562 erythroid differentiation, whereas the mRNA expression level of Kv3.3 was decreased during the differentiation. In addition, Kv2.1 was the only Kv channel that exists in K562, which was affected by the down-regulation of Kv3.3 by using siRNA-Kv3.3; Kv2.1 was increased by the siRNA-Kv3.3. In the electrophysiological speculation, it can be explained because an oxidation affects the two Kv channels differently. Oxidation increases the potassium currents through the Kv3.3 by prohibiting fast inactivation, whereas it decreases the potassium currents through the Kv2.1 by down-regulating the open probability and giving rise to non-conducting channels (Chen et al., 2000; Kanda et al., 2011). Considering the opposite electrophysiological responses and expression level changes of the two Kv channels against the oxidation, there would be some balances between Kv2.1 and Kv3.3 to regulate oxidative stress-related cellular behavior.

In the present study, increased adhesion properties in Kv3.3-silenced K562 cells were detected and integrins were turned out to be important in the observed changes. When fibronectin, which interacts well with integrins, was used, down-regulated Kv3.3 expression during hemin-induced erythroid differentiation resulted in enhanced cell adhesion. At the same time, the hemin-induced erythroid differentiation enhancing effect of siRNA-Kv3.3 disappeared, and no differences were seen between control and siRNA-Kv3.3-transfected cells for expressions of the signal molecules. Järvinen et al (1993) demonstrated that differentiation inducers alter the integrin expression of K562 cells (Jarvinen

et al., 1993). It has been demonstrated that α5β1 is the only fibronectin receptor integrin expressed in suspension-cultured K562 cells, and differentiation inducers such as TPA (12-tetradecanoyl-13-acetyl-beta-phorbol) or hemin chloride alter the expression levels of integrin; TPA increased the β3 integrin, whereas hemin chloride did not have any effect on the β3 integrin and it only decreased the β1 integrin (Jarvinen et al., 1993). K562 cells bind to fibronectin through the α5β1 integrin receptor when added to wells coated with fibronectin (Danen et al., 1995). In Figure 8E, it demonstrated that siRNA-Kv3.3 increased β3 integrin expression when the cells were incubated in the fibronectin-coated well. From the data, it could be assumed that siRNA-Kv3.3 transfection changed the original cell property of K562. In addition, from the Figure 5 and 9 it was found that siRNA-Kv3.3 transfection affected signaling pathways were changed due to the cell culture in fibronectin coated wells. It has been suggested that the Src family of tyrosine kinases-receptor tyrosine kinases-MAPK signaling is involved in integrin signaling. Figure 9 demonstrates that the transfection of siRNA-Kv3.3 to K562 cells cultured in fibronectin-coated wells does not have any effect on the expression levels of p38 and ERK, which are MAPK families. Therefore, increased β3 integrins makes transfection of siRNA-Kv3.3 in K562 cells affect signaling pathways other than the MAPK pathway, such as Rho-GTPase, PI3K/Akt or Rac1-related pathways (Huveneers and Danen, 2009; Zeller et al., 2013; Guidetti et al., 2015).

Taken together, these data suggest that in the presence of fibronectin, the erythroid differentiation-inducing effect of a decreased Kv3.3 expression level was changed to a cell adhesion-enhancing effect; as a result, there are no

increases in hemoglobin content as a potent oxidative stress inducer. Kv3.3 appears to enhance cell differentiation, and its enhancing effect may be regulated by providing hemin or hemin with fibronectin. Moreover, Kv3.3 may also be involved in the cell adhesion process, similar to the function of hERG potassium channels (Arcangeli et al., 2004), even if the effect is in the opposite direction; the hERG potassium channels enhance cell adhesion, whereas Kv3.3 inhibits cell adhesion. Further studies are warranted to identify the particular mechanisms responsible for the different regulation of these channels.

In summary, several Kv channels in K562 cells were identified and it was found that Kv3.3 is involved in K562 cell differentiation through signal cascades such as the MAPK, CREB, and c-fos signaling pathways. Kv3.3 is also involved in cell adhesion properties through the regulation of integrin β3. These results imply that Kv channels, at least Kv3.3, function in cell differentiation processes. Therefore, further knowledge of the relationship between Kv channels and cell differentiation mechanisms would open a new paradigm for understanding the regulation of cell differentiation processes.

CHAPTER II

Kv3.4 is modulated by HIF-1α to protect SH-SY5Y cells against oxidative stress-induced neural cell death

(Data in this chapter have been published in

Song et al., Sci Rep, 2017, 7(1):2075)

ABSTRACT

The Kv3.4 channel is characterized by fast inactivation and sensitivity to oxidation. However, the physiological role of Kv3.4 as an oxidation-sensitive channel has yet to be investigated. Here, this study demonstrates that Kv3.4 plays a pivotal role in oxidative stress-related neural cell damage as an oxidation-sensitive channel and that HIF-1α down-regulates Kv3.4 function, providing neuroprotection. MPP^+ and $CoCl_2$ are ROS-generating reagents that induce oxidative stress. However, only $CoCl_2$ decreases the expression and function of Kv3.4. HIF-1α, which accumulates in response to $CoCl_2$ treatment, is a key factor in Kv3.4 regulation. In particular, mitochondrial Kv3.4 was more sensitive to $CoCl_2$. Blocking Kv3.4 function using BDS-II, a Kv3.4-specific inhibitor, protected SH-SY5Y cells against MPP^+-induced neural cell death. Kv3.4 inhibition blocked MPP^+-induced cytochrome c release from the mitochondrial intermembrane space to the cytosol and mitochondrial membrane potential depolarization, which are characteristic features of apoptosis. These results highlight Kv3.4 as a possible new therapeutic paradigm for oxidative stress-related diseases, including Parkinson's disease.

INTRODUCTION

Kv channels are transmembrane channels that are specific to potassium and sensitive to voltage changes in numerous cells. In neuronal cells, Kv currents play important roles in regulating numerous neurophysiological functions, including resting membrane potential, spontaneous firing rate, and apoptosis, because Kv currents are key regulators of neuronal membrane excitability (Pongs, 1999; Pal et al., 2003; Norris et al., 2010). Shaw-related subfamily (Kv3.1–Kv3.4) Kv channels display rapid activation and deactivation kinetics, as well as relatively large conductance (Pacheco Otalora et al., 2011). Among the Kv3 subfamily, Kv3.3 and Kv3.4 are oxygen-sensitive channels, which are also known as oxidation-sensitive channels. Both channels are characterized by fast voltage-dependent inactivation; the cytoplasmic N-terminus has a positively charged ball that provokes the fast closing of the channel by occluding the pore once it is opened (Patel and Honore, 2001). Oxidation of a cysteine residue in the amino terminus of the channels interrupts their fast inactivation by forming a disulfide bond and consequently increasing current amplitude; Kv3.3 and Kv3.4 lose their fast inactivation upon the external application of H_2O_2 (Ruppersberg et al., 1991; Patel and Honore, 2001). In the rabbit carotid body, Kv3.4 participates in the chronic hypoxia sensitization of carotid body chemoreceptor cells as an oxygen-sensitive channel; Kv3.4 expression is down-regulated and Kv3.4 current is diminished under hypoxic conditions (Kaab et al., 2005).

The SH-SY5Y cell line is a thrice cloned subline of SK-N-SH cells, which were established from a neuroblastoma patient (Biedler et al., 1973). The SH-SY5Y cell line has recently been widely used as an *in vitro* Parkinson's disease model because SH-SY5Y cells express dopamine transporter, a dopaminergic neuron-specific protein within the central nervous system. 1-Methyl-4-phenylpyridinium ion (MPP^+), which is metabolized from 1-methyl-4-phenyl-1,2,3,6-tetrahydropyridine (MPTP) by monoamine oxidase-B, is a neurotoxin that selectively destroys certain dopaminergic neurons in the substantia nigra by interfering with oxidative phosphorylation in mitochondria, thereby depleting ATP and inducing cell death (Langston et al., 1984; Xie et al., 2010). MPP^+ requires dopamine transporters for neuronal uptake; therefore, SH-SY5Y cells have been widely utilized as a good model for studying MPP^+-induced neurotoxicity and the pathogenesis of MPP^+-induced Parkinson's symptoms (Xie et al., 2010). MPP^+ is an oxidative stress inducer, and studies suggest that oxidative stress generated by Parkinson's symptom-inducing reagents such as MPP^+ and rotenone contribute to their toxicity in SH-SY5Y cells; oxidative stress and free radical generation may play pivotal roles in neurodegeneration (Uttara et al., 2009). $CoCl_2$ is another often-used oxidative stress inducer in SH-SY5Y cells. However, unlike MPP^+ or rotenone, cobalt stimulates ROS generation through a non-enzymatic, non-mitochondrial mechanism and $CoCl_2$ treatment induces hypoxia-inducible factor 1α (HIF-1α) accumulation (Chandel et al., 2000). Because HIF-1α accumulates during $CoCl_2$ treatment, $CoCl_2$ is used as a hypoxia-mimetic agent to investigate the function of HIF-1α.

Kv3.4 is well documented as a potential therapeutic target for Alzheimer's disease. Kv3.4 is overexpressed in both the early and advanced stages of this neurodegenerative disease, and the up-regulation of Kv3.4 leads to altered electrical and synaptic activity that may underlie the neurodegeneration observed in Alzheimer's disease (Angulo et al., 2004). Kv3.4 and its accessory protein MinK-Related Peptide 2 (MIRP2) are involved in neuronal cell death induced by neurotoxic amyloid β-peptide, which is generated from amyloid precursor protein and whose amyloid fibrillar form is the primary component of amyloid plaques found in the brains of Alzheimer's disease patients (Pannaccione et al., 2007). The oxidation-sensitive channel Kv3.4 likely plays a pivotal role in neuronal cell death induced by oxidative stress because oxidative stress is generated from amyloid β-peptide-associated ROS. Furthermore, oxidative stress is one of the general premonitory symptoms of neurodegenerative diseases (Varadarajan et al., 2000).

Taken together, oxidative stress is one of the key factors in neurodegenerative diseases such as Alzheimer's and Parkinson's disease, and Kv3.4 may be involved in oxidative stress-related abnormal neural cell death as an oxidation-sensitive channel.

MATERIALS AND METHODS

Cell culture

SH-SY5Y cells were cultured in a minimum essential media (MEM) (Welgene, Daegu, Korea) containing $NaHCO_3$ supplemented with 10% fetal bovine serum (FBS) and 1% antibiotic-antimycotic solution (Sigma, St, Louis, MO) at 37% incubation with 5% CO_2. When the cells grew sufficiently in a T75 flask (SPL Life Sciences, Gyeonggi-do, Korea), they were subcultured in 6-well plates or 100 mm culture dishes (SPL).

Reverse transcription-polymerase chain reaction (RT-PCR)

Hybrid-R™ (GeneAll, Seoul, Korea) was used to isolate the total RNA according to the manufacturer's instructions. The cDNA was synthesized using 1 ug of isolated RNA with random hexamers and M-MLV (Promega, Madison, WI). The PCR reaction was performed with 2 ul of cDNA, 1× GoTaq® green master mix (Promega), and specific target primers in the following reaction conditions: initial denaturation at 94°C for 5 min, 35 cycles of cycling process (94°C for 40 s, the each of annealing temperatures (Kv3.3: 60°C, Kv3.4: 65°C)

for 40 s, 72°C for 1 min, and an extension at 72°C for 1 min), and a final extension at 72°C for 7 min. The PCR products were loaded on 1.6% agarose gel for electrophoresis and analyzed with an ABI Prism 3730 XL DNA Analyzer (Applied Biosystems, Foster City, CA) to confirm the channel mRNA expression in the SH-SY5Y cells.

Western blot assay

SH-SY5Y cells were lysed using a radioimmunoprecipitation assay (RIPA) buffer (Sigma), and the total protein concentration was measured with a Bicinchoninic acid (BCA) protein assay kit (Pierce, Rockford, IL). The quantified protein was loaded on a 10% Sodium Dodecyl Sulfate Polyacrylamide Gel Electrophoresis (SDS-PAGE) and then transferred to nitrocellulose membranes (Whatman, Maidstone, Kent). Blocking was performed using 1X TBS-Tween 20 containing 5% nonfat milk (Difco, Franklin Lakes, NJ), and protein-transferred membranes were then probed overnight with target protein antibodies such as HIF-1α, Kv3.3, Kv3.4 (Abcam, Cambridge, MA), β-actin, COX-4, cytochrome c, or NDFIP1 (Santa Cruz Biotechnology, Finnell St., Dallas, TX). Membranes that were probed by primary antibodies were incubated with horseradish peroxidase–conjugated goat, anti-rabbit or

anti-mouse secondary antibody (GenDEPOT, Barker, TX) for 1 hour and visualized using a WesternBright™ Quantum™ (Advansta, Menlo Park, CA).

Real-time RT-PCR

Real-time RT PCR was performed using an Applied Biosystems StepOnePlus™ Real-Time PCR System (Applied Biosystems, Foster City, CA). Each of the primer efficiencies of the specific target primer was tested using a Glyceraldehyde 3-phosphate dehydrogenase (GAPDH) (a house keeping gene) primer as a reference. The standard curve for the efficiency test was obtained from 2- or 10-fold diluted cDNAs. The real-time RT-PCR reaction was performed with 2 μl of cDNA, 1 x SYBR Green Master Mix (Applied Biosystems, Foster City, CA), and 0.2 μM forward and reverse primers (Kv3.3 forward: 5'-CCTTCCTGACCTACGTGGAG-3', reverse: 5'- CGAGATAGAA GGGCAGGATG-3', Kv3.4 forward: 5'-AATATCCCAGGGTGGTGACA-3', reverse: 5'-GGTCTTCAAAGCTCCAGTGC-3') using the following reaction condition: initial step 95°C 30 s, then 40 cycles of cycling processes (95°C for 5 s, and 60°C for 45 s. The single product synthesized by the paired primers was analyzed with the use of a dissociation curve.

Patch clamp recordings

The prepared SH-SY5Y cells for patch clamp recordings were incubated for 24 hours in 12-well plates containing 12 mm coverslips (SPL) with 2 ml of MEM medium to allow the cells to attach to the coverslips. The cell-attached coverslips were transferred to the chamber and were visualized through differential interference contrast video microscopy (Olympus, Tokyo, Japan). Patch pipettes were pulled from the borosilicate glass capillaries (1.7 mm diameter; 0.5 mm wall thickness) (World Precision Instruments, Sarasota, FL), resulting in a seal resistance ranging from 5 to 7 MΩ. The internal pipette solution (in mM concentration) consisted of 150 KCl, 1 $MgCl_2$, 10 HEPES, 5 EGTA, and 2 Mg-ATP (pH 7.2 adjustment with KOH) and the bath solution (in mM concentration) containing 143 NaCl, 5.4 KCl, 0.5 $MgCl_2$, 1.8 $CaCl_2$, 0.5 NaH_2PO_4, 10 glucose, and 5 HEPES (pH 7.4 adjustment with NaOH) were used for recordings. The Kv channel currents were recorded in the whole cell configuration using an Axoclamp 2B amplifier (Axon Instruments, Foster City, CA). Electric signal filtering was performed at 1 kHz and digitized at 10 kHz with an analog–digital converter (Digidata 1320A, Axon Instruments) and pClamp software (Version 9.0, Axon Instruments). The voltage-clamp mode was performed in the following protocol: cells were exposed to the

hyperpolarizing pulse of -90 mV for 320 ms, and the membrane currents were activated by depolarizing pulses of 400 ms from a holding potential of -80 mV to test potential in the range of -70 to 40 mV in 10 mV increments. Membrane potential was recorded in the current-clamp mode.

Cell viability test

Cell viability after 1 mM MPP^+ treatment was analyzed by an MTT assay (Sigma). SH-SY5Y cells seeded in a 6-well plate were washed with Dulbecco's phosphate-buffered saline (DPBS) and incubated with MTT solution for 4 hours. After the incubation, centrifuge the cells suspended in MTT solution to pellet the cells; SH-SY5Y cells are easily suspended, still alive, and, therefore, the modified manufacturer's protocol was applied for non-adherent cells. The cell pellet was dissolved with dimethyl sulfoxide (DMSO), and 100 ul of the solution was then transferred to a new 96-well plate for measuring the absorbance at 570 nm. Apart from the MTT assay, the cell viability of 6-well plate–seeded cells was visualized with Hemacolor® rapid staining (Millipore, Billerica, MA) according to the manufacturer's instructions. The cells were incubated for 30 seconds with each of the three Hemacolor® rapid staining solutions.

Mitochondria isolation

Mitochondria were isolated from the SH-SY5Y cells using a mitochondria isolation kit (Life Technologies, Van Allen Way Carlsbad, CA). The isolation was performed following the manufacturer's instructions, and a reagent-based method was used to isolate mitochondria. Cytosol and mitochondrial fractions were used for the western blot assay right after the isolation. The isolated mitochondrial fraction was confirmed with a COX-4 protein expression level as a reference.

Mitochondrial membrane potential (MMP) measurement

Membrane potentials of mitochondria were measured with a JC-1 Mitochondrial Membrane Potential Assay Kit (Abcam) according to the manufacturer's instructions. SH-SY5Y cells ($1x10^6$) were seeded in a 35 mm confocal dish (SPL) and incubated for 24 hours to allow them to attach to the bottom of the dish. After washing the cells with DPBS, the cells were incubated with JC-1 solution for 10 minutes at 37°C in the dark. The cells were washed again with DPBS and were treated with 1 mM of MPP^+ for 4 hours, and 100 nM of BDS-II was pretreated 10 minutes before the MPP^+ treatment if needed.

MMP was analyzed using a confocal microscope at 535 ± 17.5 nm excitation for aggregated JC-1 only or 475 ± 20 nm excitation for both the aggregated and monomer forms of JC-1. The emission wavelength was 590 ± 17.5 nm. FCCP (carbonyl cyanide 4-[trifluoromethoxy] phenylhydrazone) is an ionophore uncoupler of oxidative phosphorylation, and FCCP-treated cells were presented as an MMP depolarization positive control.

Transfection of siRNA

Cells were transfected with HIF-1α or NDFIP1 siRNA purchased from Santa Cruz Biotechnology and Lipofectamine™ 2000 reagent (Invitrogen, Carlsbad, CA, USA) following the manufacturer's instructions for adhesion cells. Control siRNA purchased from Santa Cruz Biotechnology was used for the control siRNA group. The SH-SY5Y cells (2×10^5) were plated in 6-well plates in MEM (Welgene, Daegu, Korea) containing 10% FBS without antibiotics 24 hours before the transfection step. Adhered cells were transfected with siRNA and transfection reagent using MEM containing little FBS and no antibiotics for 5 hours. After 5 hours of transfection, fresh MEM containing 10% FBS and 1% antibiotics were given to the cells and the cells were incubated for 2 days. If

$CoCl_2$ treatment was used to induce HIF-1α accumulation, 100 μM of $CoCl_2$ was added to the media 6 hours before the end of the transfection.

Immunocytochemistry

The mitochondria of SH-SY5Y cells were probed with a 250 nM MitoTracker® Deep Red FM (Life Technologies) during 30 minutes of incubation. After washing the cells twice with DPBS, the cells were treated with 4% paraformaldehyde for 20 minutes for fixation. The cells were washed again with DPBS and permeabilized using 0.3% Triton™ X-100 (Sigma) for 5 minutes at room temperature. DPBS-washed cells were incubated with 5% donkey serum solution (Sigma) for 60 minutes at room temperature and then incubated with anti-Kv3.4 (Abcam) at 4ºC overnight. DPBS-rinsed cells were treated with 5% donkey serum solution containing Alexa Fluor® 488 dye (Life Technologies) for 60 minutes. After washing, the cells were mounted using VECTASHIELD Antifade Mounting Medium with DAPI (Vector Laboratories, Burlingame, CA). Five different images were assessed in each group (the control and $CoCl_2$ treatment groups) to avoid cherry-picking.

ROS detection

ROS was analyzed using 2′,7′-dichlorodihydrofluorescein diacetate (2′,7′-dichlorofluorescin diacetate; H2DCFDA) (Invitrogen). SH-SY5Y cells were incubated with a medium containing 100 μM of $CoCl_2$ or 1 mM of MPP^+ until the indicated time points (0 to 6 hours). The cells were washed twice with DPBS and then incubated with 37°C DPBS containing 5 μM of H2DCFDA for 30 minutes. Finally, the cells were incubated with a fresh medium for 15 minutes for recovery. Fluorescence images were taken using an Axio Scope (Carl Zeiss, Hallbergmoos, Germany) and digitally recorded with a cooled charge-coupled device (CCD) camera named Micromax Kodak1317 (Princeton instruments, AZ, USA). The images were analyzed using Metamorph version 6.3r2 (Molecular Devices Corporation, PA, USA).

Statistical analysis

All data are shown as means ± standard error (SE). The Student's *t*-test or One-way ANOVA was used to analyze the data and Tukey's test was used as a post hoc test (GraphPad Prism version 5.0).

RESULTS

Kv3.4 mRNA and protein expression levels during $CoCl_2$ or MPP^+ treatment

RT-PCR analysis reveals that Kv3.3 and Kv3.4 are expressed in SH-SY5Y cells (Figure 10A). Kv3.3 and Kv3.4 mRNA and protein expression levels were measured at the indicated time-points during MPP^+ or $CoCl_2$ treatment. Kv3.3 and Kv3.4 mRNA expression levels were decreased after 100 μM $CoCl_2$ treatment, whereas no change was observed after 1 mM MPP^+ treatment (Figure 10B). Kv3.3 mRNA expression was decreased at 30 min, 1 h, and 24 h of $CoCl_2$ treatment, and Kv3.4 expression began to decrease after 4 h of $CoCl_2$ treatment. The changes in Kv3.3 and Kv3.4 protein expression levels mirrored the changes in mRNA expression during 100 μM $CoCl_2$ treatment, but Kv3.4 levels decreased more significantly during treatment. MPP^+ did not affect Kv3.3 and Kv3.4 protein expression levels, which is consistent with the mRNA expression data (Figure 10C).

Changes in BDS-II sensitive currents during $CoCl_2$ or MPP^+ treatment

Kv3.4-related currents were investigated in SH-SY5Y cells using patch-clamp recording. Currents sensitive to BDS-II, a Kv3.4-selective channel blocker, were reduced in cells treated with 100 μM $CoCl_2$, whereas 1 mM MPP^+ did not affect BDS-II-sensitive currents (Figure 11A). BDS-II-sensitive currents were detected when greater than a +20 mV pulse was applied to the control group, and BDS-II-sensitive currents were detected when greater than +30 mV pulse was applied to the MPP^+-treatment group (Figure 11B). However, in the $CoCl_2$ treatment group, only a small number of BDS-II-sensitive currents were detected in SH-SY5Y cells (Figure 11B). BDS-II-sensitive currents were analysed after applying a +40 mV pulse to the control group (327.62 ± 83.45 pA, n=12), $CoCl_2$ treatment group (138.89 ± 51.8 pA, (n=8), and MPP^+ treatment group (253.3 ± 47.98 pA, n=9) (Figure 11B). The resting membrane potential was depolarized by 1 mM MPP^+ treatment. However, 100 nM BDS-II treatment had no effect on the resting membrane potential (Figure 11C).

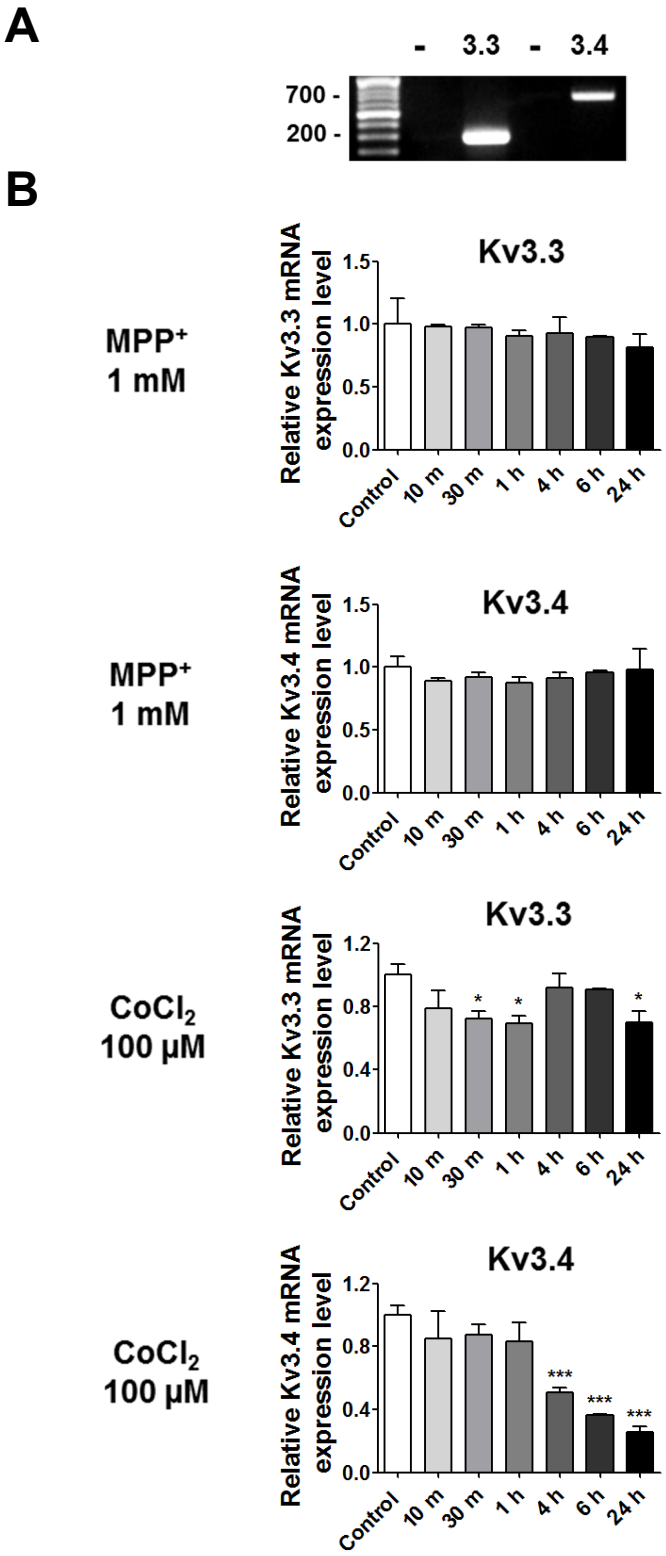
A
- 3.3 - 3.4
700 -
200 -
B
MPP+
1 mM
Kv3.3
Relative Kv3.3 mRNA expression level
1.5
1.0
0.5
0.0
Control
10 m
30 m
1 h
4 h
6 h
24 h
MPP+
1 mM
Kv3.4
Relative Kv3.4 mRNA expression level
1.5
1.0
0.5
0.0
Control
10 m
30 m
1 h
4 h
6 h
24 h
CoCl2
100 μM
Kv3.3
Relative Kv3.3 mRNA expression level
1.2
0.8
0.4
0.0
*
*
*
Control
10 m
30 m
1 h
4 h
6 h
24 h
CoCl2
100 μM
Kv3.4
Relative Kv3.4 mRNA expression level
1.2
0.8
0.4
0.0
***
***
***
Control
10 m
30 m
1 h
4 h
6 h
24 h

C

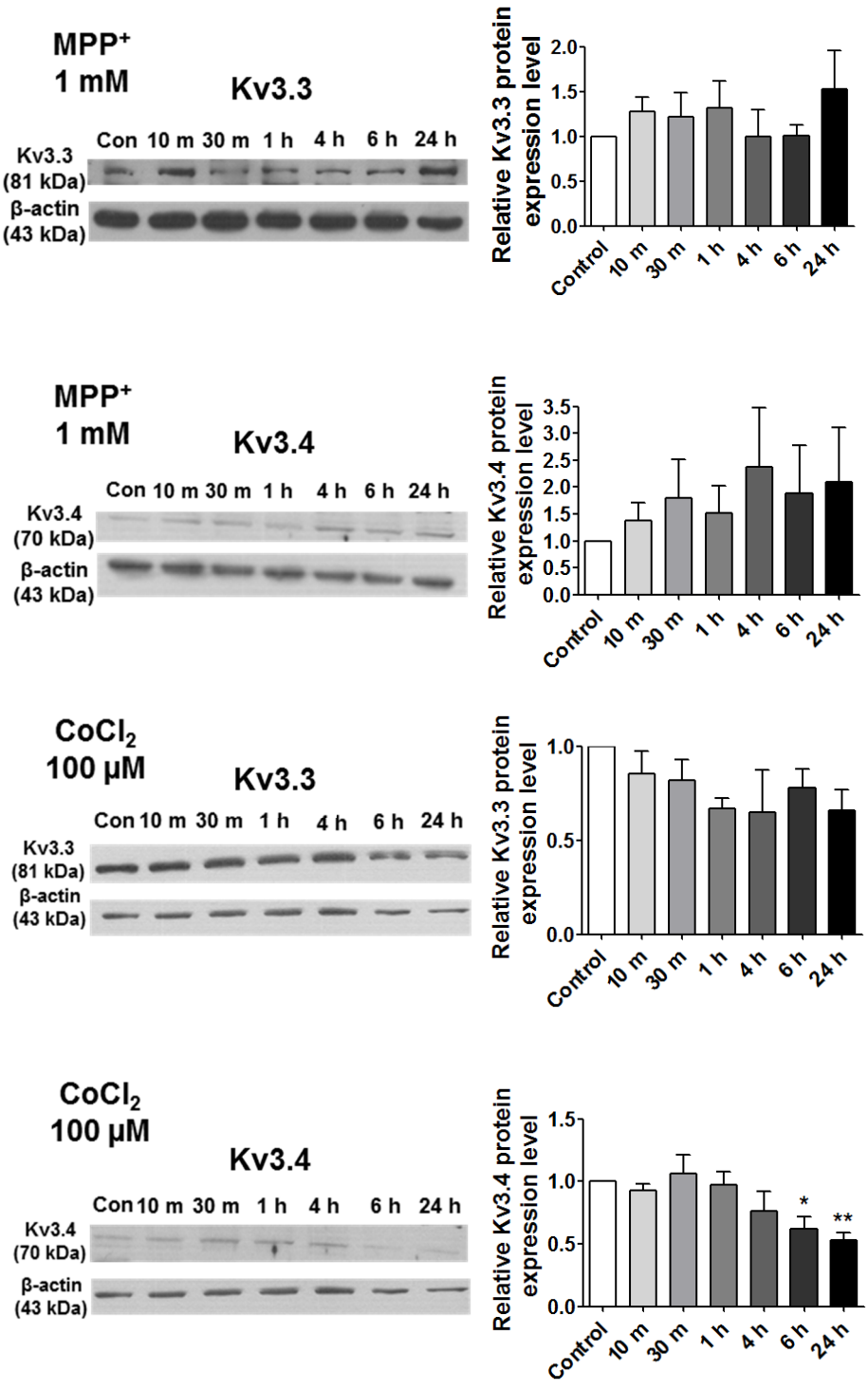
MPP+
1 mM
Kv3.3
Con 10 m 30 m 1 h 4 h 6 h 24 h
Kv3.3
(81 kDa)
β-actin
(43 kDa)
Relative Kv3.3 protein expression level
2.0
1.5
1.0
0.5
0.0
Control 10 m 30 m 1 h 4 h 6 h 24 h
MPP+
1 mM
Kv3.4
Con 10 m 30 m 1 h 4 h 6 h 24 h
Kv3.4
(70 kDa)
β-actin
(43 kDa)
Relative Kv3.4 protein expression level
3.5
3.0
2.5
2.0
1.5
1.0
0.5
0.0
Control 10 m 30 m 1 h 4 h 6 h 24 h
CoCl2
100 μM
Kv3.3
Con 10 m 30 m 1 h 4 h 6 h 24 h
Kv3.3
(81 kDa)
β-actin
(43 kDa)
Relative Kv3.3 protein expression level
1.0
0.5
0.0
Control 10 m 30 m 1 h 4 h 6 h 24 h
CoCl2
100 μM
Kv3.4
Con 10 m 30 m 1 h 4 h 6 h 24 h
Kv3.4
(70 kDa)
β-actin
(43 kDa)
Relative Kv3.4 protein expression level
1.5
1.0
0.5
0.0
*
**
Control 10 m 30 m 1 h 4 h 6 h 24 h

Figure 10. Effects of MPP^+ and $CoCl_2$ on Kv3.3 and Kv3.4 expression in SH-SY5Y cells (A) RT-PCR analysis demonstrated that Kv3.3 and Kv3.4 are expressed in SH-SY5Y cells. (B) Changes in Kv3.3 and Kv3.4 mRNA expression were measured via qPCR following treatment with 1 mM MPP^+ or 100 μM $CoCl_2$. Neither Kv3.3 nor Kv3.4 were affected by MPP^+ treatment, whereas Kv3.3 was significantly decreased after 30 min, 1 h, and 24 h of $CoCl_2$ treatment. Kv3.4 was decreased after 4, 6, and 24 h of $CoCl_2$ treatment. (C) Western blotting demonstrated that 1 mM MPP^+ did not affect Kv3.3 and Kv3.4 protein expression levels. Kv3.3 protein expression was not significantly altered by 100 μM $CoCl_2$ treatment, whereas Kv3.4 protein (70 kDa) expression was significantly decreased after 6 and 24 h of 100 μM $CoCl_2$ treatment. All experiments were performed in quadruplicate, and data represent the mean ± standard error. *$p<0.05$, **$p<0.01$ and ***$p<0.001$ versus the control value.

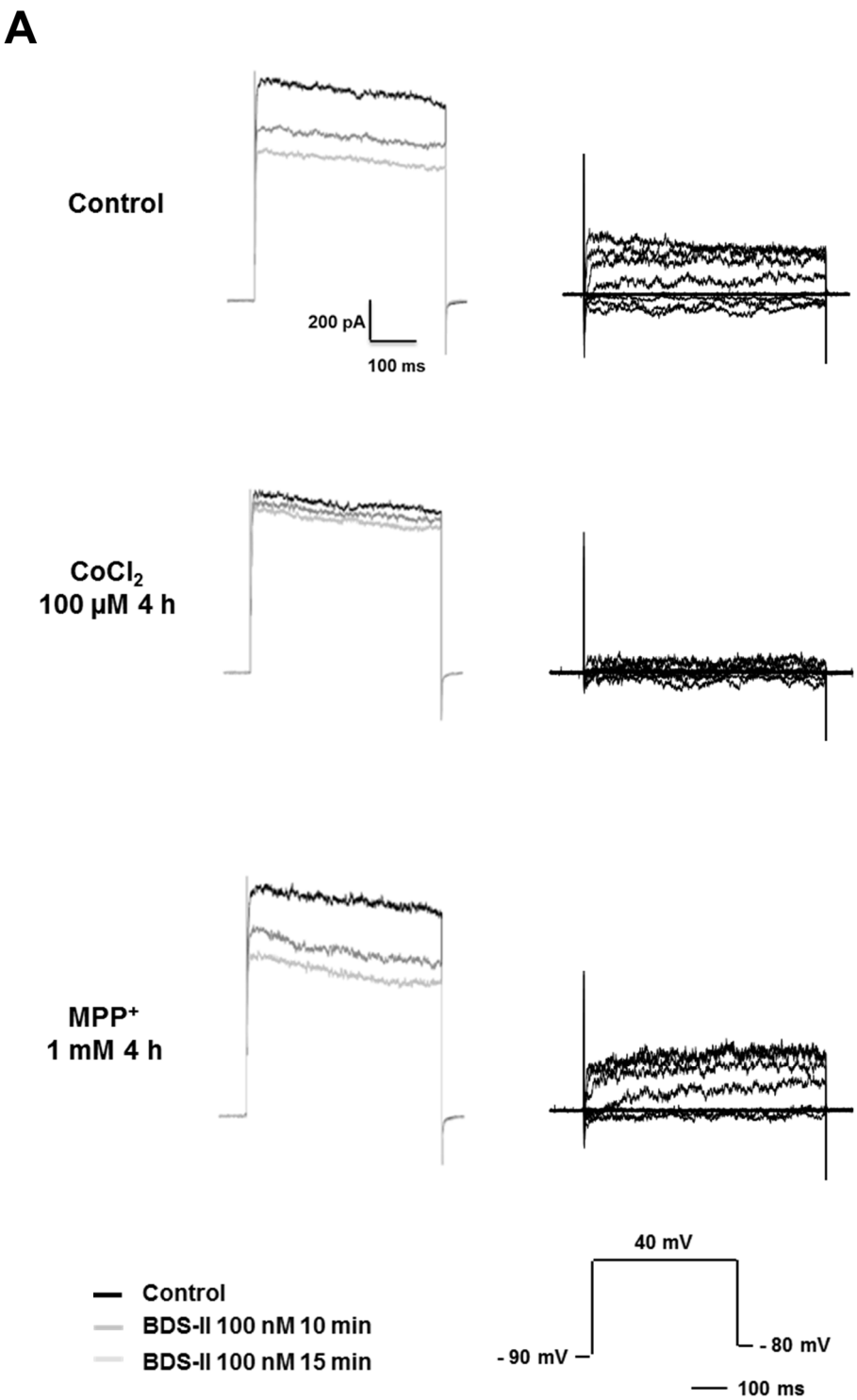
A
Control
200 pA
100 ms
CoCl2
100 μM 4 h
MPP+
1 mM 4 h
Control
BDS-II 100 nM 10 min
BDS-II 100 nM 15 min
40 mV
- 90 mV
- 80 mV
100 ms

B

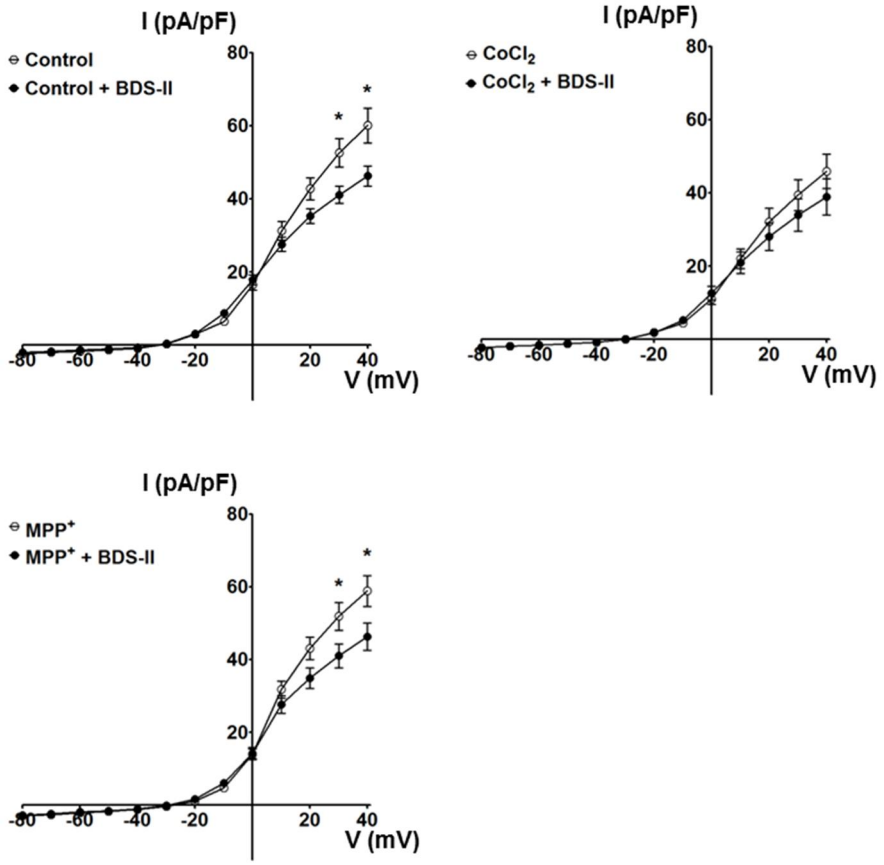
I (pA/pF)
Control
Control + BDS-II
80
60
40
20
-80
-60
-40
-20
20
40
V (mV)
*
*
I (pA/pF)
CoCl2
CoCl2 + BDS-II
80
60
40
20
-80
-60
-40
-20
20
40
V (mV)
I (pA/pF)
MPP+
MPP+ + BDS-II
80
60
40
20
-80
-60
-40
-20
20
40
V (mV)
*
*

C

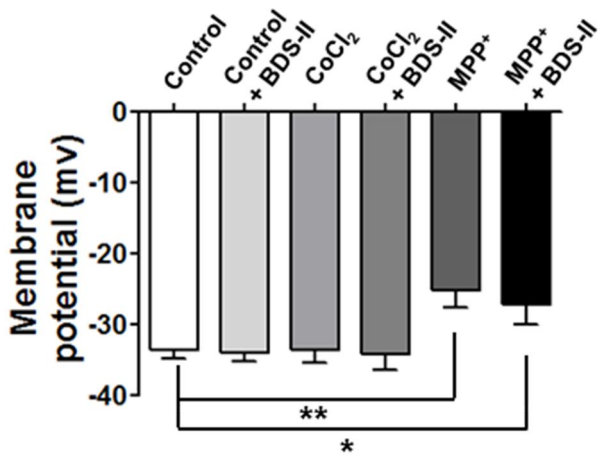
Control
Control + BDS-II
CoCl2
CoCl2 + BDS-II
MPP+
MPP+ + BDS-II
Membrane potential (mv)
0
-10
-20
-30
-40
**
*

Figure 11. Patch-clamp recordings of BDS-II-sensitive currents during $CoCl_2$ or MPP^+ treatment (A) Representative whole-cell currents recorded in SH-SY5Y cells. Currents sensitive to BDS-II (100 nM) were measured in whole-cell mode. SH-SY5Y cells were hyperpolarized by a -90 mV pulse and then depolarized by a +40 mV pulse with a -80 mV holding potential. After 10 min of BDS-II treatment, diminished currents were observed in the control group (327.62 ± 83.45 pA, n=12), the 100 μM $CoCl_2$-treatment group (138.89 ± 51.8 pA, n=8), and the 1 mM MPP^+-treatment group (253.3 ± 47.98 pA, n=9). (B) BDS-II significantly inhibited voltage-dependent currents at +20, +30, and +40 mV of depolarization in the control group and +30 and +40 mV of depolarization in the 1 mM MPP^+-treatment group, whereas no BDS-II-sensitive current was detected in cells treated with 100 μM $CoCl_2$. Experiments were repeated at the indicated times, and data are expressed as the mean ± standard error. *$p<0.05$ and ***$p<0.001$ versus the control value. (C) The resting membrane potential of SH-SY5Y cells was significantly depolarized by 1 mM MPP^+ treatment. However, 100 nM BDS-II did not affect the resting membrane potential.

HIF-1α regulates Kv3.4 expression levels in SH-SY5Y cells

Because HIF-1α accumulates in response to $CoCl_2$ but not MPP^+ treatment, HIF-1α is a strong candidate for regulating Kv3.4 expression in SH-SY5Y cells. Kv3.4 was most significantly affected by siRNA among Kv channels (Figure 12A). Treating cells with PX-478, a HIF-1α-selective inhibitor (Koh et al., 2008), led to the down-regulation of HIF-1α and also affected Kv3.4 expression levels by up-regulating Kv3.4 mRNA expression (Figure 12B and 12C). Next, it was investigated whether PX-478 inhibited the changes Kv3.4 expression during $CoCl_2$ treatment. PX-478 rescued the down-regulation of Kv3.4 mRNA expression caused by $CoCl_2$ (Figure 12D). Kv3.4 protein expression, which was down-regulated after 6 h of $CoCl_2$ treatment, was also recovered when the PX-478 was pretreated for 4 h and treated with $CoCl_2$ with PX-478 for 6 h (Figure 12E). In addition, PX-478 also recovered the reduction in BDS-II-sensitive Kv currents induced by $CoCl_2$ treatment (Figure 12F).

Mitochondrial Kv3.4 is important in oxidative stress regulation

Mitochondrial potassium channels protect neuronal tissues, and their putative

functional roles include not only physiological mitochondrial properties but also the modulation of reactive oxygen species generation in mitochondria (Szewczyk et al., 2009). Therefore, it was examined whether Kv3.4 exists in mitochondria. Immunocytochemical analysis demonstrated that Kv3.4 (green) and mitochondria (red) are co-localized and co-localization of Kv3.4 was decreased after 6 hours of $CoCl_2$ treatment (Figure 13A). Then it was explored why Kv3.4 protein expression was unaltered despite the down-regulation of Kv3.4 mRNA expression after 4 h of $CoCl_2$ treatment (Figure 10B and 10C). Figure 13B demonstrates that cytosolic Kv3.4 protein expression is not affected by 4 h of $CoCl_2$ treatment, whereas mitochondrial Kv3.4 is affected by the same experimental condition. Western blotting demonstrated that the 100 kDa Kv3.4 band was more dramatically altered compared with the 70 kDa Kv3.4 band in cells treated with $CoCl_2$ or $CoCl_2$ plus PX-478. The 100 kDa Kv3.4 band accumulated upon PX-478 treatment (Figure 13B).

HIF-1α affects the NDFIP1-related Kv3.4 regulatory system

Ubiquitination is found out to be closely related to Kv3.4 when cells enter apoptosis using GENEVESTIGATOR®, a bioinformatic tool. Ring finger protein 125, E3 ubiquitin protein ligase (RNF125), and Nedd4 family-

interacting protein 1 (NDFIP1) are highly co-expressed with Kv3.4 (Figure 14A). According to previous reports, NDFIP1 protein expression was up-regulated when SH-SY5Y cells were treated with $CoCl_2$ at concentrations above 200 μM, whereas 100 μM $CoCl_2$ did not affect NDFIP1 (Howitt et al., 2009; Schieber et al., 2011). In addition, 100 μM $CoCl_2$ did not up-regulate NDFIP1 protein expression, and NDFIP1 mRNA levels were down-regulated by 100 μM $CoCl_2$ treatment in SH-SY5Y cells (Figure 14B and 14C). To confirm the relationship between HIF-1α and NDFIP1, the cells were pretreated with PX-478 followed by PX-478 and $CoCl_2$ treatments. NDFIP1 mRNA and protein expression levels were down-regulated by $CoCl_2$ plus PX-478 (Figure 14C). It was hypothesized that $CoCl_2$-induced HIF-1α accumulation up-regulates NDFIP1. In addition, given that PX-478 pretreatment not only inhibits $CoCl_2$-induced HIF-1α accumulation but also removes the remaining HIF-1α that originally exists in SH-SY5Y cells, PX-478 treatment down-regulates NDFIP1. Next, the relationship between Kv3.4 and NDFIP1 was examined. NDFIP1 siRNA effectively down-regulated the expression of 100 kDa Kv3.4 (Figure 14D and 14E). On the other hand, NDFIP1 siRNA did not affect the expression of 100 kDa Kv3.4 in $CoCl_2$-treated cells (Figure 14E).

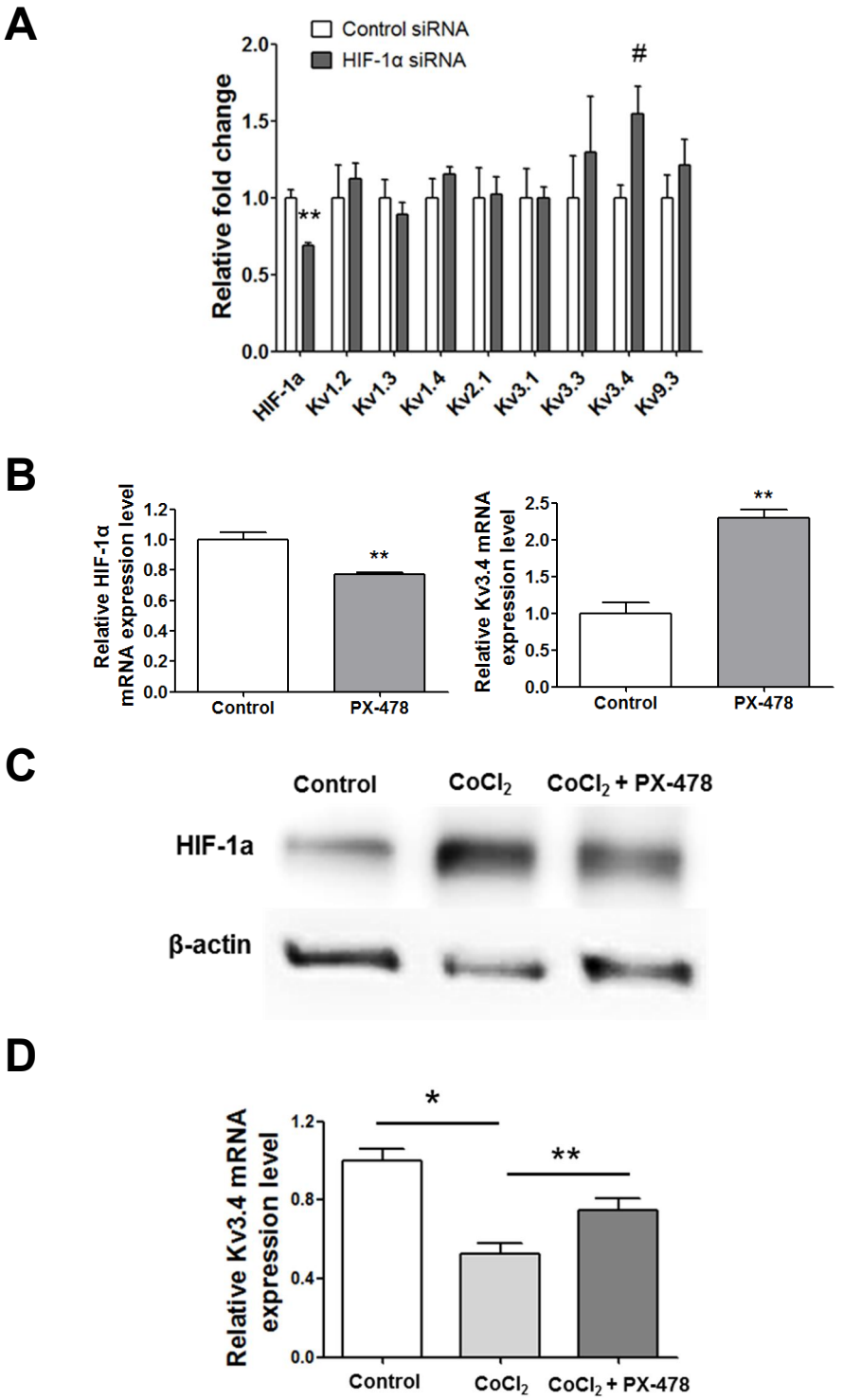
A
Control siRNA
HIF-1α siRNA
Relative fold change
2.0
1.5
1.0
0.5
0.0
**
#
HIF-1a
Kv1.2
Kv1.3
Kv1.4
Kv2.1
Kv3.1
Kv3.3
Kv3.4
Kv9.3
B
Relative HIF-1α mRNA expression level
1.2
1.0
0.8
0.6
0.4
0.2
0.0
**
Control
PX-478
Relative Kv3.4 mRNA expression level
2.5
2.0
1.5
1.0
0.5
0.0
**
Control
PX-478
C
Control
CoCl2
CoCl2 + PX-478
HIF-1a
β-actin
D
Relative Kv3.4 mRNA expression level
1.2
0.8
0.4
0.0
*
**
Control
CoCl2
CoCl2 + PX-478

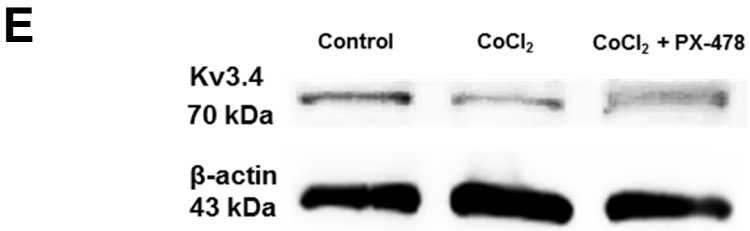
E
Control
CoCl2
CoCl2 + PX-478
Kv3.4
70 kDa
β-actin
43 kDa

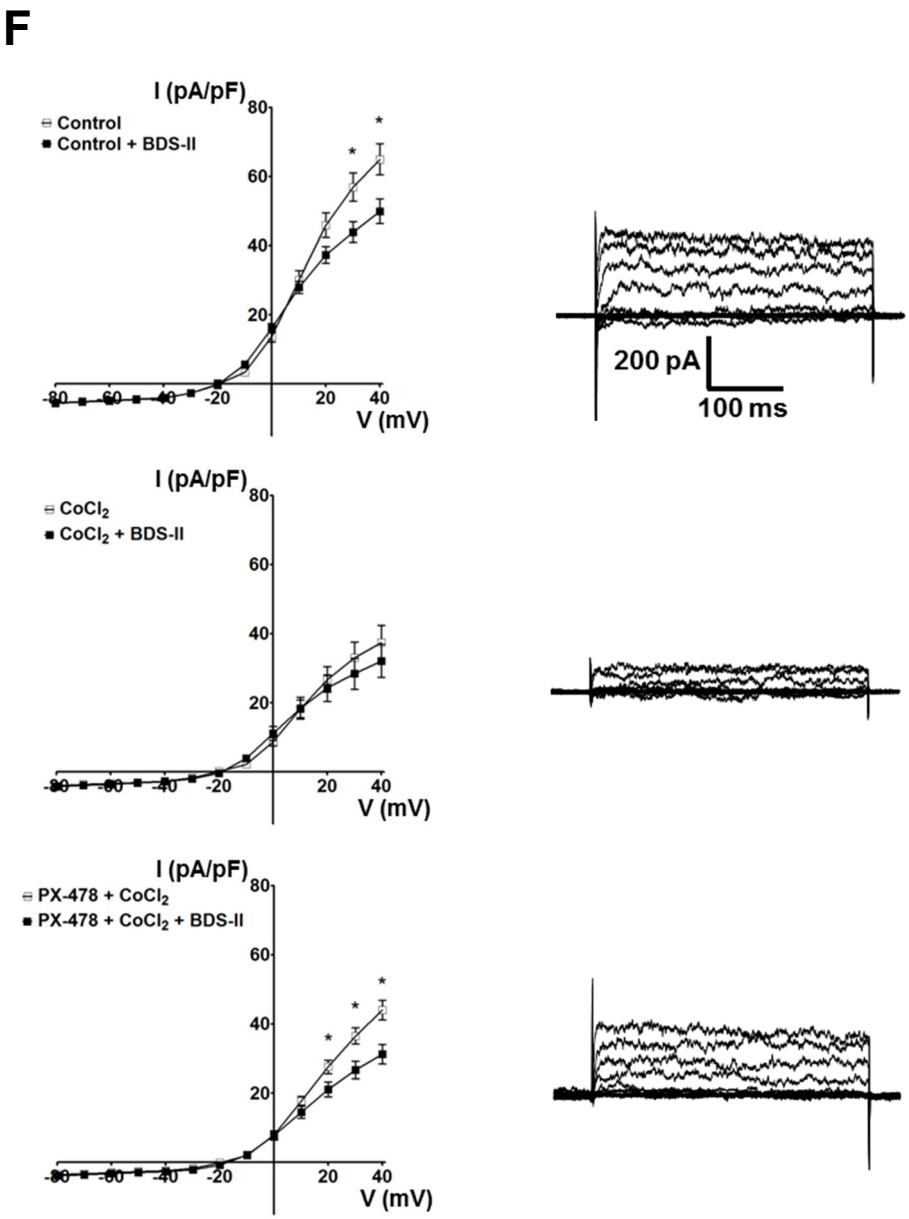
F
I (pA/pF)
Control
Control + BDS-II
V (mV)
200 pA
100 ms
I (pA/pF)
CoCl2
CoCl2 + BDS-II
V (mV)
I (pA/pF)
PX-478 + CoCl2
PX-478 + CoCl2 + BDS-II
V (mV)

Figure 12. The relationship between HIF-1α and Kv3.4 (A) Out of eight oxygen-sensitive Kv channels (Kv1.2, Kv1.3, Kv1.4, Kv2.1, Kv3.1, Kv3.3, Kv3.4, and Kv9.3), only Kv3.4 from among eight was significantly up-regulated by transient HIF-1α siRNA transfection. (B) PX-478 (40 μM), a HIF-1α-specific blocker, inhibited HIF-1α and up-regulated Kv3.4 mRNA expression. (C) HIF-1α accumulated upon 100 μM $CoCl_2$ treatment, and $CoCl_2$-induced HIF-1α accumulation was inhibited by 40 μM PX-478 treatment: 4 h of PX-478 pretreatment followed by 6 h of $CoCl_2$ and PX-478 treatment. (D) Kv3.4 mRNA expression was down-regulated after 4 h of 100 μM $CoCl_2$ treatment. PX-478 pretreatment recovered the down-regulation of Kv3.4 mRNA expression induced by $CoCl_2$. (E) Kv3.4 (70 kDa) was decreased after 6 h of $CoCl_2$ treatment. The decrease in Kv3.4 (70 kDa) expression was recovered by PX-478 pretreatment (4 h) followed by 6 h of $CoCl_2$ and PX-478 treatment. (F) Currents sensitive to BDS-II (100 nM) were detected at +20, +30, and +40 mV of depolarization (n=6), whereas BDS-II-sensitive currents were diminished by 100 μM $CoCl_2$ treatment (n=6). Diminished BDS-II-sensitive currents were recovered by 40 μM PX-478 pretreatment at +40 mV of depolarization (n=9). Experiments were repeated in triplicate or the indicated times, and data represent the mean ± standard error. *, #$p<0.05$ and **$p<0.01$ versus the control.

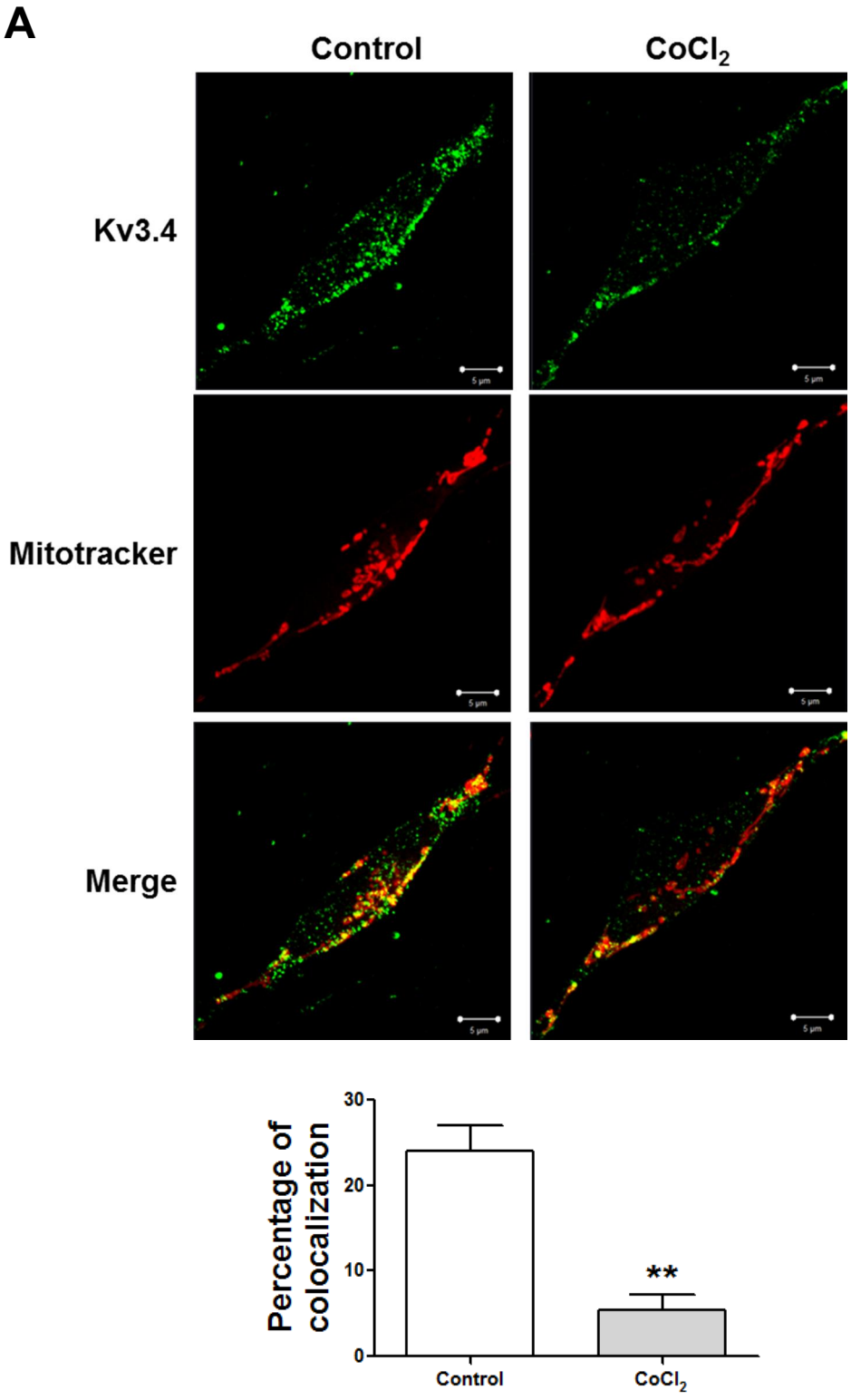
A
Control
CoCl2
Kv3.4
Mitotracker
Merge
5 μm
Percentage of colocalization
30
20
10
0
**
Control
CoCl2

B

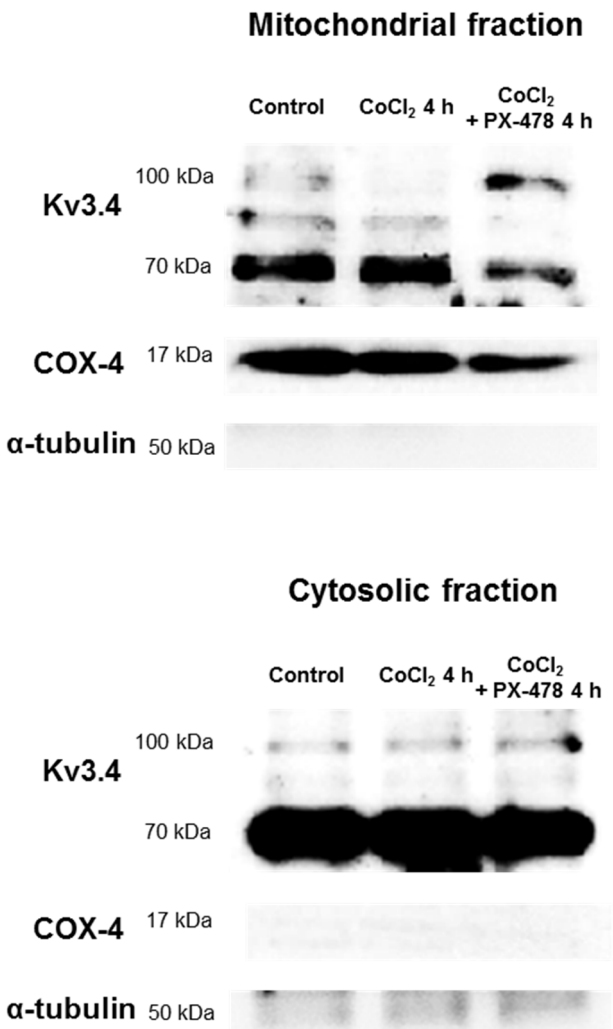
Mitochondrial fraction
Control
CoCl2 4 h
CoCl2 + PX-478 4 h
Kv3.4
100 kDa
70 kDa
COX-4
17 kDa
α-tubulin
50 kDa
Cytosolic fraction
Control
CoCl2 4 h
CoCl2 + PX-478 4 h
Kv3.4
100 kDa
70 kDa
COX-4
17 kDa
α-tubulin
50 kDa

Figure 13. Mitochondrial Kv3.4 was more sensitive to $CoCl_2$ and PX-478 (A) Immunocytochemical analysis demonstrated that Kv3.4 co-localizes with mitochondria, and co-localized Kv3.4 decreased after 6 h of 100 μM $CoCl_2$ treatment (green: Kv3.4, red: mitochondria, yellow: co-localization). Five different images were assessed in each group (the control and $CoCl_2$ treatment groups) to avoid cherry-picking; representative images are shown. (B) Mitochondrial fractionation demonstrated that Kv3.4 is present in both the mitochondria and cytosol and that mitochondrial 100 kDa Kv3.4 is sensitive to $CoCl_2$ alone or $CoCl_2$ with PX-478 treatment. Kv3.4 (100 kDa) was down-regulated by 4 h of $CoCl_2$ treatment, whereas 4 h of PX-478 pretreatment followed by 4 h of $CoCl_2$ and PX-478 treatment induced the accumulation of Kv3.4. COX-4 and α-tubulin are used as mitochondrial and cytosolic markers, respectively. All experiments were performed in quadruplicate; representative images are shown.

A

Description of the most correlated genes (top 20)

	Gene	Score	Description
1	RNF125	0.75	ring finger protein 125, E3 ubiquitin protein ligase
2	KCNC4	0.74	Potassium voltage-gated channel, Shaw-related subfamily, member 4
3	PPM1F	0.74	Protein phosphatase, Mg2+/Mn2+ dependent, 1F
4	PPM1F	0.73	Protein phosphatase, Mg2+/Mn2+ dependent, 1F
5	RAP1GAP2	0.68	RAP1 GTPase activating protein 2
6	LPHN1	0.64	latrophilin 1
7	RBP4	0.64	retinol binding protein 4, plasma
8	LOC100505483	0.64	uncharacterized LOC100505483
9	PPP1R21	0.64	protein phosphatase 1, regulator subunit 21
10	CBFA2T3	0.63	core-binding factor, runt domain, alpha subunit 2; translocated to, 3
11	ADRBK2	0.63	adrenergic, beta, receptor kinase 2
12	PRKCZ	0.63	protein kinase 3, zeta
13	236089_at	0.63	
14	HSPA12B	0.62	heat shock 70kD protein 12B
15	NDFIP1	0.62	Nedd4 family interacting protein 1
16	ALOX5	0.62	arachidonate 5-lipoxygenase
17	NPDC1	0.62	neural proliferation, differentiation and control, 1
18	RABGAP1L	0.62	RAB GTPase activating protein 1-like
19	KIAA1377	0.62	KIAA1377
20	ERG	0.62	v-ets erythroblastosis virus E26 oncogene homolog

B

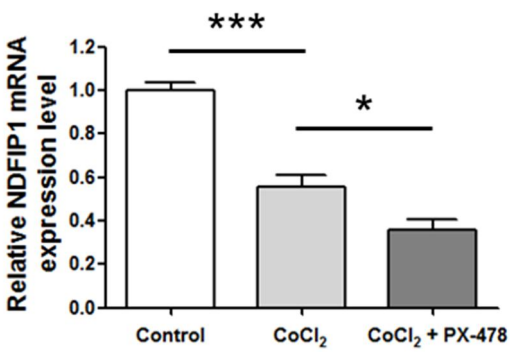

C

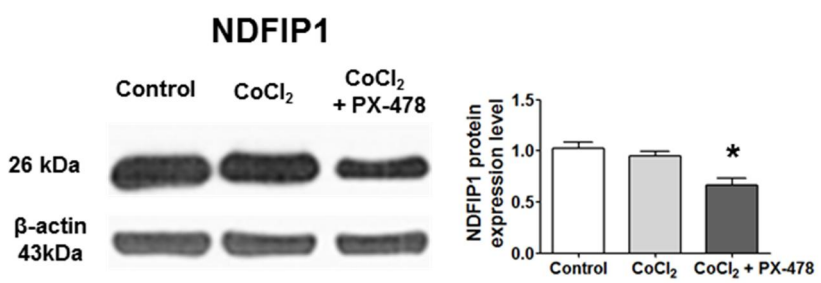

D

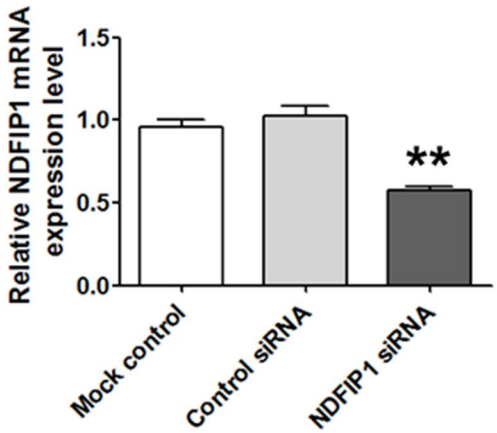
Relative NDFIP1 mRNA expression level
1.5
1.0
0.5
0.0
**
Mock control
Control siRNA
NDFIP1 siRNA

E

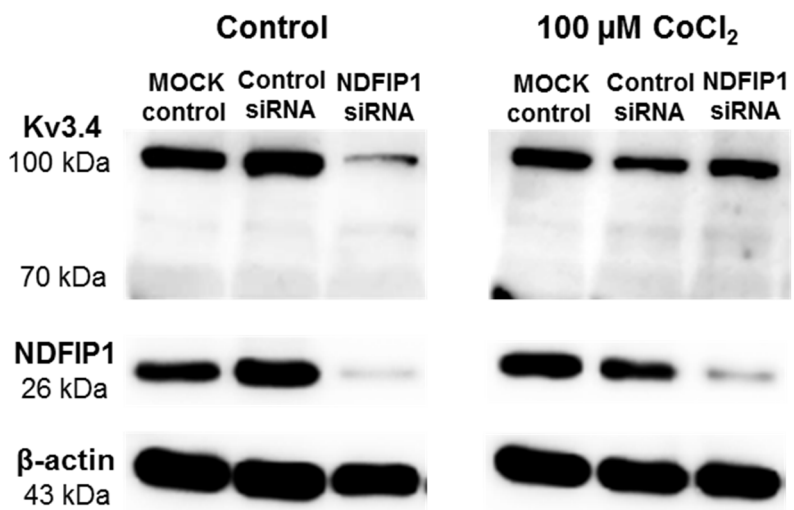
Control
100 μM CoCl2
MOCK control
Control siRNA
NDFIP1 siRNA
MOCK control
Control siRNA
NDFIP1 siRNA
Kv3.4
100 kDa
70 kDa
NDFIP1
26 kDa
β-actin
43 kDa

Figure 14. HIF-1α and NDFIP1-related Kv3.4 regulatory system (A) The co-expression analysis tool in GENEVESTIGATOR® was used to predict genes that are co-expressed with Kv3.4 during apoptosis. The genes were ranked based on their correlation coefficient. Nedd4 family interacting protein 1 (NDFIP1) ranked 15th (0.62 score). (B) NDFIP1 mRNA expression was down-regulated by 100 μM $CoCl_2$ treatment, and 40 μM PX-478 pretreatment additionally down-regulated NDFIP1 mRNA expression. (C) $CoCl_2$ (100 μM) did not affect NDFIP1 protein expression, whereas 40 μM PX-478 pretreatment followed by $CoCl_2$ and PX-478 treatment down-regulated NDFIP1 protein expression. (D) NDFIP1 siRNA efficiently down-regulated NDFIP1 mRNA expression by half. (E) NDFIP1 siRNA down-regulated NDFIP1 protein expression and 100 kDa Kv3.4 expression. When cells were treated with 100 μM $CoCl_2$, NDFIP1 siRNA did not affect 100 kDa Kv3.4 protein expression, despite the efficient down-regulation of NDFIP1 protein levels by NDFIP1 siRNA. All of the experiments were performed in triplicate, and data are expressed as the mean ± standard error. *$p<0.05$, ***$p<0.001$ versus the control value.

The neuroprotective effect of BDS-II against MPP^+-induced SH-SY5Y cell death

HIF-1α has a neuroprotective effect against rotenone-induced injury, which mimics Parkinson's disease symptoms (Wu et al., 2010). The down-regulation of Kv3.4 by HIF-1α during $CoCl_2$ treatment may have a neuroprotective effect on SH-SY5Y cells; thus, this scheme was applied to MPP^+ treatment. As shown in Figure 15A, BDS-II pretreatment protected SH-SY5Y cells from MPP^+-induced cell death. Hemacolor fast staining and MTT assay data demonstrated that 100 nM BDS-II, the lowest effective concentration indicated in the product datasheet, rescued SH-SY5Y cells from 500 μM MPP^+-induced neural cell death (Figure 15A). BDS-II treatment blocked MPP^+-induced cytochrome c release from the mitochondrial intermembrane space to the cytosol, which is one of the key steps of the apoptotic pathway (Figure 15B).

BDS-II blocked MPP^+-induced MMP depolarization in SH-SY5Y cells

MMP was also measured using JC-1 staining. The MMP of control-group cells adhered to the floor of the cell plate indicated that red normal MMP and green

depolarized MMP were co-localized, indicating that MMP is regulated by the surrounding microenvironment (Figure 16A). Following MPP^+ treatment, green JC-1 monomers increased, indicating that the MMP of the adhered cells was depolarized, whereas BDS-II pretreatment blocked the MPP^+-induced MMP depolarization (Figure 16A). Undifferentiated SH-SY5Y cells have the ability to form aggregates; when the cells are differentiated, they spread into the surrounding area (Dwane et al., 2013). Therefore, the MMP of aggregated SH-SY5Y cells was measured. MPP^+ depolarized the MMP of the SH-SY5Y aggregates, and BDS-II pretreatment again blocked depolarization (Figure 16B). The MMP of the floating SH-SY5Y cells was also measured because SH-SY5Y cells not only grow while adhered to the substrate but also grow in clumps that float in the media. The MMP of the MPP^+-treated cells was depolarized, whereas the BDS-II pretreatment group exhibited a normal MMP compared with the control group (Figure 16C). As a control, the MMP-depolarizing agent FCCP depolarized floating cells; no cells remained adhered to the plate when treated with FCCP (Figure 16C).

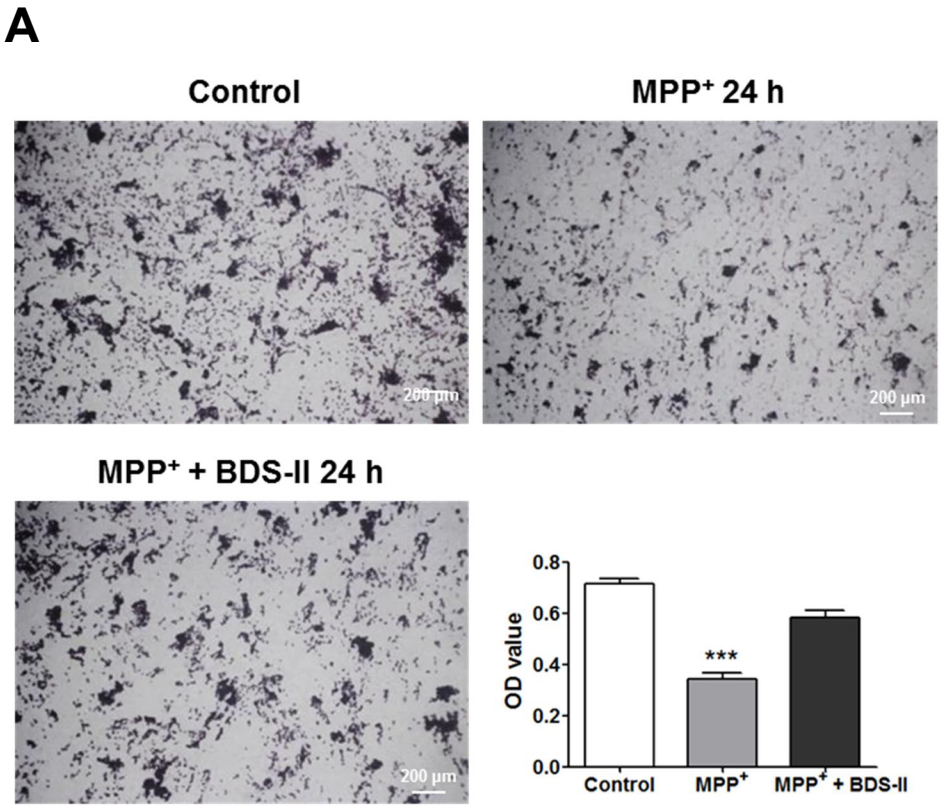
A
Control
MPP+ 24 h
MPP+ + BDS-II 24 h
200 μm
OD value
0.8
0.6
0.4
0.2
0.0
***
Control
MPP+
MPP+ + BDS-II

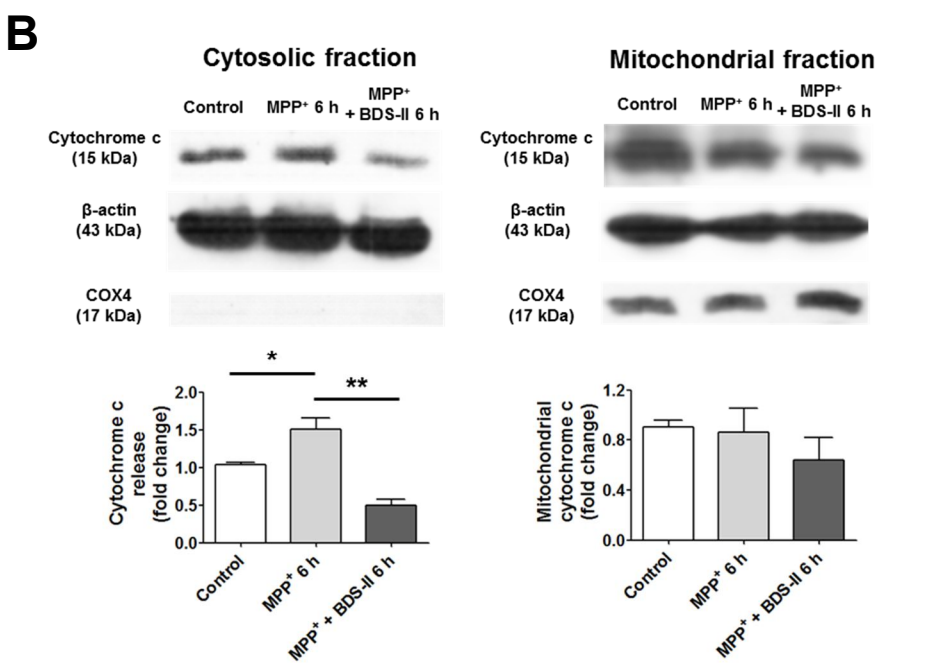
B
Cytosolic fraction
Mitochondrial fraction
Control
MPP+ 6 h
MPP+ + BDS-II 6 h
Cytochrome c (15 kDa)
β-actin (43 kDa)
COX4 (17 kDa)
Cytochrome c release (fold change)
Mitochondrial cytochrome c (fold change)
*
**
2.0
1.5
1.0
0.5
0.0
1.2
0.8
0.4
Control
MPP+ 6 h
MPP+ + BDS-II 6 h

Figure 15. The neuroprotective effect of BDS-II against MPP^+-induced SH-SY5Y cell death (A) Hemacolor-stained SH-SY5Y cells and MTT assays demonstrate that 100 nM BDS-II protected SH-SY5Y cells against 500 μM MPP^+-induced neural cell death. The MTT assay demonstrated that only 48.23 ± 2.91% of cells survived after 24 h of 500 μM MPP^+ treatment, whereas BDS-II enabled 81.68 ± 3.94% of cells to survive after 500 μM MPP^+ treatment. (B) BDS-II blocked MPP^+-induced cytochrome c release from the mitochondrial intermembrane space to the cytosol, which is a key step in the apoptosis signalling pathway. Experiments were repeated in triplicate, and data represent the mean ± standard error. *$p<0.05$, **$p<0.01$, and ***$p<0.001$ versus the control value.

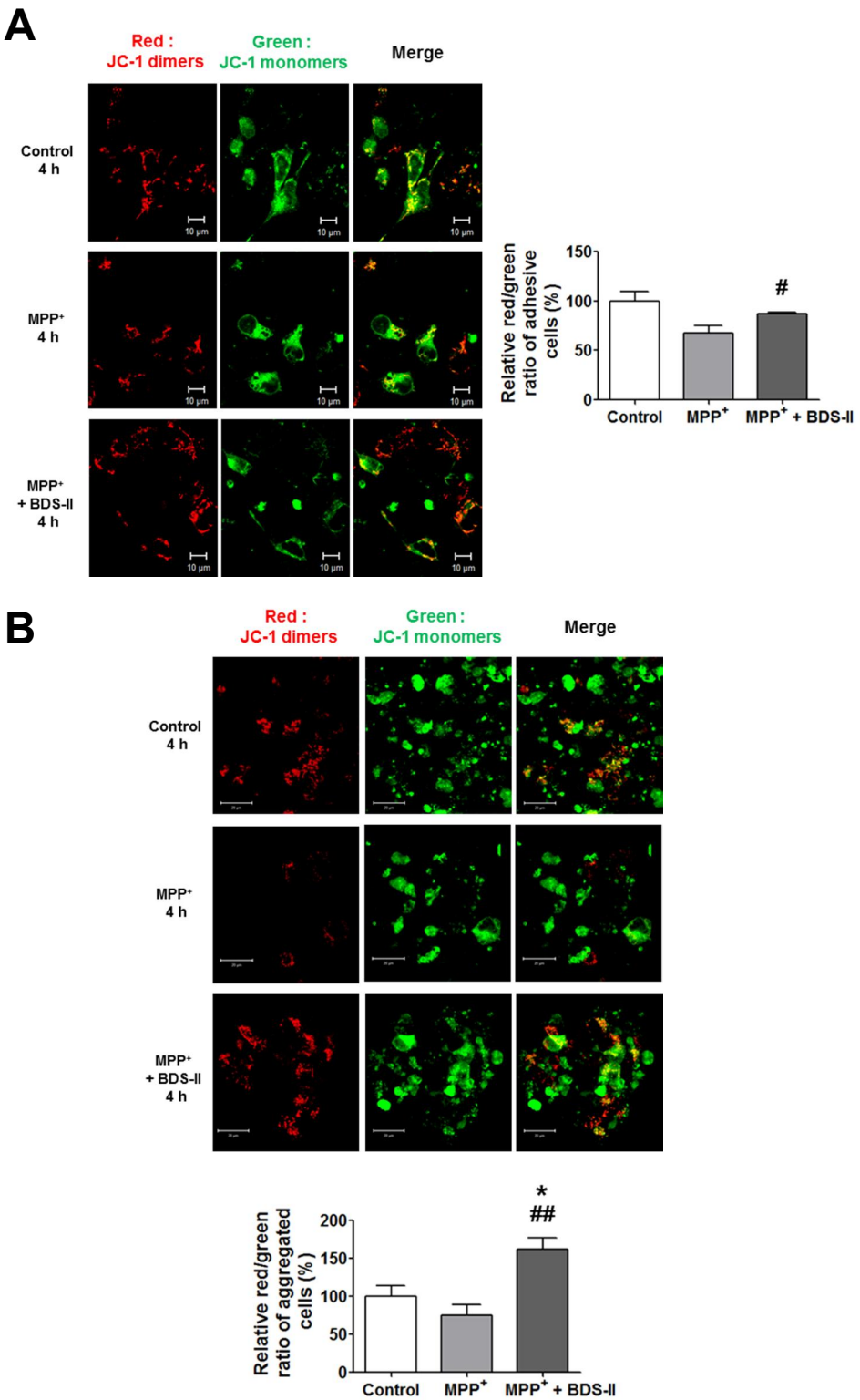
A
Red :
JC-1 dimers
Green :
JC-1 monomers
Merge
Control
4 h
MPP+
4 h
MPP+
+ BDS-II
4 h
10 μm
Relative red/green
ratio of adhesive
cells (%)
150
100
50
0
#
Control
MPP+
MPP+ + BDS-II
B
Red :
JC-1 dimers
Green :
JC-1 monomers
Merge
Control
4 h
MPP+
4 h
MPP+
+ BDS-II
4 h
Relative red/green
ratio of aggregated
cells (%)
200
150
100
50
0
*
##
Control
MPP+
MPP+ + BDS-II

C

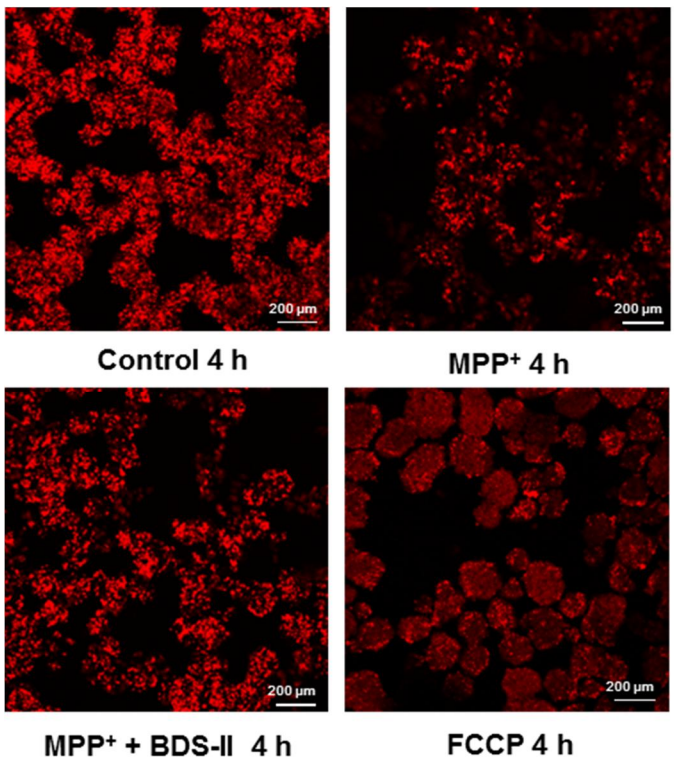
200 μm
200 μm
Control 4 h
MPP+ 4 h
200 μm
200 μm
MPP+ + BDS-II 4 h
FCCP 4 h

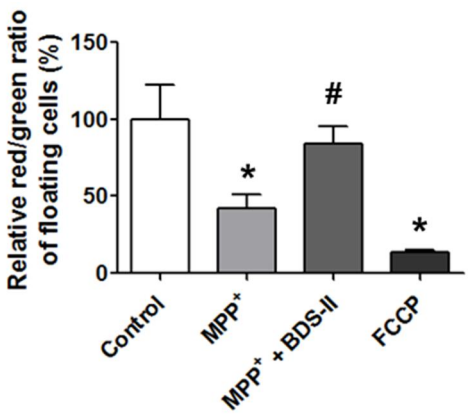
Relative red/green ratio of floating cells (%)
150
100
50
0
*
#
*
Control
MPP+
MPP+ + BDS-II
FCCP

Figure 16. BDS-II blocked MPP^+-induced MMP depolarization in SH-SY5Y cells (A) JC-1 staining revealed that BDS-II prevented the depolarization of mitochondrial membrane potential induced by 1 mM MPP^+ in SH-SY5Y cells. Red JC-1 dimers represent normal mitochondrial membrane potential. Green JC-1 monomers represent depolarized mitochondrial membrane potential. Red dimers and green monomers were co-localized in control cells. When cells were treated with 1 mM MPP^+, most of the cells showed only green monomers. When 100 nM BDS-II was pretreated for 10 min followed by 4 h of 1 mM MPP^+ and 100 nM BDS-II treatment, red dimers and green monomers co-localized again, but many cells also exclusively exhibited red dimers. (B) BDS-II also prevented the depolarization of mitochondrial membrane potential induced by 1 mM MPP^+ in aggregated SH-SY5Y cells. Red dimers and green monomers were detected in the control and MPP^++BDS-II groups, whereas almost all of the red dimers disappeared in the MPP^+ group. (C) Red JC-1 dimers indicated that 100 nM BDS-II rescued SH-SY5Y cells from MMP depolarization induced by 1 mM MPP^+ treatment. FCCP (100 μM) was used as a positive control. All of the experiments were performed in triplicate or quadruplicate, and representative images are shown.

DISCUSSION

Previous studies have revealed the cellular functions of Kv channels, including cell proliferation, apoptosis, and oxygen sensing (Patel and Honore, 2001; Wang, 2004; Lang et al., 2005; O'Grady and Lee, 2005). Kv3.4 is characterized by its fast inactivation, and the channel loses its fast inactivation property upon external application of H_2O_2 and this effect is reversible if glutathione is added as a reducing agent; therefore, Kv3.4 is an oxidation-sensitive channel (Ruppersberg et al., 1991; Patel and Honore, 2001). However, to date, most of the previous studies investigated Kv3.4 exclusively as a hypoxia-related and oxygen-sensitive channel, although there are numerous oxidation-inducing factors other than oxygen (Kaab et al., 2005; Li and Schultz, 2006).

This study demonstrated that Kv3.4 may regulate oxidative stress as an oxidation-sensitive channel. First, SH-SY5Y cells were treated with MPP^+, an *in vitro* Parkinson's disease-inducing reagent, as a ROS-generating reagent. However, no change in Kv3.4 mRNA or protein expression levels was observed, and patch-clamp recordings also demonstrated that MPP^+ treatment did not affect BDS-II-sensitive currents. It was hypothesized that Kv3.4 is not involved in the regulation of oxidative stress induced by MPP^+, perhaps because the

specific cellular defence mechanism against oxidative stress that includes Kv3.4 is not activated. Next, it was examined whether ROS generated by $CoCl_2$ may lead to Kv3.4-related oxidative stress regulation, since $CoCl_2$ is not only an oxidative stress inducer but also a hypoxia-mimetic reagent and several reports have addressed the relationship between hypoxia and Kv3.4 (Kaab et al., 2005; Li and Schultz, 2006; Guo et al., 2008). When the cells were treated with $CoCl_2$, Kv3.4 mRNA and protein expression levels were reduced; patch clamp recordings also demonstrated that BDS-II-sensitive currents disappeared after $CoCl_2$ treatment. According to the results, although both $CoCl_2$ and MPP^+ induce ROS generation, only $CoCl_2$ treatment down-regulates the Kv3.4 expression level and BDS-II-sensitive currents. These results indicate that a key factor for Kv3.4 regulation exists or is activated exclusively by $CoCl_2$ treatment, not MPP^+ treatment.

It was hypothesized that HIF-1α is a key factor in the regulation of Kv3.4 because HIF-1α accumulates under $CoCl_2$ but not under MPP^+ treatment (Wu et al., 2010). Pretreatment with the HIF-1α-specific inhibitor PX-478 prior to $CoCl_2$ treatment restored the $CoCl_2$-induced reduction in BDS-II-sensitive currents. Previous studies found that decreased reactive-oxygen intermediates, including H_2O_2, caused by a low level of available substrate oxygen during

hypoxia resulted in reduced production of oxidized Kv3.4 and that Kv3.4 currents were subsequently reduced (Patel and Honore, 2001; Kaab et al., 2005). However, Kv3.4 currents were also reduced by $CoCl_2$, a well-known ROS inducer[12, 28], in the performed experiments. Moreover, hypoxic conditions increase ROS production and oxidative stress (Chandel et al., 2000; Kaab et al., 2005; Clanton, 2007). Therefore, the reduced Kv3.4 currents during hypoxia may be regulated by HIF-1α. In fact, partial HIF-1α deficiency in pulmonary artery smooth muscle cells appeared to restore the chronic hypoxia-induced reduction in Kv currents (Shimoda et al., 2001).

Mitochondrial dysfunction has been implicated in several models of acute and chronic neuronal death, and the major chronic neurodegenerative diseases, such as Alzheimer's, Parkinson's, or Huntington's disease, display depolarized MMP and apoptosis (Mattson, 2000; Mattson and Kroemer, 2003; Kroemer et al., 2007). Therefore, agents targeting specific mitochondrial ion channels or proteins that contribute to the MMP would be useful therapeutic tools to inhibit acute cell death (Kroemer et al., 2007). In pulmonary artery smooth muscle cells, changes in the localization of mitochondria and mitochondria-dependent intracellular ATP and Mg^{2+} concentrations are closely related to Kv currents (Firth et al., 2008; Firth et al., 2009). In particular, the

existence of mitochondrial Kv1.3 has been substantiated, and mitochondrial Kv1.3 mediates Bax-induced apoptosis in lymphocytes (Szabo et al., 2008; Szewczyk et al., 2009; Bednarczyk et al., 2010). Immunocytochemistry and mitochondrial fractionation suggest that Kv3.4 is present on mitochondria and plays a role in MMP-related apoptosis in SH-SY5Y cells. Kv3.4 expression levels change during 4 h $CoCl_2$ and PX-478 treatment, which were not detected in Western blots of total protein but only in the mitochondrial fraction. Interestingly, 100 kDa Kv3.4 was more dramatically altered than 70 kDa Kv3.4 by $CoCl_2$ treatment. Although the general size of Kv3.4 is 70 kDa, the size of Kv3.4 varies because Kv channels form tetramers and have some accessory channels that regulate their currents. Kv3.4 is 100 kDa when it is glycosylated or forms a tetramer with Kv3.1 or other accessory channels, including Mirp2 (Baranauskas et al., 2003; Cartwright et al., 2007; Kanda et al., 2011). Based on the results, it was concluded that such a glycosylated form or channel heteromers, which include accessory channel proteins, aid in the subcellular localization of Kv3.4, including to mitochondria. It was also concluded that mitochondrial Kv3.4 is more sensitive to oxidative stress.

Bioinformatic analysis demonstrates that ubiquitination is closely related to Kv3.4 during cell death, and NDFIP1 was selected as research target,

because the neural precursor cell expressed developmentally down-regulated protein 4 (Nedd4) family, including Nedd4 and Nedd4-2, which use NDFIP1 as an intermediate adaptor protein, are related to the regulation of voltage-gated ion channels in excitable cells (Bongiorno et al., 2011). Nedd4 and Nedd4-2 are E3 ubiquitin ligase enzymes that target proteins for ubiquitination, and NDFIP1 is one of the adaptor proteins required to bring Nedd4 and Nedd4-2 to the target proteins (Bongiorno et al., 2011). These data demonstrate that NDFIP1 siRNA down-regulated Kv3.4 efficiently. However, when the cells were treated with $CoCl_2$, NDFIP1 siRNA did not affect Kv3.4 expression. HIF-1α plays a pivotal role in Kv3.4 regulation; therefore, it was hypothesize that accumulated HIF-1α potentially affected NDFIP1-related Kv3.4 regulation.

Considering the data, it was hypothesized that $CoCl_2$ may have an effect on the oxidative stress-regulating systems that are related to Kv3.4, whereas MPP^+ does not affect Kv3.4. The regulation of Kv3.4 protein expression by HIF-1α, which is accumulated by $CoCl_2$, may not be enough to activate the Kv3.4 related oxidative stress-regulating system, however, it was believed that it would activate the oxidative stress-regulating system. Because a low $CoCl_2$ concentration (50, 100, 150, or 200 μM) shows cytoprotection in cardiomyocytes and HepG2 cells (Piret et al., 2002; Wu et al., 2012) and Kv3.4

is down-regulated by 100 μM of $CoCl_2$ in the data. Therefore down-regulated Kv3.4 was believed to be involved in the cytoprotection induced by a low $CoCl_2$ concentration. On the other hand, a high $CoCl_2$ concentration (500 μM) prompts cell death in the SH-SY5Y cells (Stenger et al., 2011), and in this scheme, it is because ROS generated by a high concentration of $CoCl_2$ may overcome the cytoprotective effect of downregulated Kv3.4. According to the hypothesis of this study, inhibiting Kv3.4 would alter the response of SH-SY5Y cells to MPP^+ treatment. Therefore the cells were treated with the BDS-II, a selective Kv3.4 inhibitor, before MPP^+ treatment to confirm this hypothesis. BDS-II treatment protected SH-SY5Y cells against MPP^+-induced neural cell death by inhibiting apoptosis. BDS-II treatment blocked mitochondrial cytochrome c release during MPP^+ treatment. Several reports demonstrate K^+ concentrations are an important factor in apoptosis (Shah and Aizenman, 2014). Specifically, Kv2.1 is one of the most important potassium channels that are involved in apoptosis, and its functional role has been investigated in greater detail compared with other oxidation-sensitive channels (Pal et al., 2003; Yao et al., 2009; McCord and Aizenman, 2013). Kv2.1, which is abundantly expressed in the cortex and hippocampus, is oxidized in the brains of aging mice, and oxidized Kv2.1 channels, which form oligomers through disulfide bonds involving Cys-73,

accumulate in the plasma membrane as a consequence of defective endocytosis (Misonou et al., 2005; Wu et al., 2013). The membrane accumulation of Kv2.1 oligomers disrupts planar lipid raft integrity and causes apoptosis by activating the c-Src/JNK signalling pathway (Wu et al., 2013). Other Kv channels, such as Kv1.1, Kv1.3, and Kv4.2, are involved in neuronal apoptosis (Plant et al., 2006; Koeberle et al., 2010), and the data in this study demonstrate that Kv3.4 is also involved in the neuronal apoptotic pathway.

Oxidative stress has been detected in a variety of neurodegenerative diseases, such as Alzheimer's disease and Parkinson's disease, and increasing evidence suggests that oxidative stress plays a major role in these diseases (Markesbery, 1997; Gandhi and Abramov, 2012; Hwang, 2013). Several Kv channels, such as Kv2.1, Kv3.4, and Kv4.2, are thought to be connected to Alzheimer's disease. Therefore, Kv channels, including Kv3.4, are expected to be novel therapeutic targets in Parkinson's disease (Pan et al., 2004; Pannaccione et al., 2007; Cotella et al., 2012). Sesti et al suggested that the oxidation of K^+ channels by ROS might be a leading cause of neurodegenerative diseases, including Alzheimer's and Parkinson's disease. They demonstrated that highly elevated ROS levels are found in the aging brain and in many neurodegenerative diseases and therefore, oxidative modification

of K^+ channels might be a general principle underlying aging and neurodegeneration (Sesti et al., 2010). Kv3.4 has been suggested as a new therapeutic target for major neurodegenerative diseases, and the mechanisms of Kv3.4 related to these diseases have been investigated (Pannaccione et al., 2007; Boda et al., 2012). However, the relationship between the oxidative modification of Kv3.4 and neurodegenerative diseases remains unknown. This study suggests that Kv3.4 may play important roles in neurodegenerative disease as an oxidation-sensitive channel.

Taken together, Kv3.4 has an effect on the death of SH-SY5Y cells as an oxidation-sensitive channel. Kv3.4 is involved in the MPP^+-induced apoptotic pathway through, for example, cytochrome c release and MMP regulation. In addition, mitochondrial Kv3.4 may be important for such phenomena, and HIF-1α is a key regulator of Kv3.4. These data imply the pivotal function of Kv3.4 in the neuroblast cell as an oxidation-sensitive Kv channel, and further studies of the relationship between Kv3.4 and oxidative stress would provide a new therapeutic paradigm for oxidative stress-related diseases.

CHAPTER III

Kv3.1 and Kv3.4, are involved in cancer cell migration and invasion

(Data in this chapter have been published in Song et al., Int J Mol Sci, 2018, 19(4). pii: E1061)

ABSTRACT

Kv channels, including Kv3.1 and Kv3.4, are known as oxygen sensors, and their function in hypoxia has been well investigated. However, the relationship between Kv channels and tumor hypoxia has yet to be investigated. This study demonstrates that Kv3.1 and Kv3.4 are tumor hypoxia-related Kv channels involved in cancer cell migration and invasion. Kv3.1 and Kv3.4 protein expression in A549 and MDA-MB-231 cells increased in a cell density-dependent manner, whereas Kv3.3 protein expression did not change in A549 cells with an increase in cell density. The Kv3.1 and Kv3.4 blocker blood depressing substance-II (BDS-II) did not affect cell proliferation; instead, BDS-II inhibited cell migration and invasion. It was found that BDS-II inhibited intracellular pH regulation and ERK1/2 activation in A549 cells cultured at a high density, potentially resulting in BDS-II-induced inhibition of cell migration and invasion. The data in this study suggest that Kv3.1 and Kv3.4 may be new therapeutic targets for cancer metastasis.

INTRODUCTION

Tumor hypoxia is a characteristic of cancer that differs from normal tissue. Because of the rapid growth of tumors, the blood supply cannot provide sufficient oxygen to tumor cells, and as a result, the cells encounter a hypoxic microenvironment. Tumor cells alter their metabolism and increase their migratory and metastatic behavior to overcome this hypoxic microenvironment (Spill et al., 2016). Furthermore, hypoxia is associated with extracellular matrix remodeling, which plays crucial roles in metastasis (Gilkes et al., 2014). During these changes, cells are forced to induce genomic and proteomic changes that may contribute to tumor malignancy (Hockel and Vaupel, 2001; Vaupel et al., 2004; Wilson and Hay, 2011).

Hypoxia induces depolarization of membrane potential by inhibiting the activity of several oxygen-sensitive K^+ channels, including Kv channels, Ca^{2+}-activated K^+ channels, and the two-pore domain TASK-like K^+ channels (Patel and Honor, 2001; Giaccia et al., 2004). Specifically, the expression and roles of Kv channels, as oxygen-sensitive channels, have been well investigated. Hypoxia inhibits Kv channel activity in various systems that are closely related to oxygen (Buckler, 1997; Kaab et al., 2005; Mittal et al., 2012). During

hypoxia, hypoxia-inducible factors (HIFs) appear to be important for regulating O_2-sensing machinery in carotid body cells and pulmonary myocytes, and a particular HIF, HIF-1α, regulates K^+ channel activity (Shimoda et al., 2001; Kline et al., 2002; Giaccia et al., 2004; Lopez-Barneo et al., 2004). HIF-1α is one of the most important transcription factors for controlling many hypoxia-inducible genes (Wang et al., 1995), and accumulating evidence suggests that HIF-1α mediates tumor metabolic responses and promotes tumor proliferation, angiogenesis, and metastasis (Semenza, 2002; Vaupel, 2004; Semenza, 2013).

The roles of Kv channels in cancer development and progression have been well investigated. Kv channels are not only involved in cell proliferation and tumor growth but also cell migration, adhesion and metastasis (Huang and Jan, 2014; Pardo and Stuhmer, 2014). However, mechanistic studies of the functions of Kv channels have not yet been able to clearly explain all the observed phenomena. In fact, both canonical ion permeation-dependent and noncanonical ion permeation-independent processes, including signaling cascades, have been proposed to participate in cancer development and progression (Huang and Jan, 2014). Therefore, new cancer research paradigms that include Kv channels as therapeutic targets may be necessary to more clearly explain the observed phenomena.

MATERIALS AND METHODS

Cell culture

Cells were cultured in RPMI 1640 (A549, MDA-MB-231, and HT-29 cells (Welgene, Daegu, Korea)) or DMEM (L-132 cells) containing $NaHCO_3$ supplemented with 10% fetal bovine serum (FBS) and 1% antibiotic-antimycotic solution (Sigma, St, Louis, MO) at 37°C with 5% CO_2. When the cells exhibited sufficient growth in a T75 flask (SPL Life Sciences, Gyeonggi-do, Korea), they were divided into various culture dishes or culture plates (SPL). Each cell line was then grown until cells reached the desired confluence for experiments (low, medium, or high). BDS-II treatments were performed after 18 to 24 hours of incubation time for cell adherence. For the experiments, the cells were seeded, and after the cells grew to an appropriate cell density, a photo was took and percentage of the surface area of the plate or dish covered by the cells was evaluated using ImageJ software (National Institutes of Health, Bethesda, MD). Low density represents 20~30% cell confluence, medium density represents 40~60% cell confluence, and high density represents over 80% cell confluence. Cell seeding numbers are shown in Table 3, and 6-well plates

were used for all experiments except the PCR analysis (100-mm dish) and the migration and invasion assays (manufacturer's kit inserts were used).

Reverse transcription-polymerase chain reaction (RT-PCR)

RNA preparation was performed using Hybrid-R™ (GeneAll, Seoul, Korea) according to the manufacturer's instructions. Isolated RNA (1 μg) with random hexamers and M-MLV (Promega, Madison, WI) was used to synthesize cDNA. The PCR reaction was performed with 2 μl of cDNA, 1× GoTaq® green master mix (Promega), and specific target primers (Table 4) under the following reaction conditions: initial denaturation at 94°C for 5 min and then 35 cycles of 94°C for 40 s, each of the annealing temperatures for 40 s, 72°C for 1 min, and an extension at 72°C for 1 min, followed by a final extension at 72°C for 7 min. The PCR products were loaded on 1.6% agarose gel for electrophoresis and analyzed with an ABI Prism 3730 XL DNA Analyzer (Applied Biosystems, Foster City, CA) to confirm the channel mRNA expression in each of the three cancer cells.

Western blotting

Cells were lysed using RIPA buffer (Sigma), and the total protein concentration was measured with a BCA protein assay kit (Pierce, Rockford, IL). The quantified protein was loaded on a 10% acrylamide gel for SDS-PAGE and then transferred to a nitrocellulose membrane (Whatman, Maidstone, Kent). Then, 1X TBS-Tween 20 containing 5% nonfat milk (Difco, Franklin Lakes, NJ) was used to block non-specific antibody binding, and protein-transferred membranes were probed overnight with commercially purchased primary antibodies targeting the proteins HIF-1α, Kv3.1, Kv3.3 (Abcam, Cambridge, MA), Kv3.4 (Alomone labs, Jerusalem, Israel), tERK, pERK (Cell Signaling Technology, Inc., Danvers, MA), β-actin, or vinculin (Santa Cruz Biotechnology, Dallas, TX). Membranes probed with primary antibodies were incubated with horseradish peroxidase–conjugated goat, anti-rabbit or anti-mouse secondary antibody (GenDEPOT, Barker, TX) for 1 hour and visualized using a WesternBright™ Quantum™ (Advansta, Menlo Park, CA). An ImageQuant LAS 4000 image analyzer (GE Healthcare Life Sciences, Songdo, Korea) was used to visualize immunocomplexes, and ImageJ software (National Institutes of Health) was used to quantify the data.

ROS detection

ROS levels were analyzed using 2′,7′-dichlorodihydrofluorescein diacetate (H2DCFDA) (Invitrogen, Carlsbad, CA). Cells were plated at different cell densities, cultured until they reached an appropriate cell density, and then washed twice with DPBS followed by a 30 minute incubation with 37°C DPBS containing 5 μM H2DCFDA. Finally, the cells were incubated for 15 minutes with fresh medium to allow recovery. Fluorescence images were taken using an EVOStm fl Digital Inverted Fluorescence Microscope (Fisher Scientific, Paisley, UK). The images were analyzed using ImageJ software (National Institutes of Health, Bethesda, MD).

Cell proliferation assay

Cell proliferation was measured using an MTT assay (Sigma). Cells seeded in a 96-well plate were incubated with 5 mg/ml MTT solution for 2 hours. After the incubation, the formazan crystals in each well were dissolved in 100 μl of dimethyl sulfoxide (DMSO), and the absorbance was measured at 570 nm. In addition to the MTT assay, the proliferation of cells seeded in a 6-well plate was visualized with Hemacolor® rapid staining (Millipore, Billerica, MA) according

to the manufacturer's instructions. Each of the three Hemacolor® rapid staining solutions was applied for 1 minute to stain the cells. Cells were washed with DPBS after the Hemacolor® rapid staining.

Cell migration and invasion assay

Cell migration was tested with a 2-well culture insert in a 35-mm dish purchased from ibidi (ibidi, Martinsried, Germany) according to the manufacturer's instructions. Briefly, an appropriate number of A549 (5×10^4), MDA-MB-231 (7×10^4), HT-29 (2×10^5), or L-132 (5×10^4) cells was seeded in the 2-well culture insert and incubated for one day. After the culture-insert was removed, the cells were incubated again to observe their migration to the empty space in the well.

Cell invasion was confirmed with a 24-well culture insert (SPL) for a transwell invasion assay. A549 (7×10^4), MDA-MB-231 (7×10^4) or L-132 (7×10^4) cells were placed on the upper layer of a cell-permeable membrane with FBS-free medium, and medium containing 10% FBS was placed below the cell-permeable membrane. Following 24 hour incubation, the cells that migrated through the membrane were stained via Hemacolor® (Millipore) and counted using ImageJ software (National Institutes of Health).

Acridine orange staining

A low or high density of A549 and L-132 cells was seeded in a 35-mm confocal dish (SPL), and the seeding cell density was same used in 6-well plates (Table 3). After 24 h of incubation, BDS-II treatment was applied until the cells reached the required cell density (approximately 30 hours). Cells were incubated with acridine orange (2 μg/ml) (Sigma, St, Louis, MO) for 15 minutes and then washed twice using prewarmed DPBS, and the plate containing the cells was filled again with 2 ml of DPBS. Fluorescence images were acquired with an LSM710 confocal microscope (Carl Zeiss, Hallbergmoos, Germany). The acridine orange signal was detected after 488 nm excitation at an emission wavelength of 543 nm for monomer type or 633 nm for dimer type. The images were analyzed using ImageJ software (National Institutes of Health, Bethesda, MD).

siRNA transfection

Cells were transfected with 60 nM siRNA-Kv3.1 or siRNA-Kv3.4 (Santa Cruz Biotechnology) and Lipofectamine™ 3000 reagent (Invitrogen) following the manufacturer's instructions for adherent cells. Mock control and control siRNA

transfection (Santa Cruz Biotechnology) were used as negative controls. Briefly, the A549 cells (1 x 10^5) were plated in 6-well plates and incubated for 24 hours prior to the transfection step in RPMI 1640 (Welgene, Daegu, Korea) containing 10% FBS without antibiotics. After 24 hours of incubation, the cells were transfected using siRNA-Kv3.1 or siRNA-Kv3.4. After 48 hours of transfection, the transfected cells were transferred to the cell migration kit and cell invasion kit to confirm the cell migration and invasion. The transfected cells were also transferred to a new 6-well plate at high density to confirm ERK activation.

Statistical analysis

All data are shown as the mean ± standard error (SE). Student's *t*-test was applied for statistical analysis of two groups of data, and one-way ANOVA with Tukey's post hoc test was used for more than two groups of data. Two-way ANOVA was used for analysis of the acridine orange staining data in Figure 22 (GraphPad Prism version 5.0).

Table 3. Cell seeding numbers

Culture place	Cell line	Cell density	Number of cells	Culture time
6-well plate	A549	low	2×10^4	2~3 days
		med	4×10^4	
		high	1.2×10^5	
	MDA-MB-231	low	2×10^4	
		med	4×10^4	
		high	1.2×10^5	
	HT-29	low	5×10^4	
		med	1.5×10^5	
		high	5×10^5	
	L-132	low	1×10^4	
		med	4×10^4	
		high	1.2×10^5	
100 mm dish	A549	low	2×10^5	2~3 days
		med	4×10^5	
		high	1×10^6	
	MDA-MB-231	low	2×10^5	
		med	4×10^5	
		high	1×10^6	
	HT-29	low	5×10^5	
		med	1.5×10^6	
		high	1×10^7	

Table 4. RT-PCR primers for Kv channel screening in A549, MDA-MB-231, HT-29, and L-132 cells

Subtype	Accession No.	Size (bp)	Primer sequence (Forward/Reverse)	Annealing (°C)
Kv1.2	L02752	513	5'-GGGACAGAGTTGGCTGAGAA-3' 5'-GGAGGATGGGATCTTTGGAC-3'	60
Kv1.5	M55513	917	5'-TGCGTCATCTGGTTCACCTTCG-3' 5'-TGTTCAGCAAGCCTCCCATTCC-3'	60
Kv2.1	L02840	451	5'-GGAAGCCTGCTGTCTTCTTG-3' 5'-CTTCATCTGAGAGCCCAAGG-3'	65
Kv3.1	S56770	550	5'-AACCCCATCGTGAACAAGACGG-3' 5'-TCATGGTGACCACGGCCCA-3'	60
Kv3.3	AF055989	284	5'-CCTCATCTCCATCACCACCT-3' 5'-CGAGATAGAAGGGCAGGATG-3'	60
Kv3.4	M64676	631	5'-TTCAAGCTCACACGCCACTTCG-3' 5'-TGCCAAATCCCAAGGTCTGAGG-3'	65
Kv4.2	NM_012281.2	157	5'-GCCTTCTTCTGCTTGGACAC-3' 5'-TCATCACCAGCCCAATGTAA-3'	60
Kv9.3	AF043472	395	5'-CTGGGGAAGCTGCTTACTTG-3' 5'-CAGATTTTCTTCCGGAGCTG-3'	60

RESULTS

Increases in HIF-1α and ROS levels related to increased cell density

A549, MDA-MB-231, and HT-29 cells were cultured until they reached optimal cell confluency. A low cell density was defined as approximately 20~30% cell confluency, a medium cell density was approximately 40~60% cell confluency, and a high cell density was over 80% confluency. The representative cell-seeding conditions for each of the cell lines are presented in Figure 17.

HIF-1α expression, which represents cell density-related pericellular hypoxia, increased approximately 4-fold and 6-fold in A549 and MDA-MB-231 cells, respectively, according to the increase in cell density, whereas HIF-1α expression did not significantly increase in HT-29 cells (Figure 18A). ROS levels also increased in A549 and MDA-MB-231 cells according to the increase in cell density. In HT-29 cells, only cells cultured at a high density showed significantly higher ROS levels than the low-density cultured cells (Figure 18B).

mRNA and protein expression changes according to increased cell density

RT-PCR analysis demonstrated that among the 8 oxygen-sensitive Kv channels

(Patel and Honore, 2001), Kv3.1, Kv3.3, and Kv3.4 were highly expressed in A549, MDA-MB-231, and HT-29 cells (Figure 19). Even though several Kv channels, including Kv1.2, Kv2.1, and Kv9.3, were also expressed in the cell lines, the three Kv3 subfamilies were commonly and stably expressed in all of the cell lines (Figure 19A). The Kv3.1 and Kv3.4 protein expression levels were increased in a cell density-dependent manner in A549 cells (Figure 19B). However, Kv3.3 protein expression in A549 cells was not altered by cell density (Figure 19B). Therefore, it was decided to focus on the Kv3.1 and Kv3.4 protein expression levels in the other two cell lines. The same increase in the Kv3.1 and Kv3.4 expression levels was observed according to cell density in MDA-MB-231 cells (Figure 19C). However, in HT-29 cells, Kv3.1 expression was only increased in the high-density cells and not in those cultured at a medium density (Figure 19D). Interestingly, unlike Kv3.1 in A549 and MDA-MB-231 cells, Kv3.4 expression was not increased in HT-29 cells in a cell density-dependent manner (Figure 19D).

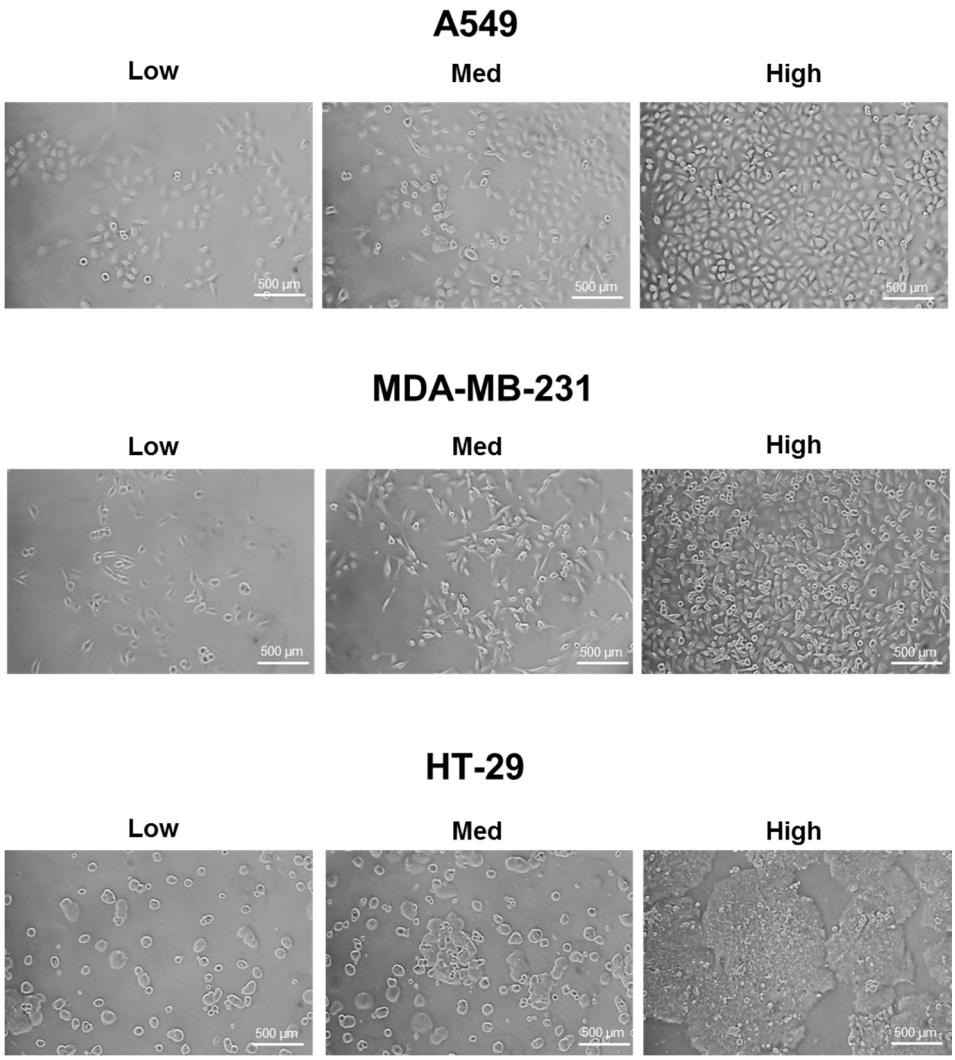
A549
Low
Med
High
500 µm
500 µm
500 µm
MDA-MB-231
Low
Med
High
500 µm
500 µm
500 µm
HT-29
Low
Med
High
500 µm
500 µm
500 µm

Figure 17. The three cell confluency conditions of A549, MDA-MB-231, and HT-29 cells A549, MDA-MB-231, and HT-29 cells were grown until they reached the appropriate cell densities. Low cell density was defined as approximately 20~30% cell confluency, medium density as approximately 40~60% cell confluency, and high density as approximately 80~90% cell confluency. Representative images of each cell condition are shown in the figure.

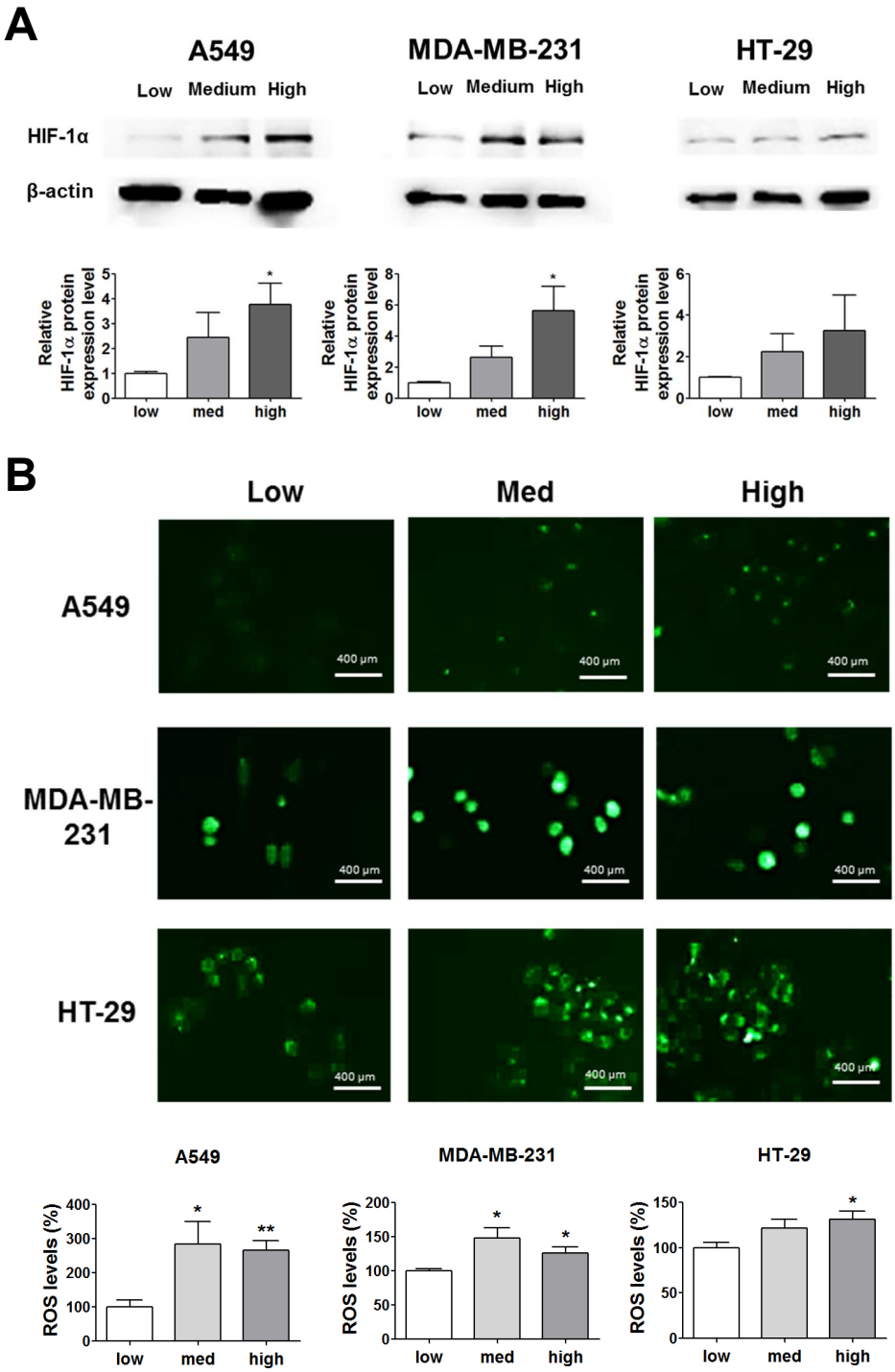
A
A549
MDA-MB-231
HT-29
Low Medium High
HIF-1α
β-actin
Relative HIF-1α protein expression level
low med high
B
Low
Med
High
A549
MDA-MB-231
HT-29
400 μm
ROS levels (%)
low med high

Figure 18. Increased pericellular hypoxia and ROS levels according to the increase in cell density (A) Western blot data demonstrate that HIF-1α expression, which was considered to be induced by pericellular hypoxia in the experiments, was significantly higher in high-density A549 and MDA-MB-231 cells than in low-density A549 and MDA-MB-231 cells, whereas HIF-1α expression was not increased in high-density HT-29 cells compared with that in low-density HT-29 cells. The cells cultured at a medium density did not show a significant increase in the HIF-1α expression level compared with that in the low-density cells. (B) Representative images show increased ROS signals (green) according to the increase in cell density. The graphs show the quantitative analysis of the ROS data. ROS levels were significantly increased with an increase in cell density in A549 and MDA-MB-231 cells, whereas ROS levels in HT-29 cells were significantly increased only when the cells were cultured at a high density. All experiments were performed in triplicate, and the data represent the mean ± standard error. *$p<0.05$ and **$p<0.01$ versus the low-density value.

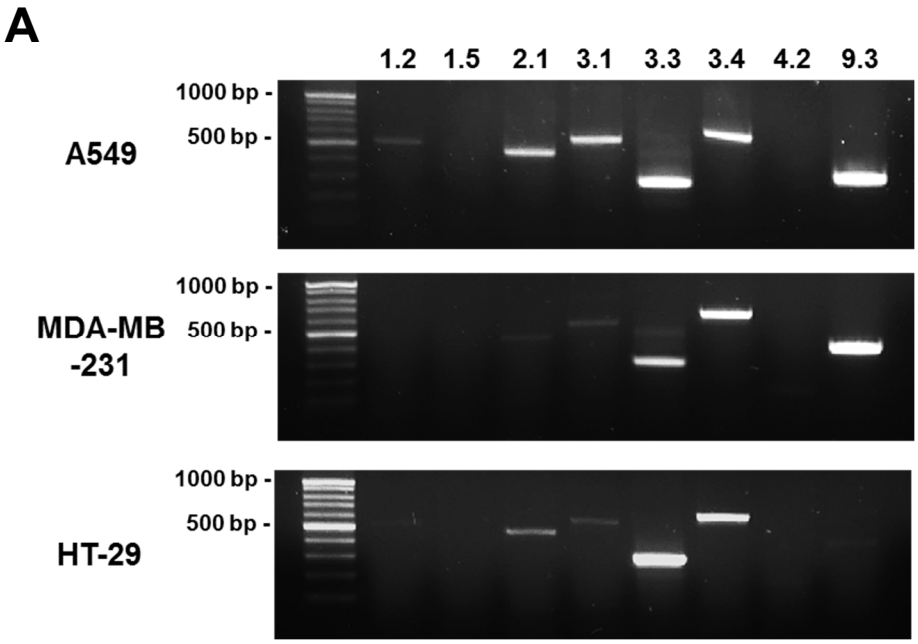
A
1.2
1.5
2.1
3.1
3.3
3.4
4.2
9.3
1000 bp -
500 bp -
A549
MDA-MB
-231
HT-29

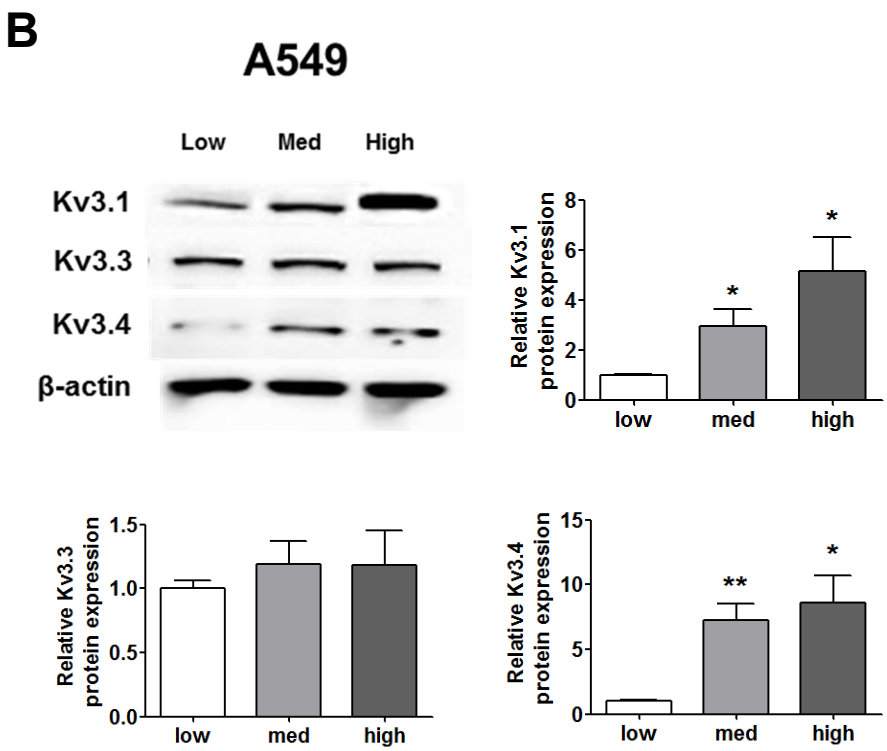
B
A549
Low
Med
High
Kv3.1
Kv3.3
Kv3.4
β-actin
Relative Kv3.1
protein expression
Relative Kv3.3
protein expression
Relative Kv3.4
protein expression
low
med
high

C

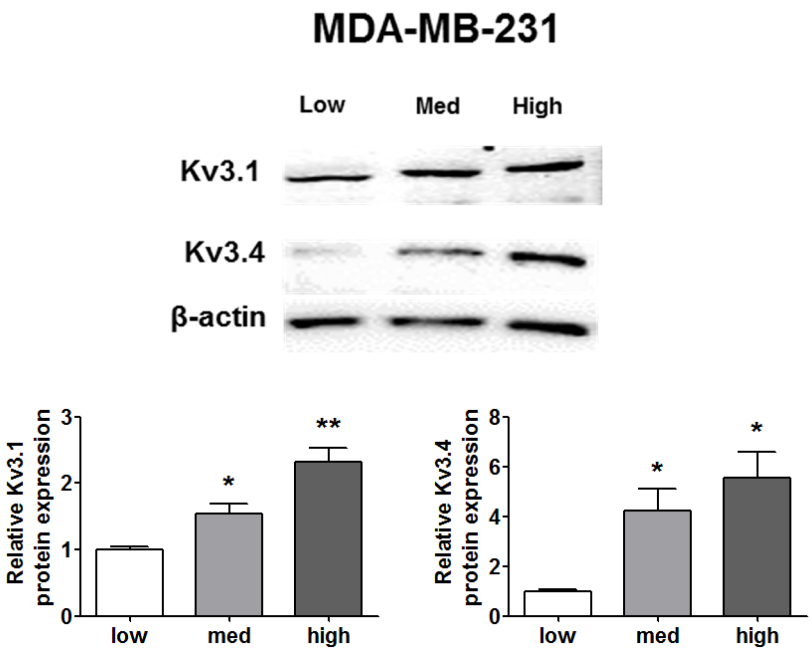
MDA-MB-231
Low
Med
High
Kv3.1
Kv3.4
β-actin
Relative Kv3.1 protein expression
Relative Kv3.4 protein expression
low
med
high

D

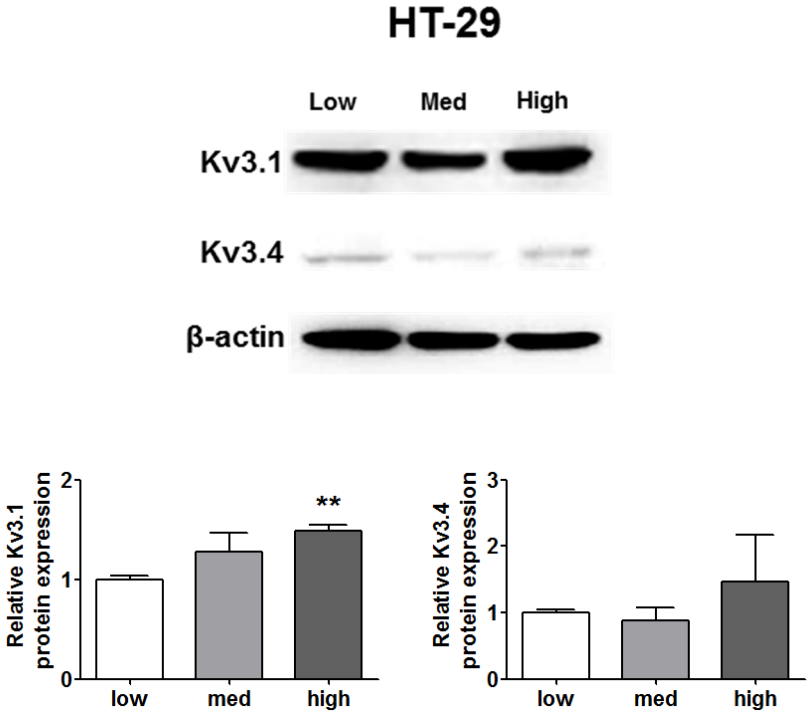
HT-29
Low
Med
High
Kv3.1
Kv3.4
β-actin
Relative Kv3.1 protein expression
Relative Kv3.4 protein expression
low
med
high

Figure 19. Changes in mRNA and protein expression of Kv3.1, Kv3.3, and Kv3.4 according to cell density (A) RT-PCR data demonstrating that Kv3.1, Kv3.3, and Kv3.4 mRNA was expressed in A549, MDA-MB-231, and HT-29 cells. (B) The protein expression levels of Kv3.1, Kv3.3, and Kv3.4 were analyzed by western blot. Kv3.1 and Kv3.4 were increased in A549 cells dependent on the cell density, whereas Kv3.3 was not altered according to the cell density. (C), (D) Kv3.1 and Kv3.4 protein expression levels, which were cell density-dependently increased in A549 cells, were also analyzed in MDA-MB-231 and HT-29 cells by western blot. Kv3.1 and Kv3.4 were increased in MDA-MB-231 cells according to the increase in cell density. Only Kv3.1 was significantly increased in high-density HT-29 cells compared to that in low-density HT-29 cells. Unlike A549 and MDA-MB-231 cells, which showed changes in Kv3.4 expression, Kv3.4 expression was not significantly increased in HT-29 cells as the cell density increased. All experiments were performed in triplicate, and the data represent the mean ± standard error. *$p<0.05$ and **$p<0.01$ versus the low-density value.

The effect of BDS-II-mediated Kv3.1 and Kv3.4 inhibition on cell proliferation, migration, and invasion

The effect of blood depressing substance-II (BDS-II) on cell proliferation and cell movement was investigated. Cells cultured at a low or medium density were tested to investigate the effect of 500 nM BDS-II on cell proliferation, and an effect of BDS-II on cell proliferation in A549, MDA-MB-231, or HT-29 cells was not observed (Figure 20A). However, it was found that 500 nM BDS-II affected cell migration and invasion. After 24 h of BDS-II treatment, the cell migration area was reduced by almost half in A549, MDA-MB-231, and HT-29 cells compared with that in the control group (Figure 20B). Cell migration was also inhibited by knockdown of Kv3.4 (Figure 21D), a specific target of BDS-II, using siRNA in A549 cells, whereas Kv3.1 downregulation (Figure 21A) did not have any effect on cell migration (Figure 21B and 21E). The number of invasive cells was significantly reduced by 500 nM BDS-II in A549 and MDA-MB-231 cells (Figure 20C). Knockdown of Kv3.1 or Kv3.4 also efficiently inhibited A549 cell invasion (Figure 21C and 21F). However, almost no invasive cells was observed in the HT-29 cultures, even though Matrigel was used in those experiments.

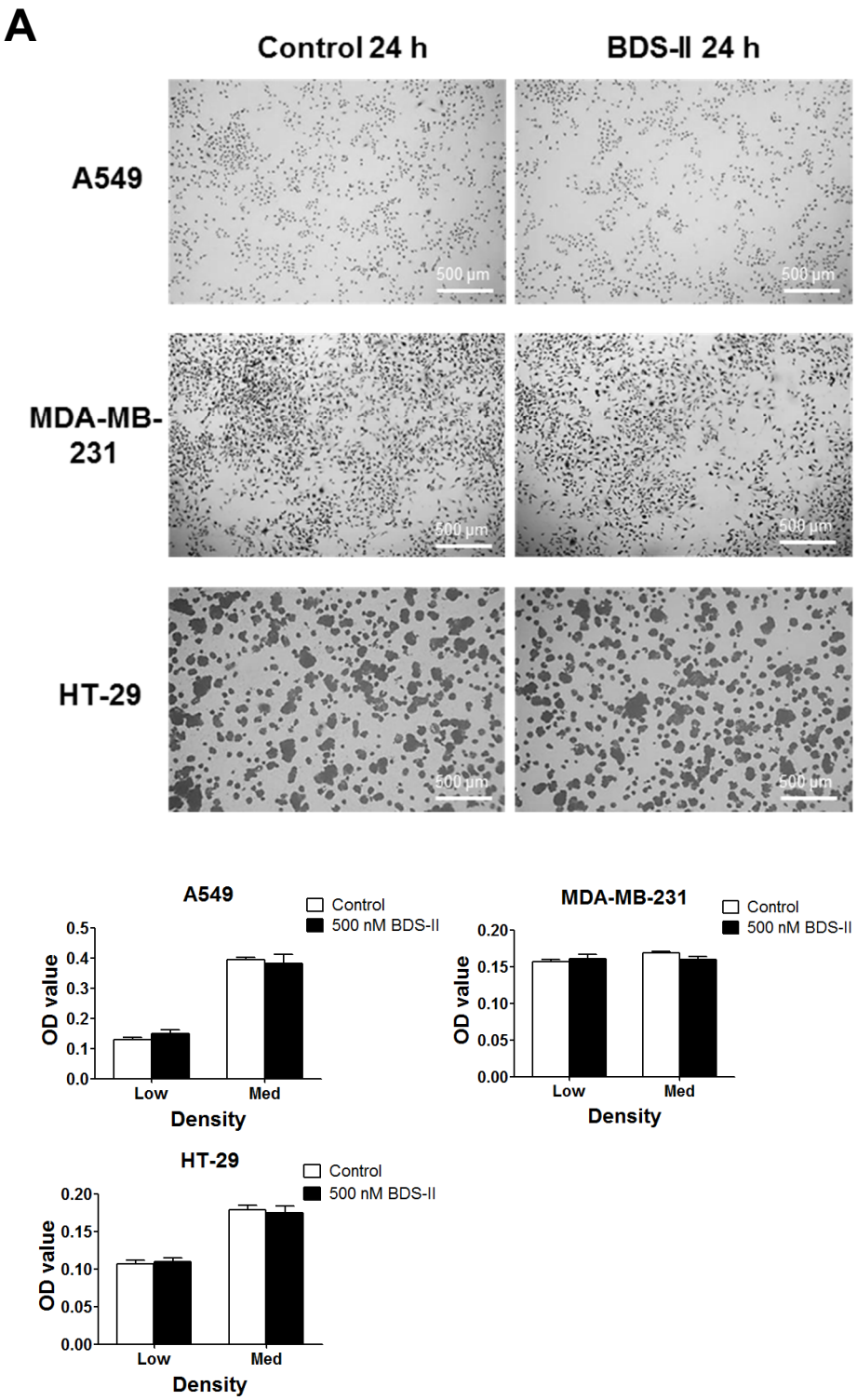
A
Control 24 h
BDS-II 24 h
A549
MDA-MB-231
HT-29
500 μm
A549
Control
500 nM BDS-II
OD value
0.0
0.1
0.2
0.3
0.4
0.5
Low
Med
Density
MDA-MB-231
Control
500 nM BDS-II
OD value
0.00
0.05
0.10
0.15
0.20
Low
Med
Density
HT-29
Control
500 nM BDS-II
OD value
0.00
0.05
0.10
0.15
0.20
Low
Med
Density

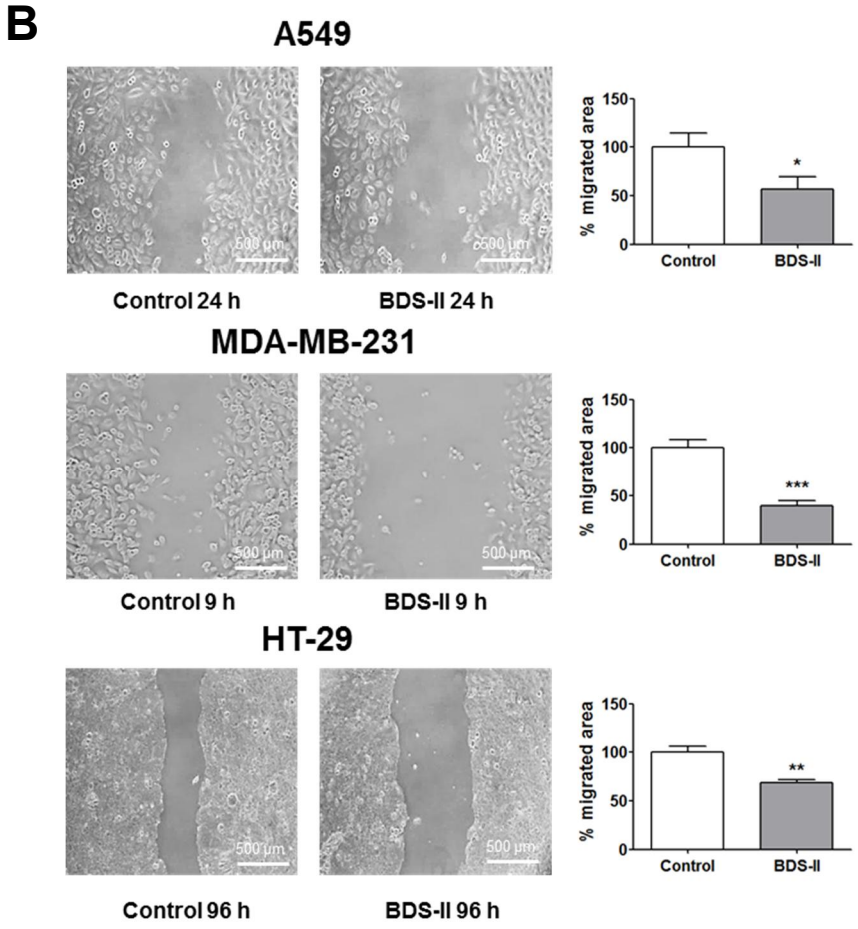
B
A549
500 μm
500 μm
% migrated area
150
100
50
0
*
Control
BDS-II
Control 24 h
BDS-II 24 h
MDA-MB-231
500 μm
500 μm
% migrated area
150
100
50
0
***
Control
BDS-II
Control 9 h
BDS-II 9 h
HT-29
500 μm
500 μm
% migrated area
150
100
50
0
**
Control
BDS-II
Control 96 h
BDS-II 96 h

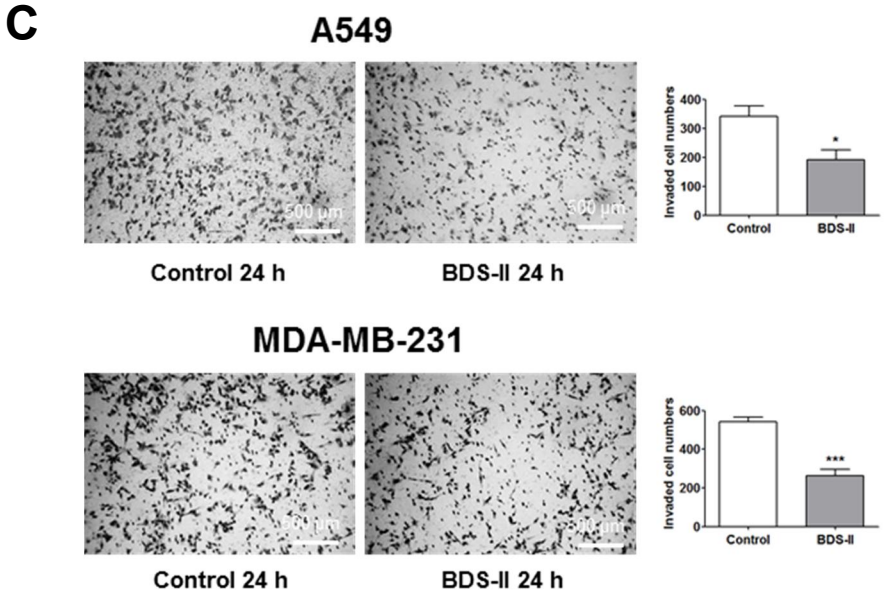
C
A549
500 μm
500 μm
Invaded cell numbers
400
300
200
100
0
*
Control
BDS-II
Control 24 h
BDS-II 24 h
MDA-MB-231
Invaded cell numbers
600
400
200
0
***
Control
BDS-II
Control 24 h
BDS-II 24 h

Figure 20. Effect of BDS-II on cell proliferation, migration, and invasion (A) Hemacolor® rapid staining was only performed in cells cultured at a medium density, and the MTT assay was performed in cells cultured at a low density and medium density. Representative Hemacolor® rapid staining images demonstrate that 24 h of 500 nM BDS-II treatment did not affect the proliferation of A549, MDA-MB-231, and HT-29 cells. MTT data are shown in graphical form. The MTT data also demonstrated that BDS-II did not affect cell proliferation in the three cell lines. (B) Cell migration was observed until the cells covered almost all of the empty space between the culture insert (A549: 48 h, MDA-MB-231: 24 h, and HT-29: 120 h). Representative images demonstrate that 500 nM BDS-II significantly inhibited migration by almost half in A549, MDA-MB-231, and HT-29 cells. The graphs show the quantified percentage of the migration area in the control and BDS-II-treated groups. (C) Hemacolor® rapid staining images demonstrate that the number of cells that migrated through the membrane was reduced in A549 and MDA-MB-231 cells by 500 nM BDS-II treatment. The graphs show the quantification of the invasive cell numbers in the control and BDS-II-treated groups. All experiments were performed in triplicate or quadruplicate, and the data represent the mean ± standard error. *$p<0.05$, **$p<0.01$, and ***$p<0.001$ versus the control value.

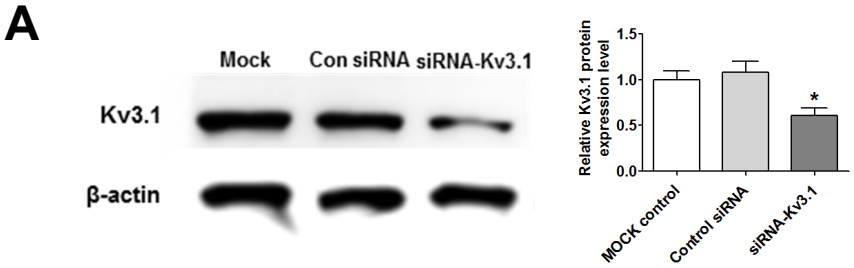
A
Mock
Con siRNA
siRNA-Kv3.1
Kv3.1
β-actin
Relative Kv3.1 protein expression level
1.5
1.0
0.5
0.0
*
MOCK control
Control siRNA
siRNA-Kv3.1

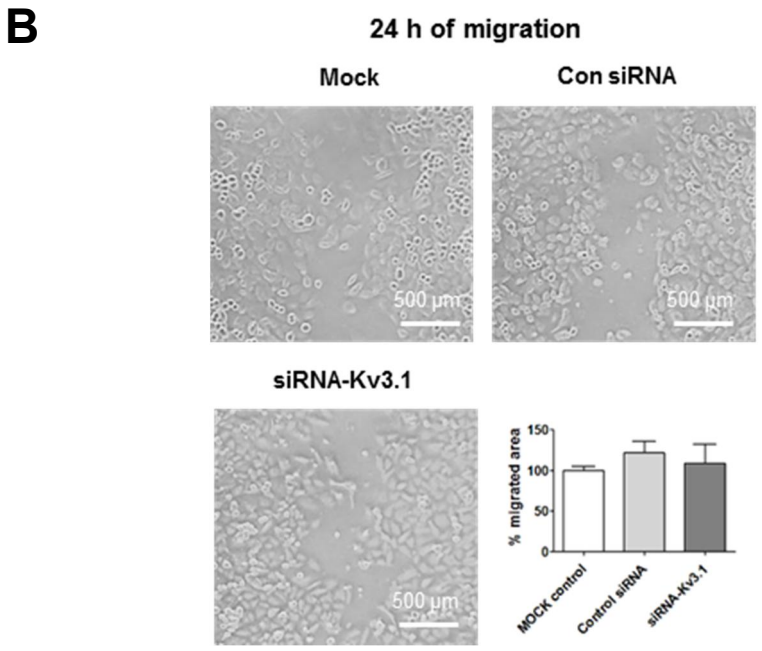
B
24 h of migration
Mock
Con siRNA
500 μm
500 μm
siRNA-Kv3.1
500 μm
% migrated area
150
100
50
0
MOCK control
Control siRNA
siRNA-Kv3.1

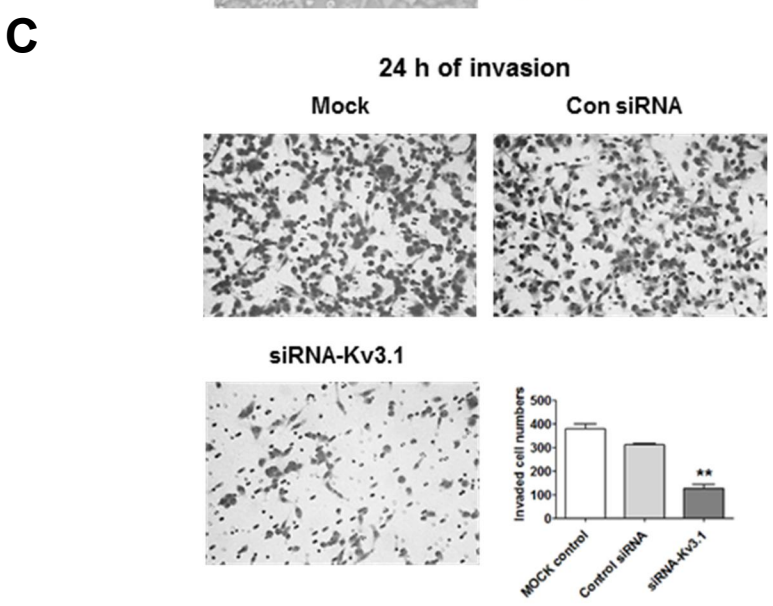
C
24 h of invasion
Mock
Con siRNA
siRNA-Kv3.1
Invaded cell numbers
500
400
300
200
100
0
**
MOCK control
Control siRNA
siRNA-Kv3.1


D
Mock
Con siRNA
siRNA-Kv3.4
Kv3.4
Vinculin
Relative Kv3.4 protein expression level
1.5
1.0
0.5
0.0
*
MOCK control
Control siRNA
siRNA-Kv3.4

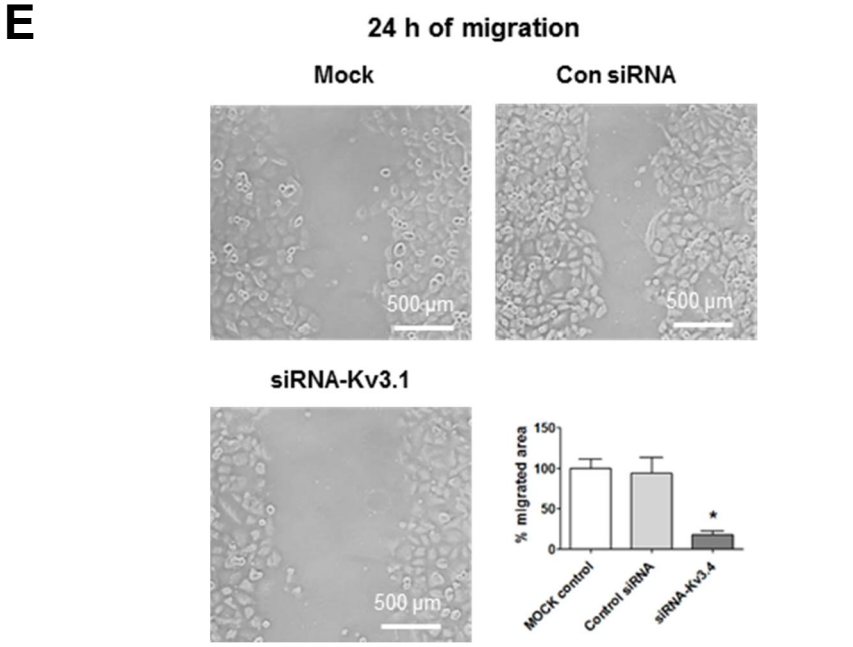
E
24 h of migration
Mock
Con siRNA
500 μm
500 μm
siRNA-Kv3.1
500 μm
% migrated area
150
100
50
0
*
MOCK control
Control siRNA
siRNA-Kv3.4

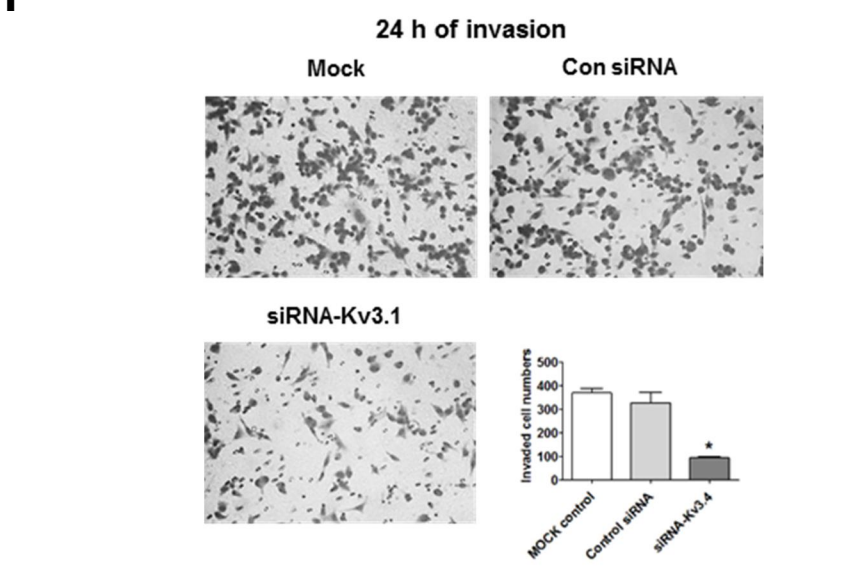
F
24 h of invasion
Mock
Con siRNA
siRNA-Kv3.1
Invaded cell numbers
500
400
300
200
100
0
*
MOCK control
Control siRNA
siRNA-Kv3.4

Figure 21. The effect of Kv3.1 or Kv3.4 downregulation using siRNA on A549 cell migration and invasion (A), (D) Kv3.1 and Kv3.4 were efficiently downregulated by siRNA-Kv3.1 and siRNA-Kv3.4, respectively. (B), (E) siRNA-Kv3.1 did not have an effect on A549 cell migration, whereas siRNA-Kv3.4 significantly inhibited A549 cell migration. (C), (F) A549 cell invasion was significantly inhibited by siRNA-Kv3.1 or siRNA-Kv3.4.

Cell density-dependent Kv channel expression and the effect of BDS-II on L-132 cells

Next, it was determined whether the observed phenomena were cancer specific or not. The same experiments using L-132 cells, a normal human lung cell line, were performed. RT-PCR analysis demonstrated that L-132 cells also highly express Kv3.1, Kv3.3, and Kv3.4 (Figure 22A); however, unlike A549 cells, the expression levels of Kv3.1, Kv3.3, and Kv3.4 were not increased according to cell density in L-132 cells (Figure 22B). In addition, 500 nM BDS-II did not have an effect on L-132 cell migration and invasion (Figure 22C and 22D).

Cell density-dependent alterations in the diameter of acidic compartments in A549 and L-132 cells

It was found that the number of small (0.4-0.6 μm) acidic compartments (Okamoto et al., 2008) in A549 and L-132 cells was significantly increased and that the number of large (1-1.2 μm) acidic compartments in A549 and L-132 cells was decreased when the cells reached high density compared with those of the low-density cells (Figure 23A and 23C). Therefore, how BDS-II affects this cell density-dependent alteration was investigated. When A549 cells were

cultured at a low density, BDS-II did not have an effect on the intracellular acidic compartments in A549 cells, whereas when A549 cells were cultured at a high density, 500 nM BDS-II decreased the number of small (0.4-0.6 and 0.8-1.0 μm) acidic compartments and increased the number of large (1-1.2 μm) acidic compartments (Figure 23B). In contrast, 500 nM BDS-II had little effect on L-132 cells cultured at either a low or high density (Figure 23D).

Effect of BDS-II on ERK activation according to increased A549 and L-132 cell density

It was found that ERK activation was higher in high-density cultured A549 cells compared with that in low-density cultured A549 cells (Figure 24A), whereas L-132 cells showed no cell density-related changes in ERK activation (Figure 24B). BDS-II had no effect on ERK activation when either A549 or L-132 cells were cultured at a low or medium density; however, when A549 or L-132 cells were cultured at a high density, BDS-II inhibited ERK activation (Figure 24A and 24B). BDS-II (500 nM) treatment induced the same effect in both cell lines. Knockdown of Kv3.1 or Kv3.4 using siRNA also inhibited ERK activation (Figure 24C and 24D).

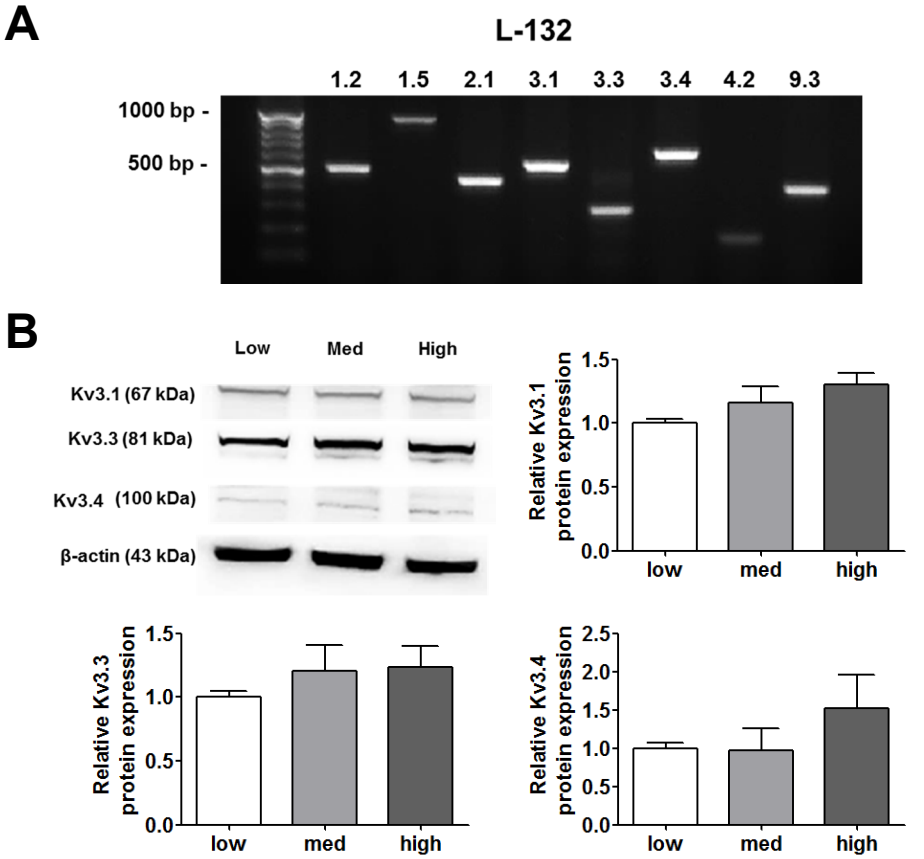
A
L-132
1.2
1.5
2.1
3.1
3.3
3.4
4.2
9.3
1000 bp -
500 bp -
B
Low
Med
High
Kv3.1 (67 kDa)
Kv3.3 (81 kDa)
Kv3.4 (100 kDa)
β-actin (43 kDa)
Relative Kv3.1 protein expression
Relative Kv3.3 protein expression
Relative Kv3.4 protein expression
low
med
high
C
Control 10 h
BDS-II 10 h
% migrated area
Control
BDS-II
D
Control 24 h
BDS-II 24 h
Invaded cell numbers
Control
BDS-II

Figure 22. The expression of Kv3.1, Kv3.3, and Kv3.4 and the effect of BDS-II on L-132 cells (A) RT-PCR data demonstrate that L-132 cells express all of the 8 oxygen-sensitive Kv channels at the mRNA level. (B) The protein expression levels of Kv3.1, Kv3.3, and Kv3.4 were analyzed by western blot in L-132 cells. The expression of all three Kv channels was not significantly altered according to the cell density. (C) Cell migration was observed until the L-132 cells covered almost all of the empty space between the culture insert (approximately 24 hours). Representative images demonstrate that 500 nM BDS-II did not affect L-132 cell migration. The graph shows the quantified percentage of the migration area in the control and BDS-II-treated group. (D) Hemacolor® rapid staining images demonstrate that the number of L-132 cells that migrated through the membrane was not altered by 500 nM BDS-II treatment. The graph shows the quantification of the invasive cell numbers in the control and BDS-II-treated groups. All experiments were performed in quadruplicate, and the data represent the mean ± standard error.

A

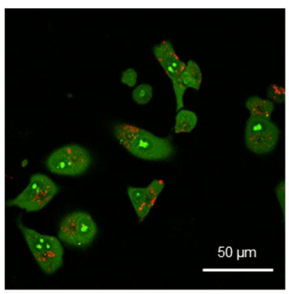

A549 low density

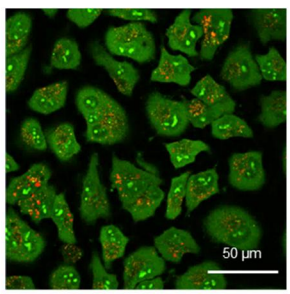

A549 high density

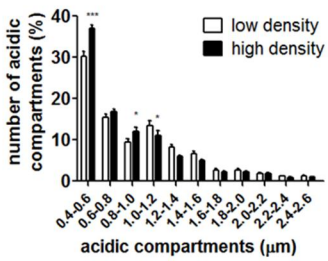

A549 low vs high

B

A549 low density

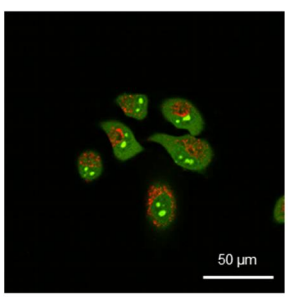

Control

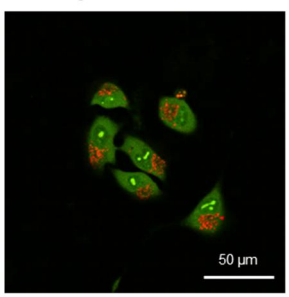

BDS-II

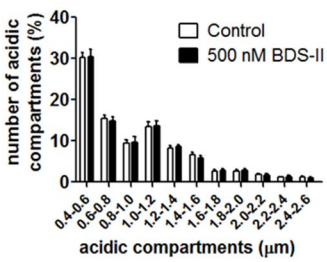

Control vs BDS-II

A549 high density

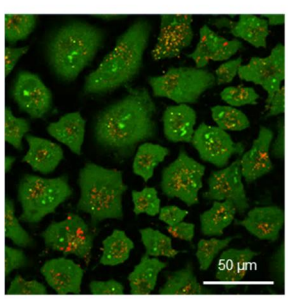

Control

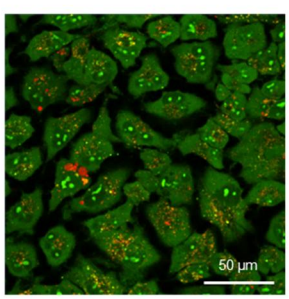

BDS-II

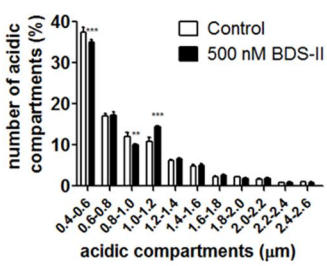

Control vs BDS-II

A

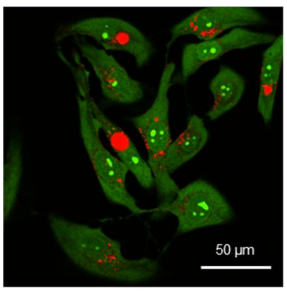

L-132 low density

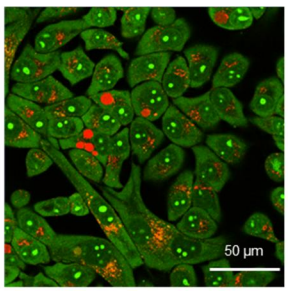

L-132 high density

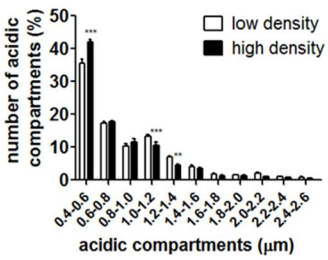

L-132 low vs high

B

L-132 low density

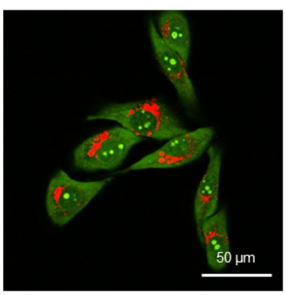

Control

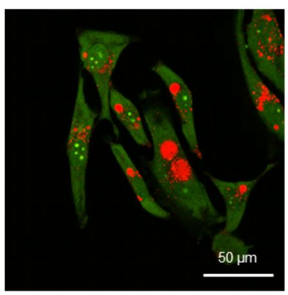

BDS-II

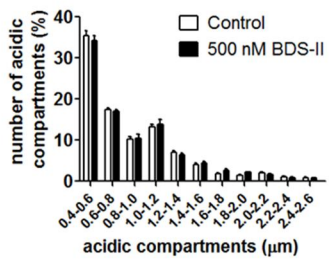

Control vs BDS-II

L-132 high density

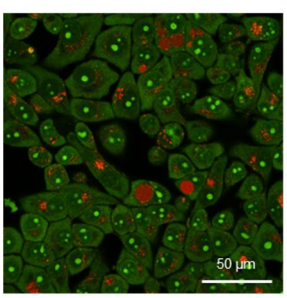

Control

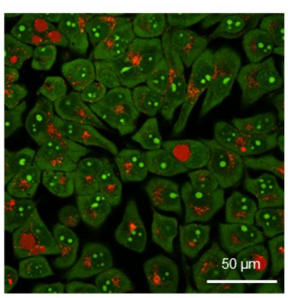

BDS-II

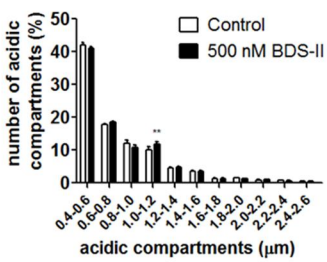

Control vs BDS-II

Figure 23. Acridine orange staining represents alterations in the diameter of acidic compartments in A549 and L-132 cells according to cell density

The orange-red fluorescence of acridine orange staining demonstrates the acidic compartments, including the intracellular organelles, and the yellow-green color indicates a slightly acidic or neutral pH. (A) The number of small (0.4-0.6 μm) acidic compartments in A549 cells was significantly increased and the number of large (1-1.2 μm) acidic compartments in A549 cells was decreased when the cells reached a high density compared to that of A549 cells at a low density. (B) When A549 cells were incubated with 500 nM BDS-II for 30 h, BDS-II had no effect on A549 cells cultured at a low density (n=13), whereas the same concentration of BDS-II decreased the number of small (0.4-0.6 and 0.8-1.0 μm) acidic compartments and increased the number of large (1-1.2 μm) acidic compartments in A549 cells cultured at a high density (n=17). (C) The number of small acidic compartments in L-132 cells was also significantly increased when the cells reached a high density compared with that of L-132 cells cultured at a low density. (D) L-132 cells were also incubated with 500 nM BDS-II for 30 h, and BDS-II had no effect on the size of the acidic compartments in L-132 cells cultured at either a low (n=13) or high density (n=17). The quantified graphs demonstrate the size of the acidic compartments

in the cells. The particle analysis function of ImageJ was used to analyze the images. All experiments were repeated the indicated number of times, and the data represent the mean ± standard error. *$p<0.05$, **$p<0.01$, and ***$p<0.001$ versus the control value.

A

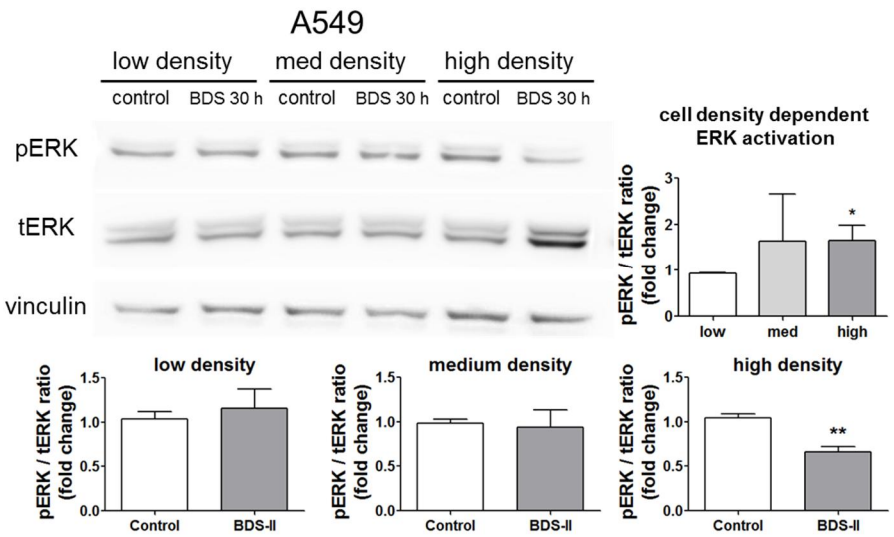
A549
low density
med density
high density
control
BDS 30 h
control
BDS 30 h
control
BDS 30 h
pERK
tERK
vinculin
cell density dependent
ERK activation
pERK / tERK ratio
(fold change)
low
med
high
*
low density
medium density
high density
Control
BDS-II
**

B

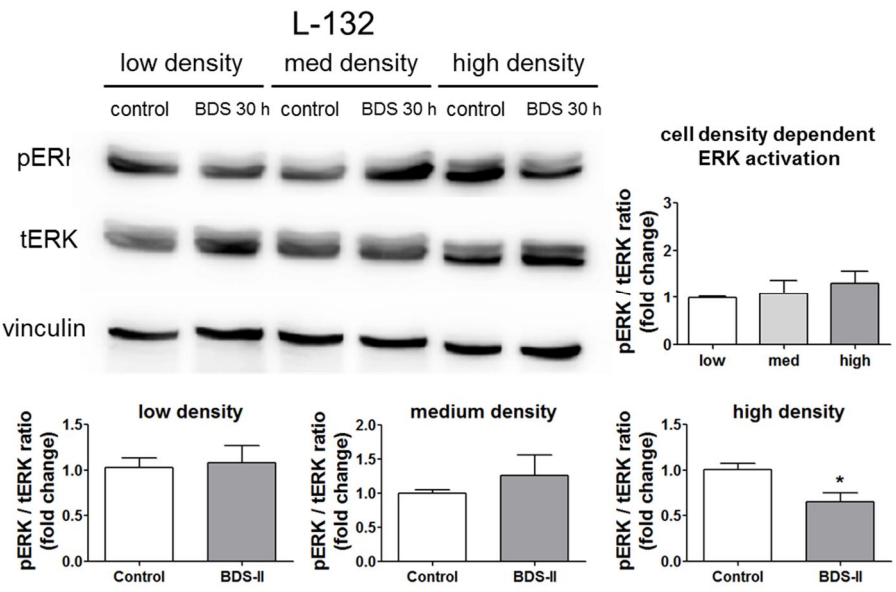
L-132
low density
med density
high density
control
BDS 30 h
control
BDS 30 h
control
BDS 30 h
pERK
tERK
vinculin
cell density dependent
ERK activation
pERK / tERK ratio
(fold change)
low
med
high
low density
medium density
high density
Control
BDS-II
*

C

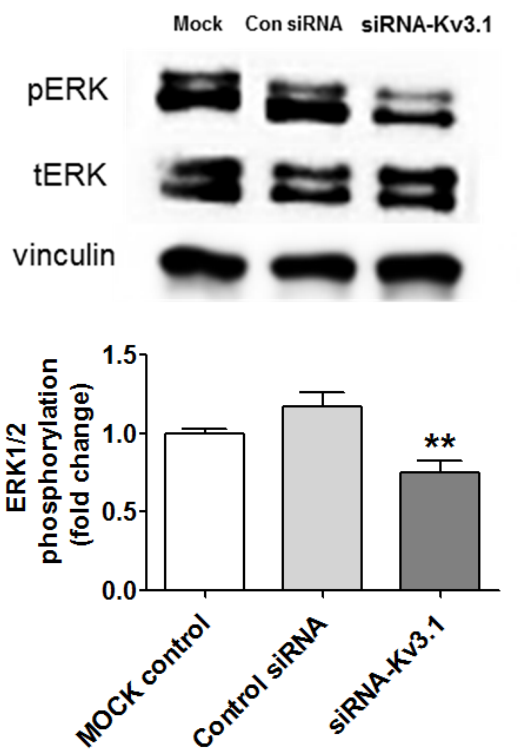
Mock
Con siRNA
siRNA-Kv3.1
pERK
tERK
vinculin
ERK1/2 phosphorylation (fold change)
1.5
1.0
0.5
0.0
**
MOCK control
Control siRNA
siRNA-Kv3.1

D

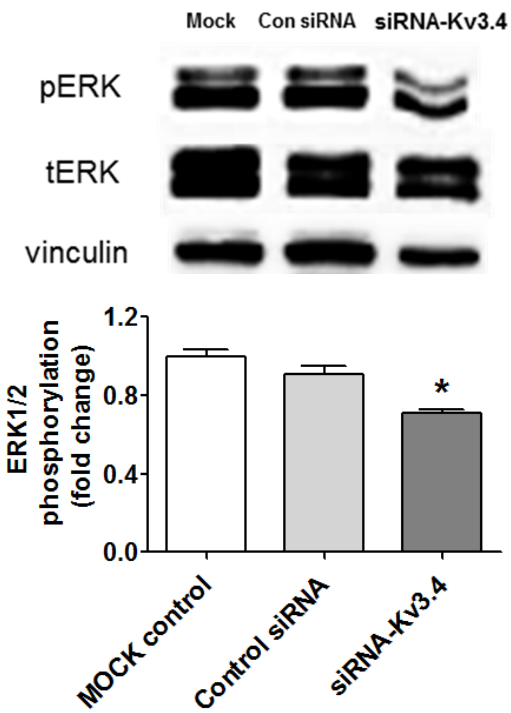
Mock
Con siRNA
siRNA-Kv3.4
pERK
tERK
vinculin
ERK1/2 phosphorylation (fold change)
1.2
0.8
0.4
0.0
*
MOCK control
Control siRNA
siRNA-Kv3.4

Figure 24. Effect of Kv3.1 and Kv3.4 downregulation using BDS-II and siRNA on ERK activation ERK activation according to the increase in cell density was analyzed in A549 and L-132 cells using the ratio of phosphorylated ERK (pERK) to total ERK (tERK) protein expression. (A) Quantitative data demonstrate that ERK was activated in A549 cells cultured at a high density compared with A549 cells cultured at a low density. ERK activation in medium-density A549 cells did not significantly differ from that in low-density A549 cells. (B) ERK activation was not altered according to the cell density in L-132 cells. When the cells were incubated with 500 nM BDS-II for 30 h, ERK activation in the high-density A549 or L-132 cells was inhibited. BDS-II had no effect on ERK activation in A549 or L-132 cells cultured at either a low or medium density. (C), (D) ERK activation in A549 cells was significantly inhibited by siRNA-Kv3.1 or siRNA-Kv3.4. All experiments were performed in triplicate, and the data represent the mean ± standard error. *$p<0.05$ and **$p<0.01$ versus the low-density or control value.

DISCUSSION

The relationship between tumors and microenvironmental changes around tumor cells during their growth, including hypoxia and oxidative damage accumulation, has been investigated in several previous studies (Bissell and Hines, 2011; Balkwill et al., 2012; Semenza, 2016). The microenvironment induces broad changes in gene and protein expression, metabolism, and extracellular matrix remodeling, and in turn, tumor cells may be forced to undergo metastasis, which involves escape from the primary tumor, seeding at distinct sites and cell growth (Vaupel, 2004; Joyce and Pollard, 2009; Gilkes et al., 2014; Spill et al., 2016). Metastasis is suggested to represent an integrated strategy for cancer cells to avoid oxidative damage and excessive ROS accumulation in the primary tumor site (Pani et al., 2010). This study tried to mimic the microenvironmental changes and tumor response in an *in vitro* system by increasing the cell density of highly aggressive lung, breast and colon cancer cell lines.

These data demonstrated a close relationship between several oxygen-sensitive Kv channel subunits and tumor hypoxia, as well as the importance of these channels in cancer progression. Kv3.1, Kv3.3, and Kv3.4 belong to the

Kv3 subfamily, which is a class of Kv channels characterized by positively shifted voltage dependencies and very fast deactivation rates (Rudy and McBain, 2001), and these Kv channels were examined as tumor hypoxia-related Kv channels in A549, MDA-MB-23, and HT-29 cells. Each of these cell lines is highly aggressive lung, breast, and colon cancer cell lines, and all three cell lines expressed Kv3.1, Kv3.3, and Kv3.4. A cell density-dependent increase in HIF-1α in A549 and MDA-MB-231 cells were observed, whereas HIF-1α was not significantly increased in a cell density-dependent manner in HT-29 cells, which grow in an aggregate form. Interestingly, Kv3.1 and Kv3.4 protein expression showed almost the same pattern as HIF-1α in all three cell lines, suggesting that Kv3.1 and Kv3.4 are tumor hypoxia-related Kv channels. In addition, it was also assumed that the cell density-dependent increases in Kv3.1 and Kv3.4 expression are a tumor cell-specific property because Kv3.1 and Kv3.4 were not increased in a cell density-dependent manner in L-132 cells, a normal cell line.

HIF-1α expression is increased by oxygen depletion or the balance between oxygen and oxidative stress (Bonello et al., 2007; Qutub and Popel, 2008; Hagen, 2012). Kv3.3 and Kv3.4 are oxygen-sensitive channels as well as oxidation-sensitive channels. Oxidation of a cysteine residue at the amino

terminus of the channels interrupts their capacity for rapid inactivation due to the formation of a disulfide bond, consequently increasing their electrophysiological function (Ruppersberg et al., 1991; Patel and Honore, 2001). Kv3.1 is also reported to have a potential role as an oxygen sensor (Osipenko et al., 2000). Based on the results, it was hypothesize that the same expression pattern between HIF-1α and the two Kv channels was caused by cell density-induced pericellular hypoxia. Furthermore, considering that HIF-1α has been reported to regulate Kv currents during chronic hypoxia or the mitochondrial pathway normally used for oxygen sensing (Shimoda et al., 2001; Bonnet et al., 2006), it was concluded that accumulated HIF-1α during cell growth might induce the increase in Kv3.1 and Kv3.4. In HT-29 cells, HIF-1α levels were not significantly increased with an increase in cell density. In this study, it was hypothesized that the HIF-1α accumulation induced by pericellular hypoxia might already be present in HT-29 cells because of their aggregated form (Marsters et al., 2014). The comparatively slight increase in the ROS level in HT-29 cells with the increase in cell density can also be interpreted in this scheme. Interestingly, despite the pre-existence of pericellular hypoxia, a cell density-dependent increase in Kv3.1 protein expression was observed when HT-29 cells were seeded at a high density.

Next, BDS-II, a Kv3 subfamily-specific blocker, was used to confirm whether the increased expression of Kv channels had a potential role in cell density regulation by avoiding hypoxia or oxidative damage during cell growth. When cells were treated with BDS-II, cancer cell migration and invasion were inhibited in all three cell lines without an effect on cancer cell proliferation. Cell migration and invasion are important in the initial steps of cancer metastasis, and metastatic cancer cells must go through several steps to spread to new parts of the body; cancer cells must break away from the primary tumor and enter the bloodstream by invading the blood vessels. Therefore, according to the data, Kv3.1 and Kv3.4, which are specific targets of BDS-II, may be good biomarkers and therapeutic targets for cancer metastasis. In fact, Kv3.4 has already been suggested to be a strong biomarker candidate for predicting the malignant progression of laryngeal epithelial precursor lesions (Rodrigo et al., 2012) or head and neck squamous cell carcinomas (Menendez et al., 2010).

Dysregulated pH is one of the hallmarks of cancer because cancer cells have a reversed pH gradient (a high intracellular pH (pH_i) >7.4 and a low extracellular pH (pH_e) of 6.7–7.1) and this reversed gradient enables cancer progression by promoting proliferation, evasion of apoptosis, metabolic adaptation, migration and invasion (Webb et al., 2011). Extracellular

acidification is one of the major features of tumor tissues, and acidic pH_e is known to stimulate metastatic potential by affecting several enzymes and the extracellular matrix (Webb et al., 2011; Damaghi et al., 2013; Kato et al., 2013). Cells cultured at a high density exhaust medium faster than cells cultured at a low density, which may cause a rapid drop in pH due to lactic acid production, a by-product of cellular metabolism; therefore, cells cultured at a high density are forced to adapt to microenvironmental alterations in pH. The data from this study demonstrate that cells cultured at a high density have a higher proportion of small acidic compartments than cells cultured at a low density. BDS-II increased the size of the acidic compartments in high-density cultured A549 cells, and the altered size of the acidic compartments seemed to be similar to the acidic compartments in A549 cells cultured at a low density. However, BDS-II had no effect on the size of the acidic compartments in A549 cells cultured at a low density or in L-132 cells. Considering that regulation of acidic compartments, including lysosomes and acidic vacuoles, is important for cancer progression and adaptation to alterations in the extracellular environment (Glunde et al., 2003; Fais et al., 2007), the data from this study suggest that BDS-II only inhibited the cell density-dependent microenvironmental adaptation of A549 cells, in which Kv3.1 and Kv3.4 were increased according

to the cell density. Furthermore, ROS levels and the two tumor hypoxia-related Kv channels were similarly increased according to cell density in all three cancer cell lines. As mentioned above, cancer may metastasize to avoid oxidative damage and excessive ROS accumulation at the primary tumor site (Pani et al., 2010). Along this line of speculation, Kv3.1 and Kv3.4 may be sensors of a poor microenvironment around cancer cells and that an increase in the expression of these channels forces cancer cells to initiate migration or invasion.

ROS levels were increased in a cell density-dependent manner in the three cancer cell lines. ROS induce ERK activation (Storz, 2005; Reuter et al., 2010), which is known to be linked to regulation of tumor cell proliferation, migration, and invasion (Jimenez et al., 1997; Storz, 2005; McCubrey et al., 2007; Reuter et al., 2010). Therefore, it could be inferred that ERK activation, induced by ROS production during cell growth, initiates cell migration or invasion to avoid oxidative damage and excessive ROS accumulation. Based on this scheme, it was hypothesized that BDS-II might inhibit cell migration and invasion by interrupting ERK activation along with the increase in cell density. In addition, previously, an altered redox environment upon contact inhibition was shown to enhance ERK inactivation by inhibiting MAP kinase

phosphatases (Wayne et al., 2006). Therefore, it can be also assumed that an altered redox system upon contact inhibition induced by Kv3.1 and Kv3.4 inhibition by BDS-II might inhibit ERK activation in high-density A549 cells. ERK activation in high-density cultured normal cells and malignant tumor cells is different. ERK activation is inhibited by cell-cell contact inhibition in non-tumorigenic cells (Zhang et al., 2002; Wayne et al., 2006), but malignant tumor cells, including MDA-MB-231 cells, show ERK activation when they are cultured at a high density (Zhang et al., 2002; Wayne et al., 2006). The data from this study demonstrate that although ERK was not inhibited in L-132 cells when the cells reached a high density, ERK was not activated in L-132 cells in a cell density-dependent manner; however, ERK was activated in A549 cells according to the cell density increment, which is consistent with the data of previous studies and it may explain why inhibition of ERK activation induced by BDS-II only affected A549 cell migration and invasion even though ERK activation was inhibited in both A549 and L-132 cells cultured at a high density. In addition, although Kv3.1 and Kv3.4 were not cell density-dependently increased in L-132 cells, BDS-II inhibited ERK activation in L-132 cells cultured at a high density. Therefore, it was concluded that BDS-II-sensitive Kv channels, including Kv3.1 and Kv3.4, are important and are related to ERK

activation when the cells reach a high density, and only cancer cells, including A549 cells, at a high density utilize this relationship to coordinate migration and invasion. This might be the reason that Kv3.1, Kv3.4 and ERK activation are increased in a cell density-dependent manner only in A549 cells. Because cell-cell contact inhibition is an important regulatory mechanism of cell growth, the loss of cell-cell contact inhibition through ERK activation may be related to an invasive tumor phenotype (Zhang et al., 2002), and the observed BDS-II effect may be obtained by inhibition of this tumorigenic property.

In summary, tumor hypoxia-related oxygen-sensitive Kv channels, including Kv3.1 and Kv3.4, were increased in a cell density-dependent manner in three representative tumor cell lines but not in L-132 cells, a normal cell line. BDS-II, which blocks the channels of the Kv3 subfamily, efficiently inhibited tumor cell migration and invasion but had no effect on tumor cell proliferation or normal cell migration and invasion. In addition, ERK activation and alterations in the diameter of acidic compartments, which were observed in a cell density-dependent manner in A549 cells, were inhibited by BDS-II, and inhibition of these cell density-dependent changes may be the key mechanism by which BDS-II inhibits tumor cell migration and invasion. These data indicate that Kv3.1 and Kv3.4 may be new therapeutic targets for cancer metastasis.

GENERAL CONCLUSION

Although oxidation sensing is a well-known Kv channel function, research into the specific role of Kv channels as oxidation-sensitive channels is scarce. Only a few Kv channels, i.e., Kv2.1, have been extensively investigated in this regard (Sesti et al., 2014; Yu et al., 2017). Increasing evidence indicates that oxidation-sensitive Kv channels have a pivotal role in oxidative stress-related disease and cell behavior. For example, it has been proposed that Kv3.4, one of the well-recognized oxidation-sensitive Kv channels, is closely associated with Alzheimer's disease and that oxidative stress is influential in the development of this common neurodegenerative disease (Pannaccione et al., 2007; Kim et al., 2015). However, there have been no interpretations dealing with the relationship between the oxidation sensitive Kv channel and oxidative stress.

An attempt was made in the current study to identify the roles of oxidation-sensitive Kv channels in oxidative stress-related disease and in relation to cell behavior. It was demonstrated that Kv3.1, Kv3.3, and Kv3.4 were responsible for a number of functions in several different types of cells. Kv3.1 and Kv3.4 were involved in tumor hypoxia-related cancer cell migration and invasion. It was found that Kv3.4 was pivotal in the death of MPP^+-induced human neuroblastoma SH-SY5Y cells, while HIF-1α inhibited Kv3.4 to protect the cells against oxidative stress-induced neural cell death. Kv3.3 was involved in hemin-induced human leukemia cell (K562) differentiation, but in the absence of hemin, an oxidative stress inducer, it did not have any effect on K562 cell differentiation. From this, it can be inferred that Kv3.3 is involved as

an oxidation sensor in K562 differentiation.

In the presence of an oxidative stress inducer (i.e., hemin, MPP^+, or tumor hypoxia), Kv3.1, Kv3.3, and Kv3.4 were observed to function as oxidation-sensitive channels. They affected the cell physiology, i.e., cell differentiation, cell apoptosis, and cell migration and invasion, in instances where the cells were required to respond to oxidative stress. In addition, it is likely that the signal molecules, i.e., HIF-1α, MAPK, CREB, and c-fos (which have a proven relationship with oxidative stress) interact with oxidation-sensitive Kv channels.

Taken together, the implication of the current study findings is that Kv3.1, Kv3.3, and Kv3.4 have a pivotal role in oxidative stress-related disease or in relation to cell behavior. The inference is that that they would be good therapeutic targets for a variety of oxidative stress-related diseases. Treatment that targets the oxidation-sensitive Kv channels could be efficacious, especially for difficult-to-treat oxidative stress-related diseases owing to a lack of adequate understanding of their underlying mechanisms. It is proposed that Kv3.4 could be a new therapeutic target for Parkinson's disease or tumor metastasis. This study shows that investigating the data from studies dealing with Kv channels and oxidative stress-related phenomena in the perspective of oxidation sensing of Kv channel would be useful for interpreting channel study. In addition, further studies are warranted on the roles of other Kv channels, i.e., Kv1, Kv7, Kv10.1, and Kv11.1, with the potential for oxidative modulation by ROS (Sahoo et al., 2014), with the objective of securing a greater understanding of oxidative stress-related disease.

REFERENCES

Akel, S., Bertolette, D., Petrow-Sadowski, C. and Ruscetti, F. W., 2007. Levels of Smad7 regulate Smad and mitogen activated kinases (MAPKs) signaling and controls erythroid and megakaryocytic differentiation of erythroleukemia cells. Platelets. 18(8): 566-578.

Angulo, E., Noe, V., Casado, V., Mallol, J., Gomez-Isla, T., Lluis, C., Ferrer, I., Ciudad, C. J. and Franco, R., 2004. Up-regulation of the Kv3.4 potassium channel subunit in early stages of Alzheimer's disease. J Neurochem. 91(3): 547-557.

Arcangeli, A., Becchetti, A., Cherubini, A., Crociani, O., Defilippi, P., Guasti, L., Hofmann, G., Pillozzi, S., Olivotto, M. and Wanke, E., 2004. Physical and functional interaction between integrins and hERG potassium channels. Biochem Soc Trans. 32(Pt 5): 826-827.

Balkwill, F. R., Capasso, M. and Hagemann, T., 2012. The tumor microenvironment at a glance. J Cell Sci. 125(Pt 23): 5591-5596.

Baranauskas, G., Tkatch, T., Nagata, K., Yeh, J. Z. and Surmeier, D. J., 2003. Kv3.4 subunits enhance the repolarizing efficiency of Kv3.1 channels in fast-spiking neurons. Nat Neurosci. 6(3): 258-266.

Bardou, O., Trinh, N. T. and Brochiero, E., 2009. Molecular diversity and function of K^+ channels in airway and alveolar epithelial cells. Am J Physiol Lung Cell Mol Physiol. 296(2): L145-155.

Barrera, G., 2012. Oxidative stress and lipid peroxidation products in cancer progression and therapy. ISRN Oncol. 2012: 137289.

Barzilai, A. and Yamamoto, K., 2004. DNA damage responses to oxidative stress. DNA Repair (Amst). 3(8-9): 1109-1115.

Bednarczyk, P., Kowalczyk, J. E., Beresewicz, M., Dolowy, K., Szewczyk, A. and Zablocka, B., 2010. Identification of a voltage-gated potassium channel in gerbil hippocampal mitochondria. Biochem Biophys Res Commun. 397(3): 614-620.

Biedler, J. L., Helson, L. and Spengler, B. A., 1973. Morphology and growth, tumorigenicity, and cytogenetics of human neuroblastoma cells in continuous culture. Cancer Res. 33(11): 2643-2652.

Bissell, M. J. and Hines, W. C., 2011. Why don't we get more cancer? A proposed role of the microenvironment in restraining cancer progression. Nat Med. 17(3): 320-329.

Blesa, J., Trigo-Damas, I., Quiroga-Varela, A. and Jackson-Lewis, V. R., 2015. Oxidative stress and Parkinson's disease. Front Neuroanat. 9: 91.

Boda, E., Hoxha, E., Pini, A., Montarolo, F. and Tempia, F., 2012. Brain expression of Kv3 subunits during development, adulthood and aging and in a murine model of Alzheimer's disease. J Mol Neurosci. 46(3): 606-615.

Bonello, S., Zahringer, C., BelAiba, R. S., Djordjevic, T., Hess, J., Michiels, C., Kietzmann, T. and Gorlach, A., 2007. Reactive oxygen species activate the HIF-1alpha promoter via a functional NFkappaB site. Arterioscler Thromb Vasc Biol. 27(4): 755-761.

Bongiorno, D., Schuetz, F., Poronnik, P. and Adams, D. J., 2011. Regulation of voltage-gated ion channels in excitable cells by the ubiquitin ligases Nedd4 and Nedd4-2. Channels (Austin). 5(1): 79-88.

Bonnet, S., Michelakis, E. D., Porter, C. J., Andrade-Navarro, M. A., Thebaud, B., Haromy, A., Harry, G., Moudgil, R., McMurtry, M. S., Weir, E. K. and Archer, S. L., 2006. An abnormal mitochondrial-hypoxia inducible factor-1alpha-Kv channel pathway disrupts oxygen sensing and triggers pulmonary arterial hypertension in fawn hooded rats: similarities to human pulmonary arterial hypertension. Circulation. 113(22): 2630-2641.

Buckler, K. J., 1997. A novel oxygen-sensitive potassium current in rat carotid body type I cells. J Physiol. 498 (Pt 3): 649-662.

Cartwright, T. A., Corey, M. J. and Schwalbe, R. A., 2007. Complex oligosaccharides are N-linked to Kv3 voltage-gated K^+ channels in rat brain. Biochim Biophys Acta. 1770(4): 666-671.

Chandel, N. S., McClintock, D. S., Feliciano, C. E., Wood, T. M., Melendez, J. A., Rodriguez, A. M. and Schumacker, P. T., 2000. Reactive oxygen species generated at mitochondrial complex III stabilize hypoxia-inducible factor-1alpha during hypoxia: a mechanism of O_2 sensing. J Biol Chem. 275(33): 25130-25138.

Chen, J., Avdonin, V., Ciorba, M. A., Heinemann, S. H. and Hoshi, T., 2000. Acceleration of P/C-type inactivation in voltage-gated K^+ channels by methionine oxidation. Biophys J. 78(1): 174-187.

Clanton, T. L., 2007. Hypoxia-induced reactive oxygen species formation in skeletal muscle. J Appl Physiol (1985). 102(6): 2379-2388.

Cotella, D., Hernandez-Enriquez, B., Wu, X., Li, R., Pan, Z., Leveille, J., Link, C. D., Oddo, S. and Sesti, F., 2012. Toxic role of K^+ channel oxidation in mammalian brain. J Neurosci. 32(12): 4133-4144.

Damaghi, M., Wojtkowiak, J. W. and Gillies, R. J., 2013. pH sensing and regulation in cancer. Front Physiol. 4: 370.

Danen, E. H., Aota, S., van Kraats, A. A., Yamada, K. M., Ruiter, D. J. and van Muijen, G. N., 1995. Requirement for the synergy site for cell adhesion to fibronectin depends on the activation state of integrin alpha 5 beta 1. J Biol Chem. 270(37): 21612-21618.

de Nigris, F., Lerman, A., Ignarro, L. J., Williams-Ignarro, S., Sica, V., Baker, A. H., Lerman, L. O., Geng, Y. J. and Napoli, C., 2003. Oxidation-sensitive mechanisms, vascular apoptosis and atherosclerosis. Trends Mol Med. 9(8): 351-359.

Di Pietro, R., di Giacomo, V., Caravatta, L., Sancilio, S., Rana, R. A. and Cataldi, A., 2007. Cyclic nucleotide response element binding (CREB) protein activation is involved in K562 erythroleukemia cells differentiation. J Cell Biochem. 100(4): 1070-1079.

Duprat, F., Guillemare, E., Romey, G., Fink, M., Lesage, F., Lazdunski, M. and Honore, E., 1995. Susceptibility of cloned K^+ channels to reactive oxygen species. Proc Natl Acad Sci U S A. 92(25): 11796-11800.

Dwane, S., Durack, E. and Kiely, P. A., 2013. Optimising parameters for the

differentiation of SH-SY5Y cells to study cell adhesion and cell migration. BMC Res Notes. 6: 366.

Fais, S., De Milito, A., You, H. and Qin, W., 2007. Targeting vacuolar H+-ATPases as a new strategy against cancer. Cancer Res. 67(22): 10627-10630.

Fernandez, F. R., Morales, E., Rashid, A. J., Dunn, R. J. and Turner, R. W., 2003. Inactivation of Kv3.3 potassium channels in heterologous expression systems. J Biol Chem. 278(42): 40890-40898.

Firth, A. L., Gordienko, D. V., Yuill, K. H. and Smirnov, S. V., 2009. Cellular localization of mitochondria contributes to Kv channel-mediated regulation of cellular excitability in pulmonary but not mesenteric circulation. Am J Physiol Lung Cell Mol Physiol. 296(3): L347-360.

Firth, A. L., Yuill, K. H. and Smirnov, S. V., 2008. Mitochondria-dependent regulation of Kv currents in rat pulmonary artery smooth muscle cells. Am J Physiol Lung Cell Mol Physiol. 295(1): L61-70.

Florence, T. M., 1995. The role of free radicals in disease. Aust N Z J Ophthalmol. 23(1): 3-7.

Friguet, B., 2006. Oxidized protein degradation and repair in ageing and oxidative stress. FEBS Lett. 580(12): 2910-2916.

Gandhi, S. and Abramov, A. Y., 2012. Mechanism of oxidative stress in neurodegeneration. Oxid Med Cell Longev. 2012: 428010.

Giaccia, A. J., Simon, M. C. and Johnson, R., 2004. The biology of hypoxia: the role of oxygen sensing in development, normal function, and disease. Genes Dev. 18(18): 2183-2194.

Gilkes, D. M., Semenza, G. L. and Wirtz, D., 2014. Hypoxia and the extracellular matrix: drivers of tumour metastasis. Nat Rev Cancer. 14(6): 430-439.

Glunde, K., Guggino, S. E., Solaiyappan, M., Pathak, A. P., Ichikawa, Y. and Bhujwalla, Z. M., 2003. Extracellular acidification alters lysosomal trafficking in human breast cancer cells. Neoplasia. 5(6): 533-545.

Golding, B., Pillemer, S. R., Roussou, P., Peters, E. A., Tsokos, G. C., Ballow, J.

E. and Hoffman, T., 1988. Inverse relationship between proliferation and differentiation in a human TNP-specific B cell line. Cell cycle dependence of antibody secretion. J Immunol. 141(8): 2564-2568.

Guidetti, G. F., Canobbio, I. and Torti, M., 2015. PI3K/Akt in platelet integrin signaling and implications in thrombosis. Adv Biol Regul. 59: 36-52.

Guo, L., Tang, X., Tian, H., Liu, Y., Wang, Z., Wu, H., Wang, J., Guo, S. and Zhu, D., 2008. Subacute hypoxia suppresses Kv3.4 channel expression and whole-cell K^+ currents through endogenous 15-hydroxyeicosatetraenoic acid in pulmonary arterial smooth muscle cells. Eur J Pharmacol. 587(1-3): 187-195.

Hagen, T., 2012. Oxygen versus Reactive Oxygen in the Regulation of HIF-1alpha: The Balance Tips. Biochem Res Int. 2012: 436981.

Halliwell, B., 1994. Free radicals, antioxidants, and human disease: curiosity, cause, or consequence?, Lancet. 344(8924): 721-724.

Hemmerlein, B., Weseloh, R. M., Mello de Queiroz, F., Knotgen, H., Sanchez, A., Rubio, M. E., Martin, S., Schliephacke, T., Jenke, M., Heinz Joachim, R., Stuhmer, W. and Pardo, L. A., 2006. Overexpression of Eag1 potassium channels in clinical tumours. Mol Cancer. 5: 41.

Hille, B., 2001. Ion channels of excitable membranes. Sunderland, 3rd edition.

Hockel, M. and Vaupel, P., 2001. Tumor hypoxia: definitions and current clinical, biologic, and molecular aspects. J Natl Cancer Inst. 93(4): 266-276.

Hocking, J. C., Pollock, N. S., Johnston, J., Wilson, R. J., Shankar, A. and McFarlane, S., 2012. Neural activity and branching of embryonic retinal ganglion cell dendrites. Mech Dev. 129(5-8): 125-135.

Holt, S. M., Scemama, J. L., Panayiotidis, M. I. and Georgakilas, A. G., 2009. Compromised repair of clustered DNA damage in the human acute lymphoblastic leukemia MSH2-deficient NALM-6 cells. Mutat Res. 674(1-2): 123-130.

Howitt, J., Putz, U., Lackovic, J., Doan, A., Dorstyn, L., Cheng, H., Yang, B., Chan-Ling, T., Silke, J., Kumar, S. and Tan, S. S., 2009. Divalent metal

transporter 1 (DMT1) regulation by Ndfip1 prevents metal toxicity in human neurons. Proc Natl Acad Sci U S A. 106(36): 15489-15494.

Huang, H. M., Chang, T. W. and Liu, J. C., 2004. Basic fibroblast growth factor antagonizes activin A-mediated growth inhibition and hemoglobin synthesis in K562 cells by activating ERK1/2 and deactivating p38 MAP kinase. Biochem Biophys Res Commun. 320(4): 1247-1252.

Huang, X. and Jan, L. Y., 2014. Targeting potassium channels in cancer. J Cell Biol. 206(2): 151-162.

Huveneers, S. and Danen, E. H., 2009. Adhesion signaling - crosstalk between integrins, Src and Rho. J Cell Sci. 122(Pt 8): 1059-1069.

Hwang, O., 2013. Role of oxidative stress in Parkinson's disease. Exp Neurobiol. 22(1): 11-17.

Ida, C., Ogata, S., Okumura, K. and Taguchi, H., 2009. Induction of differentiation in k562 cell line by nicotinic acid-related compounds. Biosci Biotechnol Biochem. 73(1): 79-84.

Jang, S. H., Choi, C., Hong, S. G., Yarishkin, O. V., Bae, Y. M., Kim, J. G., O'Grady, S. M., Yoon, K. A., Kang, K. S., Ryu, P. D. and Lee, S. Y., 2009. Silencing of Kv4.1 potassium channels inhibits cell proliferation of tumorigenic human mammary epithelial cells. Biochem Biophys Res Commun. 384(2): 180-186.

Jang, S. H., Choi, S. Y., Ryu, P. D. and Lee, S. Y., 2011. Anti-proliferative effect of Kv1.3 blockers in A549 human lung adenocarcinoma in vitro and in vivo. Eur J Pharmacol. 651(1-3): 26-32.

Jang, S. H., Ryu, P. D. and Lee, S. Y., 2011. Dendrotoxin-kappa suppresses tumor growth induced by human lung adenocarcinoma A549 cells in nude mice. J Vet Sci. 12(1): 35-40.

Jarvinen, M., Ylanne, J. and Virtanen, I., 1993. The effect of differentiation inducers on the integrin expression of K562 erythroleukemia cells. Cell Biol Int. 17(4): 399-407.

Jimenez, L. A., Zanella, C., Fung, H., Janssen, Y. M., Vacek, P., Charland, C., Goldberg, J. and Mossman, B. T., 1997. Role of extracellular signal-

regulated protein kinases in apoptosis by asbestos and H_2O_2. Am J Physiol. 273(5 Pt 1): L1029-1035.

Joyce, J. A. and Pollard, J. W., 2009. Microenvironmental regulation of metastasis. Nat Rev Cancer. 9(4): 239-252.

Kaab, S., Miguel-Velado, E., Lopez-Lopez, J. R. and Perez-Garcia, M. T., 2005. Down regulation of Kv3.4 channels by chronic hypoxia increases acute oxygen sensitivity in rabbit carotid body. J Physiol. 566(Pt 2): 395-408.

Kanda, V. A., Lewis, A., Xu, X. and Abbott, G. W., 2011. KCNE1 and KCNE2 inhibit forward trafficking of homomeric N-type voltage-gated potassium channels. Biophys J. 101(6): 1354-1363.

Kato, Y., Ozawa, S., Miyamoto, C., Maehata, Y., Suzuki, A., Maeda, T. and Baba, Y., 2013. Acidic extracellular microenvironment and cancer. Cancer Cell Int. 13(1): 89.

Kim, G. H., Kim, J. E., Rhie, S. J. and Yoon, S., 2015. The Role of Oxidative Stress in Neurodegenerative Diseases. Exp Neurobiol. 24(4): 325-340.

Kim, S. J., Widenmaier, S. B., Choi, W. S., Nian, C., Ao, Z., Warnock, G. and McIntosh, C. H., 2012. Pancreatic beta-cell prosurvival effects of the incretin hormones involve post-translational modification of Kv2.1 delayed rectifier channels. Cell Death Differ. 19(2): 333-344.

Klaunig, J. E. and Kamendulis, L. M., 2004. The role of oxidative stress in carcinogenesis. Annu Rev Pharmacol Toxicol. 44: 239-267.

Klaunig, J. E., Kamendulis, L. M. and Hocevar, B. A., 2010. Oxidative stress and oxidative damage in carcinogenesis. Toxicol Pathol. 38(1): 96-109.

Kline, D. D., Peng, Y. J., Manalo, D. J., Semenza, G. L. and Prabhakar, N. R., 2002. Defective carotid body function and impaired ventilatory responses to chronic hypoxia in mice partially deficient for hypoxia-inducible factor 1 alpha. Proc Natl Acad Sci U S A. 99(2): 821-826.

Koeberle, P. D., Wang, Y. and Schlichter, L. C., 2010. Kv1.1 and Kv1.3 channels contribute to the degeneration of retinal ganglion cells after optic nerve transection in vivo. Cell Death Differ. 17(1): 134-144.

Koeffler, H. P. and Golde, D. W., 1980. Human myeloid leukemia cell lines: a

review. Blood. 56(3): 344-350.

Koh, M. Y., Spivak-Kroizman, T., Venturini, S., Welsh, S., Williams, R. R., Kirkpatrick, D. L. and Powis, G., 2008. Molecular mechanisms for the activity of PX-478, an antitumor inhibitor of the hypoxia-inducible factor-1alpha. Mol Cancer Ther. 7(1): 90-100.

Kroemer, G., Galluzzi, L. and Brenner, C., 2007. Mitochondrial membrane permeabilization in cell death. Physiol Rev. 87(1): 99-163.

Kryston, T. B., Georgiev, A. B., Pissis, P. and Georgakilas, A. G., 2011. Role of oxidative stress and DNA damage in human carcinogenesis. Mutat Res. 711(1-2): 193-201.

Kunzelmann, K., 2005. Ion channels and cancer. Journal of Membrane Biology. 205(3): 159-173.

Lang, F., Foller, M., Lang, K. S., Lang, P. A., Ritter, M., Gulbins, E., Vereninov, A. and Huber, S. M., 2005. Ion channels in cell proliferation and apoptotic cell death. Journal of Membrane Biology. 205(3): 147-157.

Langdon, S. P., Richards, F. M. and Hickman, J. A., 1988. Investigations of the relationship between cell proliferation and differentiation of HL-60 cells induced to differentiate by N-methylformamide. Leuk Res. 12(3): 211-216.

Langston, J. W., Irwin, I., Langston, E. B. and Forno, L. S., 1984. 1-Methyl-4-phenylpyridinium ion (MPP^+): identification of a metabolite of MPTP, a toxin selective to the substantia nigra. Neurosci Lett. 48(1): 87-92.

Leung, Y. M., 2012. Involvement of C-type inactivation gating in the actions of voltage-gated K^+ channel inhibitors. Pharmacol Ther. 133(2): 151-158.

Li, Y. L. and Schultz, H. D., 2006. Enhanced sensitivity of Kv channels to hypoxia in the rabbit carotid body in heart failure: role of angiotensin II. J Physiol. 575(Pt 1): 215-227.

Limb, J. K., Yoon, S., Lee, K. E., Kim, B. H., Lee, S., Bae, Y. S., Jhon, G. J. and Kim, J., 2009. Regulation of megakaryocytic differentiation of K562 cells by FosB, a member of the Fos family of AP-1 transcription

factors. Cell Mol Life Sci. 66(11-12): 1962-1973.

Liu, K., Xing, H., Zhang, S., Liu, S. and Fung, M., 2010. Cucurbitacin D induces fetal hemoglobin synthesis in K562 cells and human hematopoietic progenitors through activation of p38 pathway and stabilization of the gamma-globin mRNA. Blood Cells Mol Dis. 45(4): 269-275.

Liu, Q. H., Fleischmann, B. K., Hondowicz, B., Maier, C. C., Turka, L. A., Yui, K., Kotlikoff, M. I., Wells, A. D. and Freedman, B. D., 2002. Modulation of Kv channel expression and function by TCR and costimulatory signals during peripheral CD4(+) lymphocyte differentiation. J Exp Med. 196(7): 897-909.

Liu, Y. and Gutterman, D. D., 2002. Oxidative stress and potassium channel function. Clin Exp Pharmacol Physiol. 29(4): 305-311.

Lopez-Barneo, J., del Toro, R., Levitsky, K. L., Chiara, M. D. and Ortega-Saenz, P., 2004. Regulation of oxygen sensing by ion channels. J Appl Physiol (1985). 96(3): 1187-1195; discussion 1170-1182.

Lozzio, C. B. and Lozzio, B. B., 1975. Human chronic myelogenous leukemia cell-line with positive Philadelphia chromosome. Blood. 45(3): 321-334.

Markesbery, W. R., 1997. Oxidative stress hypothesis in Alzheimer's disease. Free Radic Biol Med. 23(1): 134-147.

Marsters, P., Alhamdan, R. and Campbell, B. K., 2014. Cell density-mediated pericellular hypoxia and the local dynamic regulation of VEGF-a splice variants in ovine ovarian granulosa cells. Biol Reprod. 91(2): 35.

Martinez, Y., Li, X., Liu, G., Bin, P., Yan, W., Mas, D., Valdivie, M., Hu, C. A., Ren, W. and Yin, Y., 2017. The role of methionine on metabolism, oxidative stress, and diseases. Amino Acids. 49(12): 2091-2098.

Mattson, M. P., 2000. Apoptosis in neurodegenerative disorders. Nat Rev Mol Cell Biol. 1(2): 120-129.

Mattson, M. P., 2004. Pathways towards and away from Alzheimer's disease. Nature. 430(7000): 631-639.

Mattson, M. P. and Kroemer, G., 2003. Mitochondria in cell death: novel targets

for neuroprotection and cardioprotection. Trends Mol Med. 9(5): 196-205.

McCord, M. C. and Aizenman, E., 2013. Convergent Ca2+ and Zn2+ signaling regulates apoptotic Kv2.1 K^+ currents. Proc Natl Acad Sci U S A. 110(34): 13988-13993.

McCubrey, J. A., Steelman, L. S., Chappell, W. H., Abrams, S. L., Wong, E. W., Chang, F., Lehmann, B., Terrian, D. M., Milella, M., Tafuri, A., Stivala, F., Libra, M., Basecke, J., Evangelisti, C., Martelli, A. M. and Franklin, R. A., 2007. Roles of the Raf/MEK/ERK pathway in cell growth, malignant transformation and drug resistance. Biochim Biophys Acta. 1773(8): 1263-1284.

Menendez, S. T., Rodrigo, J. P., Allonca, E., Garcia-Carracedo, D., Alvarez-Alija, G., Casado-Zapico, S., Fresno, M. F., Rodriguez, C., Suarez, C. and Garcia-Pedrero, J. M., 2010. Expression and clinical significance of the Kv3.4 potassium channel subunit in the development and progression of head and neck squamous cell carcinomas. J Pathol. 221(4): 402-410.

Milei, J., Forcada, P., Fraga, C. G., Grana, D. R., Iannelli, G., Chiariello, M., Tritto, I. and Ambrosio, G., 2007. Relationship between oxidative stress, lipid peroxidation, and ultrastructural damage in patients with coronary artery disease undergoing cardioplegic arrest/reperfusion. Cardiovasc Res. 73(4): 710-719.

Misonou, H., Mohapatra, D. P. and Trimmer, J. S., 2005. Kv2.1: a voltage-gated K^+ channel critical to dynamic control of neuronal excitability. Neurotoxicology. 26(5): 743-752.

Mittal, M., Gu, X. Q., Pak, O., Pamenter, M. E., Haag, D., Fuchs, D. B., Schermuly, R. T., Ghofrani, H. A., Brandes, R. P., Seeger, W., Grimminger, F., Haddad, G. G. and Weissmann, N., 2012. Hypoxia induces Kv channel current inhibition by increased NADPH oxidase-derived reactive oxygen species. Free Radic Biol Med. 52(6): 1033-1042.

Norris, A. J., Foeger, N. C. and Nerbonne, J. M., 2010. Neuronal voltage-gated K^+ (Kv) channels function in macromolecular complexes. Neurosci Lett. 486(2): 73-77.

Nunomura, A., Moreira, P. I., Takeda, A., Smith, M. A. and Perry, G., 2007. Oxidative RNA damage and neurodegeneration. Curr Med Chem. 14(28): 2968-2975.

O'Grady, S. M. and Lee, S. Y., 2005. Molecular diversity and function of voltage-gated (Kv) potassium channels in epithelial cells. International Journal of Biochemistry & Cell Biology. 37(8): 1578-1594.

Okamoto, F., Kajiya, H., Toh, K., Uchida, S., Yoshikawa, M., Sasaki, S., Kido, M. A., Tanaka, T. and Okabe, K., 2008. Intracellular ClC-3 chloride channels promote bone resorption in vitro through organelle acidification in mouse osteoclasts. Am J Physiol Cell Physiol. 294(3): C693-701.

Osipenko, O. N., Tate, R. J. and Gurney, A. M., 2000. Potential role for kv3.1b channels as oxygen sensors. Circ Res. 86(5): 534-540.

Pacheco Otalora, L. F., Skinner, F., Oliveira, M. S., Farrell, B., Arshadmansab, M. F., Pandari, T., Garcia, I., Robles, L., Rosas, G., Mello, C. F., Ermolinsky, B. S. and Garrido-Sanabria, E. R., 2011. Chronic deficit in the expression of voltage-gated potassium channel Kv3.4 subunit in the hippocampus of pilocarpine-treated epileptic rats. Brain Res. 1368: 308-316.

Pal, S., Hartnett, K. A., Nerbonne, J. M., Levitan, E. S. and Aizenman, E., 2003. Mediation of neuronal apoptosis by Kv2.1-encoded potassium channels. J Neurosci. 23(12): 4798-4802.

Palme, D., Misovic, M., Schmid, E., Klumpp, D., Salih, H. R., Rudner, J. and Huber, S. M., 2013. Kv3.4 potassium channel-mediated electrosignaling controls cell cycle and survival of irradiated leukemia cells. Pflugers Arch. 465(8): 1209-1221.

Pan, Y., Xu, X., Tong, X. and Wang, X., 2004. Messenger RNA and protein expression analysis of voltage-gated potassium channels in the brain of

Abeta(25-35)-treated rats. J Neurosci Res. 77(1): 94-99.

Pani, G., Galeotti, T. and Chiarugi, P., 2010. Metastasis: cancer cell's escape from oxidative stress. Cancer Metastasis Rev. 29(2): 351-378.

Pankov, R. and Yamada, K. M., 2002. Fibronectin at a glance. J Cell Sci. 115(Pt 20): 3861-3863.

Pannaccione, A., Boscia, F., Scorziello, A., Adornetto, A., Castaldo, P., Sirabella, R., Taglialatela, M., Di Renzo, G. F. and Annunziato, L., 2007. Up-regulation and increased activity of KV3.4 channels and their accessory subunit MinK-related peptide 2 induced by amyloid peptide are involved in apoptotic neuronal death. Mol Pharmacol. 72(3): 665-673.

Pardo, L. A., 2004. Voltage-gated potassium channels in cell proliferation. Physiology (Bethesda). 19: 285-292.

Pardo, L. A. and Stuhmer, W., 2014. The roles of K(+) channels in cancer. Nat Rev Cancer. 14(1): 39-48.

Pardo, L. A. and Suhmer, W., 2008. Eag1 as a cancer target. Expert Opin Ther Targets. 12(7): 837-843.

Patel, A. J. and Honore, E., 2001. Molecular physiology of oxygen-sensitive potassium channels. Eur Respir J. 18(1): 221-227.

Pettiford, S. M. and Herbst, R., 2003. The protein tyrosine phosphatase HePTP regulates nuclear translocation of ERK2 and can modulate megakaryocytic differentiation of K562 cells. Leukemia. 17(2): 366-378.

Pham-Huy, L. A., He, H. and Pham-Huy, C., 2008. Free radicals, antioxidants in disease and health. Int J Biomed Sci. 4(2): 89-96.

Pillozzi, S. and Becchetti, A., 2012. Ion channels in hematopoietic and mesenchymal stem cells. Stem Cells Int. 2012: 217910.

Piret, J. P., Mottet, D., Raes, M. and Michiels, C., 2002. $CoCl_2$, a chemical inducer of hypoxia-inducible factor-1, and hypoxia reduce apoptotic cell death in hepatoma cell line HepG2. Ann N Y Acad Sci. 973: 443-447.

Plant, L. D., Webster, N. J., Boyle, J. P., Ramsden, M., Freir, D. B., Peers, C. and Pearson, H. A., 2006. Amyloid beta peptide as a physiological modulator of neuronal 'A'-type K^+ current. Neurobiol Aging. 27(11): 1673-1683.

Pongs, O., 1999. Voltage-gated potassium channels: from hyperexcitability to excitement. FEBS Lett. 452(1-2): 31-35.

Qutub, A. A. and Popel, A. S., 2008. Reactive oxygen species regulate hypoxia-inducible factor 1alpha differentially in cancer and ischemia. Mol Cell Biol. 28(16): 5106-5119.

Rae, J. L. and Shepard, A. R., 2000. Kv3.3 potassium channels in lens epithelium and corneal endothelium. Exp Eye Res. 70(3): 339-348.

Reuter, S., Gupta, S. C., Chaturvedi, M. M. and Aggarwal, B. B., 2010. Oxidative stress, inflammation, and cancer: how are they linked?, Free Radic Biol Med. 49(11): 1603-1616.

Rodrigo, J. P., Garcia-Pedrero, J. M., Suarez, C., Takes, R. P., Thompson, L. D., Slootweg, P. J., Woolgar, J. A., Westra, W. H., Brakenhoff, R. H., Rinaldo, A., Devaney, K. O., Williams, M. D., Gnepp, D. R. and Ferlito, A., 2012. Biomarkers predicting malignant progression of laryngeal epithelial precursor lesions: a systematic review. Eur Arch Otorhinolaryngol. 269(4): 1073-1083.

Rudy, B. and McBain, C. J., 2001. Kv3 channels: voltage-gated K^+ channels designed for high-frequency repetitive firing. Trends Neurosci. 24(9): 517-526.

Ruppersberg, J. P., Frank, R., Pongs, O. and Stocker, M., 1991. Cloned neuronal IK(A) channels reopen during recovery from inactivation. Nature. 353(6345): 657-660.

Ruppersberg, J. P., Stocker, M., Pongs, O., Heinemann, S. H., Frank, R. and Koenen, M., 1991. Regulation of fast inactivation of cloned mammalian IK(A) channels by cysteine oxidation. Nature. 352(6337): 711-714.

Rutherford, T. R., Clegg, J. B. and Weatherall, D. J., 1979. K562 human leukaemic cells synthesise embryonic haemoglobin in response to

haemin. Nature. 280(5718): 164-165.

Ryter, S. W. and Tyrrell, R. M., 2000. The heme synthesis and degradation pathways: role in oxidant sensitivity. Heme oxygenase has both pro- and antioxidant properties. Free Radic Biol Med. 28(2): 289-309.

Sahoo, N., Hoshi, T. and Heinemann, S. H., 2014. Oxidative modulation of voltage-gated potassium channels. Antioxid Redox Signal. 21(6): 933-952.

Sangerman, J., Lee, M. S., Yao, X., Oteng, E., Hsiao, C. H., Li, W., Zein, S., Ofori-Acquah, S. F. and Pace, B. S., 2006. Mechanism for fetal hemoglobin induction by histone deacetylase inhibitors involves gamma-globin activation by CREB1 and ATF-2. Blood. 108(10): 3590-3599.

Schieber, C., Howitt, J., Putz, U., White, J. M., Parish, C. L., Donnelly, P. S. and Tan, S. S., 2011. Cellular up-regulation of Nedd4 family interacting protein 1 (Ndfip1) using low levels of bioactive cobalt complexes. J Biol Chem. 286(10): 8555-8564.

Schlief, T., Schonherr, R. and Heinemann, S. H., 1996. Modification of C-type inactivating Shaker potassium channels by chloramine-T. Pflugers Arch. 431(4): 483-493.

Semenza, G. L., 2002. HIF-1 and tumor progression: pathophysiology and therapeutics. Trends Mol Med. 8(4 Suppl): S62-67.

Semenza, G. L., 2013. HIF-1 mediates metabolic responses to intratumoral hypoxia and oncogenic mutations. J Clin Invest. 123(9): 3664-3671.

Semenza, G. L., 2016. The hypoxic tumor microenvironment: A driving force for breast cancer progression. Biochim Biophys Acta. 1863(3): 382-391.

Sesti, F., 2016. Oxidation of K(+) Channels in Aging and Neurodegeneration. Aging Dis. 7(2): 130-135.

Sesti, F., Liu, S. and Cai, S. Q., 2010. Oxidation of potassium channels by ROS: a general mechanism of aging and neurodegeneration?, Trends Cell Biol. 20(1): 45-51.

Sesti, F., Wu, X. and Liu, S., 2014. Oxidation of KCNB1 K(+) channels in

central nervous system and beyond. World J Biol Chem. 5(2): 85-92.

Shah, N. H. and Aizenman, E., 2014. Voltage-gated potassium channels at the crossroads of neuronal function, ischemic tolerance, and neurodegeneration. Transl Stroke Res. 5(1): 38-58.

Shimoda, L. A., Manalo, D. J., Sham, J. S., Semenza, G. L. and Sylvester, J. T., 2001. Partial HIF-1alpha deficiency impairs pulmonary arterial myocyte electrophysiological responses to hypoxia. Am J Physiol Lung Cell Mol Physiol. 281(1): L202-208.

Spill, F., Reynolds, D. S., Kamm, R. D. and Zaman, M. H., 2016. Impact of the physical microenvironment on tumor progression and metastasis. Curr Opin Biotechnol. 40: 41-48.

Stenger, C., Naves, T., Verdier, M. and Ratinaud, M. H., 2011. The cell death response to the ROS inducer, cobalt chloride, in neuroblastoma cell lines according to p53 status. Int J Oncol. 39(3): 601-609.

Storz, P., 2005. Reactive oxygen species in tumor progression. Front Biosci. 10: 1881-1896.

Szabo, I., Bock, J., Grassme, H., Soddemann, M., Wilker, B., Lang, F., Zoratti, M. and Gulbins, E., 2008. Mitochondrial potassium channel Kv1.3 mediates Bax-induced apoptosis in lymphocytes. Proc Natl Acad Sci U S A. 105(39): 14861-14866.

Szewczyk, A., Jarmuszkiewicz, W. and Kunz, W. S., 2009. Mitochondrial potassium channels. IUBMB Life. 61(2): 134-143.

Tong, H., Steinert, J. R., Robinson, S. W., Chernova, T., Read, D. J., Oliver, D. L. and Forsythe, I. D., 2010. Regulation of Kv channel expression and neuronal excitability in rat medial nucleus of the trapezoid body maintained in organotypic culture. J Physiol. 588(Pt 9): 1451-1468.

Uttara, B., Singh, A. V., Zamboni, P. and Mahajan, R. T., 2009. Oxidative stress and neurodegenerative diseases: a review of upstream and downstream antioxidant therapeutic options. Curr Neuropharmacol. 7(1): 65-74.

van den Berg, R., Haenen, G. R., van den Berg, H. and Bast, A., 2001.

Transcription factor NF-kappaB as a potential biomarker for oxidative stress. Br J Nutr. 86 Suppl 1: S121-127.

Varadarajan, S., Yatin, S., Aksenova, M. and Butterfield, D. A., 2000. Review: Alzheimer's amyloid beta-peptide-associated free radical oxidative stress and neurotoxicity. J Struct Biol. 130(2-3): 184-208.

Vaupel, P., 2004. The role of hypoxia-induced factors in tumor progression. Oncologist. 9 Suppl 5: 10-17.

Vaupel, P., Mayer, A. and Hockel, M., 2004. Tumor hypoxia and malignant progression. Methods Enzymol. 381: 335-354.

Vega-Saenz de Miera, E. and Rudy, B., 1992. Modulation of K^+ channels by hydrogen peroxide. Biochem Biophys Res Commun. 186(3): 1681-1687.

Volpi, N., Petrini, M., Conte, A., Valentini, P., Venturelli, T., Bolognani, L. and Ronca, G., 1994. Effects of glycosaminoglycans on U-937 leukemia cell proliferation and differentiation: structure-function relationship. Exp Cell Res. 215(1): 119-130.

Wang, G. L., Jiang, B. H., Rue, E. A. and Semenza, G. L., 1995. Hypoxia-inducible factor 1 is a basic-helix-loop-helix-PAS heterodimer regulated by cellular O_2 tension. Proc Natl Acad Sci U S A. 92(12): 5510-5514.

Wang, H., Zhang, Y., Cao, L., Han, H., Wang, J., Yang, B., Nattel, S. and Wang, Z., 2002. HERG K^+ channel, a regulator of tumor cell apoptosis and proliferation. Cancer Res. 62(17): 4843-4848.

Wang, X., Wang, W., Li, L., Perry, G., Lee, H. G. and Zhu, X., 2014. Oxidative stress and mitochondrial dysfunction in Alzheimer's disease. Biochim Biophys Acta. 1842(8): 1240-1247.

Wang, Z., 2004. Roles of K^+ channels in regulating tumour cell proliferation and apoptosis. Pflugers Arch. 448(3): 274-286.

Wayne, J., Sielski, J., Rizvi, A., Georges, K. and Hutter, D., 2006. ERK regulation upon contact inhibition in fibroblasts. Mol Cell Biochem. 286(1-2): 181-189.

Webb, B. A., Chimenti, M., Jacobson, M. P. and Barber, D. L., 2011. Dysregulated pH: a perfect storm for cancer progression. Nat Rev Cancer. 11(9): 671-677.

Wilson, W. R. and Hay, M. P., 2011. Targeting hypoxia in cancer therapy. Nat Rev Cancer. 11(6): 393-410.

Witt, O., Sand, K. and Pekrun, A., 2000. Butyrate-induced erythroid differentiation of human K562 leukemia cells involves inhibition of ERK and activation of p38 MAP kinase pathways. blood. 95: 2391-2396.

Wu, K., Xu, W., You, Q., Guo, R., Feng, J., Zhang, C. and Wu, W., 2012. Increased expression of heat shock protein 90 under chemical hypoxic conditions protects cardiomyocytes against injury induced by serum and glucose deprivation. Int J Mol Med. 30(5): 1138-1144.

Wu, X., Hernandez-Enriquez, B., Banas, M., Xu, R. and Sesti, F., 2013. Molecular mechanisms underlying the apoptotic effect of KCNB1 K^+ channel oxidation. J Biol Chem. 288(6): 4128-4134.

Wu, Y., Li, X., Xie, W., Jankovic, J., Le, W. and Pan, T., 2010. Neuroprotection of deferoxamine on rotenone-induced injury via accumulation of HIF-1 alpha and induction of autophagy in SH-SY5Y cells. Neurochem Int. 57(3): 198-205.

Xie, H. R., Hu, L. S. and Li, G. Y., 2010. SH-SY5Y human neuroblastoma cell line: in vitro cell model of dopaminergic neurons in Parkinson's disease. Chin Med J (Engl). 123(8): 1086-1092.

Xu, L., Enyeart, J. A. and Enyeart, J. J., 2001. Neuroprotective agent riluzole dramatically slows inactivation of Kv1.4 potassium channels by a voltage-dependent oxidative mechanism. J Pharmacol Exp Ther. 299(1): 227-237.

Yang, G. H., Wang, F., Yu, J., Wang, X. S., Yuan, J. Y. and Zhang, J. W., 2009. MicroRNAs are involved in erythroid differentiation control. J Cell Biochem. 107(3): 548-556.

Yao, H., Zhou, K., Yan, D., Li, M. and Wang, Y., 2009. The Kv2.1 channels

mediate neuronal apoptosis induced by excitotoxicity. J Neurochem. 108(4): 909-919.

Yi, Z. C., Wang, Z., Li, H. X., Liu, M. J., Wu, R. C. and Wang, X. H., 2004. Effects of chebulinic acid on differentiation of human leukemia K562 cells. Acta Pharmacol Sin. 25(2): 231-238.

You, M. H., Song, M. S., Lee, S. K., Ryu, P. D., Lee, S. Y. and Kim, D. Y., 2013. Voltage-gated K(+) channels in adipogenic differentiation of bone marrow-derived human mesenchymal stem cells. Acta Pharmacol Sin. 34(1): 129-136.

Yu, W., Gowda, M., Sharad, Y., Singh, S. A. and Sesti, F., 2017. Oxidation of KCNB1 potassium channels triggers apoptotic integrin signaling in the brain. Cell Death Dis. 8(4): e2737.

Zeller, K. S., Riaz, A., Sarve, H., Li, J., Tengholm, A. and Johansson, S., 2013. The role of mechanical force and ROS in integrin-dependent signals. PLoS One. 8(5): e64897.

Zhang, D., Cho, E. and Wong, J., 2007. A critical role for the co-repressor N-CoR in erythroid differentiation and heme synthesis. Cell Res. 17(9): 804-814.

Zhang, L., Bewick, M. and Lafrenie, R. M., 2002. Role of Raf-1 and FAK in cell density-dependent regulation of integrin-dependent activation of MAP kinase. Carcinogenesis. 23(7): 1251-1258.

ABSTRACT IN KOREAN

국문초록

산화 감지자로서 전압의존성 K+ 채널 Kv3.3과 Kv3.4의 역할

송민석

서울대학교 대학원
수의학과 수의약리학 전공

(지도교수: 이소영)

전압의존성 K^+ 채널의 세포 내 기능 및 여러 세포생리현상과의 관계에 대한 연구는 그간 활발하게 진행되어 왔다. 그러나 전압의존성 K^+ 채널의 주요 기능 중 하나인 산화감지 기능의 관점에서 전압의존성 K^+ 채널이 여러 세포생리현상과 관련하여 어떠한 역할을 갖는지 살펴보는 연구는 현재까지 거의 이루어지지 않았다.

이에 전압의존성 K^+ 채널 중 산화감지 기능이 있는 것으로 알

려져 있지만 다른 전압의존성 K^+ 채널에 비해서는 그간 연구가 활발히 진행되지 못했던 Kv3.1, Kv3.3, Kv3.4를 대상으로 연구를 진행할 필요성이 있었다. 따라서 본 논문에서는 Kv3.1, Kv3.3, Kv3.4와 같이 산화감지 기능이 있는 전압의존성 K^+ 채널이 산화적 스트레스와 밀접한 연관이 있을 것으로 예상되는 다양한 세포생리현상에 어떠한 역할을 미치는지 살펴봄으로써 전압의존성 K^+ 채널이 산화감지 채널로서 세포 내에서 갖는 역할을 규명하고자 하였다.

Kv3.3의 경우 hemin이라는 산화적 스트레스 유발인자에 의해 K562 세포가 적혈구로 분화되는 과정에 밀접하게 관여하고 있다는 사실을 확인할 수 있었으며, 그 과정에서 MAPK, CREB, c-fos와 같은 세포 내 신호전달 물질과 상호작용함을 확인하였다. siRNA 기법을 이용하여 Kv3.3의 발현을 억제한 결과, hemin에 의한 K562 세포의 적혈구로의 분화가 증가한 반면 Kv3.3을 과발현 시킨 경우에는 K562 세포 분화에 어떠한 영향도 미치지 못함을 확인하였다. Kv3.3 발현 억제를 통한 K562 세포분화증가 효과는 fibronectin을 공급해주는 경우에는 적혈구 분화에 영향을 주지 않고 세포의 부착 기능만을 증가시키는 쪽으로 유도될 수 있었다.

또한 Kv3.4가 neuroblastoma인 SH-SY5Y 세포가 산화적 스트레스 유발인자에 의한 신경세포사멸 과정에 중요한 역할을 하고 있으며, 여기에는 HIF-1α가 조절인자로서 관여한다는 사실을 확인하였다. $CoCl_2$에 의해서 축적된 HIF-1α는 $CoCl_2$에 의한 산화적 손상으로부터 SH-SY5Y 세포를 보호하는 작용을 하고 있었다. HIF-1α에 희한 신경세포 보호효과를 참고로 하여 Kv3.4 선택적 차단제인 BDS-II를 사용했을 때, 미토콘드리아 막에서 세포질로의 cytochrome c의 분비와 미토콘드리아 막전위의 탈분극이 억제됨으로써 세포사멸 과정이 억제되고 이로 인해 MPP^+에 의한 SH-SY5Y 세포의 사멸과정을 억제할 수 있었다.

한편 정상세포와는 달리 A549, MDA-MB-231과 같은 암세포에서는 세포밀도에 따른 저산소상태 및 활성산소 증가 과정에서 Kv3.1과 Kv3.4의 발현이 증가된다는 사실을 확인할 수 있었다. 발현이 증가된 Kv3.1과 Kv3.4는 산화적 스트레스에 의한 손상을 피하기 위해 세포가 이동 및 침투과정을 거치는 데에 관여하고 있었다. Kv3.1과 Kv3.4를 모두 억제할 수 있는 농도로 BDS-II를 처리하자 암세포의 pH 조절기능과 ERK 활성화를 억제함으로써 암세포의 이동

및 침투과정을 억제할 수 있었다.

본 연구의 결과는 전압의존성 K^+ 채널이 산화감지 채널로서 세포 내에서 어떠한 역할을 수행하는지에 대한 정보를 제공할 뿐만 아니라 그와 관련한 기전에 대한 정보도 제공하고 있다. 따라서 향후 전압의존성 K^+ 채널을 이용한 질병기전 및 치료 연구에 있어서 새로운 패러다임을 제시해 줄 수 있을 것으로 기대되며, 더 나아가 산화적 스트레스 관련 질병의 바이오 마커 및 치료 타겟으로서 전압의존성 K^+ 채널의 연구 가능성을 제시해 주고 있다.

주요어: 산화감지 기능, 세포 분화, 세포 사멸, 세포 이동 및 침투, 전압의존성 K^+ 채널, Kv3

학번: 2012-21540